Biogeochemical Modeling of Microbially Induced Desaturation and Precipitation

by

Caitlyn A. Hall

A Dissertation Presented in Partial Fulfillment
of the Requirements for the Degree
Doctor of Philosophy

Approved April 2021 by the
Graduate Supervisory Committee:

Bruce Rittmann, Co-Chair
Edward Kavazanjian, Co-Chair
Leon van Paassen
Jason DeJong

ARIZONA STATE UNIVERSITY
May 2021

ABSTRACT

Earthquake-induced soil liquefaction poses a significant global threat, especially to vulnerable populations. There are no existing cost-effective techniques for mitigation of liquefaction under or around existing infrastructure. Microbially Induced Desaturation and Precipitation (MIDP) via denitrification is a potentially sustainable, non-disruptive bio-based ground improvement technique under existing structures. MIDP has been shown to reduce liquefaction triggering potential under lab conditions in two ways: 1) biogenic gas desaturation in the short-term (treatment within hours to days) and 2) calcium carbonate precipitation and soil strengthening in the long-term (treatment within weeks to months). However, these experiments have not considered MIDP behavior under field stresses and pressures, nor have they considered challenges from process inhibition or microbial competition that may be encountered when upscaled to field applications.

This study presents results from centrifuge experiments and simplified modeling to explore scaling effects on biogenic gas formation, distribution, and retention when simulating field pressures and stresses. Experimental results from the centrifuge demonstrated MIDP's potential to mitigate the potential liquefaction triggering through desaturation. This study also includes the development of a biogeochemical model to explore the impact of water constituents, process inhibition, and alternative biochemical metabolisms on MIDP and the subsequent impact of MIDP on the surrounding environment. The model was used to explore MIDP behavior when varying the source-water used as the substrate recipe solute (i.e., groundwater and seawater) and when varying the electron donor (i.e., acetate, glucose, and molasses) in different substrate recipes. The

i

predicted products and by-products were compared for cases when desaturation was the targeted improvement mechanism and for the case when precipitation was the primary targeted ground improvement mechanism. From these modeling exercises, MIDP can be applied in all tested natural environments and adjusting the substrate recipe may be able to mitigate unwanted long-term environmental impacts. A preliminary techno-economic analysis using information gained from the modeling exercises was performed, which demonstrated MIDP's potential as a cost-effective technique compared to currently used ground improvement techniques, which can be costly, impractical, and unsustainable. The findings from this study are critical to develop treatment MIDP plans for potential field trials to maximize treatment effectiveness, promote sustainability and cost-effectiveness, and limit unwanted by-products.

ACKNOWLEDGEMENTS

I have too many people to thank for supporting me. I joke that it took a community to "raise me" through my Ph.D., but it's true. I am so grateful to everyone who celebrated all of my successes and listened while I anguished over whatever seemed like a catastrophe.

Thank you to my committee for helping me become a more critical thinker and explore science outside of the lab. Bruce Rittmann: When we met you said (paraphrased), "I want someone with the right attitude – the one who is willing to learn and try, not the one who thinks they already have the most experience." This set the tone for my Ph.D. and I appreciate your support, red pen editing, and asking hard questions. Edward Kavazanjian: Your practical and pragmatic advice always came at the best times, even if I didn't want to hear it. Thank you for all of your advice and support during research, existential, and travel crises, especially when my tendency to start new projects tried your patience. Leon van Paassen: Thank you for always including me in so many projects - working with you led to my growth as a scientist and person. Jason DeJong: Thank you for your confidence in me and having my best interests in mind, even if I didn't realize it then.

To my mom, Traci Hall, Rob Braymiller, and grandparents, Annemarie and Roger Alderman and Dennis Moyers: Thank you for providing me so much and always reminding me about the value of education. Thank you especially for being there for me through every flat tire and "I don't know what I'm doing" moment. Charity Hill: I know that I'll never have to build a birdhouse alone. Thank you for validating when a Tuesday felt like a *Tuesday*. Erik Aidukas: Thank you for always hearing me out, and

Knowing when a tattoo was (or wasn't) *just* a tattoo. Ethan Howley: Thank you for always supporting all of my ideas from adopting stray cats to starting a science policy group. I would not be the person I am without you. John Malloy: Thank you for picking up my pieces after a long run and in every other way - no one believes in me more. I can't wait to keeping crushing and sending it. Blake Dirks: No one makes me laugh harder (anthropomorphic dinosaurs or not) and I am grateful to have met you. Rolf Hut, Tim van Emmerik, and Anna Solcerova: We'll always have Dino's and side projects. Taylor Davis: For helping me talk through everything, swapping stories at the crag, and still going with me to Harry Potter Land after game night. Kate Williams: Your no-nonsense "Dude, obviously, you're gonna be great" has given me the confidence to always go for it.

Thank you to my friends and colleagues that helped me grow professionally and personally. To those at Swette Center and CBBG: lab mom Carole, Elizabeth Stallings, Andrew Marcus, Juan Maldonado, Jean Larson, Chris Hunt, Rod Borela, Nariman Mahabadi, Rick Kupferer, Michelle Young, Sarah Arrowsmith, Katerina Ziotopoulou, Peter Fox. To those that I met at AGU and EGU, for the community and encouraging me to MC every event: Sam Illingworth, Sheila Saia, Nilay Dogulu, Leila Saberi, Andrea Popp, Yuhan Rao, Niels Drost, Stan Schymanski, Scott Tyler, Charlie Luce, Leslie Marasco. To those I met in Davis, late nights dancing and trudging through experiments: Kevin Marti, Matthew Burrall, Kate Darby, Nick Paull, Gabby Hernandez. To those, I met finding my passion in civil rights and science policy: Matt Chrisler, Griffin McCutcheon, Oscar Lopez, Natasha Udu-gama, Melissa Goodwin, Cassandra Barrett, Nich Weller, Michelle Sullivan Govani, Liza Kurtz, Danielle McMahon. To those I met that helped me

TABLE OF CONTENTS

LIST OF TABLES

xiii

CHAPTER 1

INTRODUCTION AND SIGNIFICANCE

Every civil engineering structure relies on the strength and resilience of the ground beneath it and around it, such that it can retain its integrity and prevent loss of life. As urbanization increases, large centralized populations and infrastructure are made increasingly vulnerable to threats by natural disasters and geologic hazards, like earthquake-induced liquefaction. Current ground-improvement solutions to reduce risk are costly or impractical when applied at large-scale underneath or near existing structures. Often, these methods require significant resources that may lead to greenhouse gas emissions (e.g., Portland cement).

Bio-based ground-improvement techniques have emerged as a potential solution (DeJong et al., 2010; Karatas et al., 2008; Kavazanjian et al., 2015; Phillips et al., 2013; van Paassen, Daza, et al., 2010; van Paassen, Ghose, et al., 2010; Whiffin et al., 2007). These technologies encourage building with nature using cost-effective, sustainable methods to strengthen earthen structures and reduce the risk of failure (Burbank et al., 2011; DeJong et al., 2010; Montoya & DeJong, 2015; Montoya et al., 2013; Phillips et al., 2013; Whiffin et al., 2007). Bio-based ground stabilization techniques are potentially non-disruptive to deploy and monitor, allowing application underneath existing structures (Khodadadi et al., 2017; Mitchell & Santamarina, 2005).

One proposed bio-based ground-improvement process is Microbially Induced Desaturation and Precipitation (MIDP) via denitrification. MIDP is a two-stage ground-improvement process, in which biogenic gas desaturation and calcium carbonate ($CaCO_3$) precipitation can provide short-and long-term liquefaction resistance, respectively

(O'Donnell, 2016; van Paassen, Daza, et al., 2010; van Paassen, Ghose, et al., 2010). MIDP influences the geochemical environment and the hydro-mechanical behavior of soils through biogenic gas production, precipitation of calcium carbonate, and biomass growth. Whereas biogenic gas can reduce pore pressure build-up during cyclic loading, calcium carbonate has the potential to improve soil strength and dilatancy. Biomass growth can also reduce the available pore space for gas production and mineral precipitation, as well as reduce permeability.

All three components influence the biogeochemical environment and subsurface permeability, thereby affecting the transport of substrates and subsequent product formation. The products of MIDP have shown potential to address mitigate liquefaction at the lab-scale, but field-scale application and modeling have been limited to date. Natural biogeochemical processes, including biochemical process competition, microbial inhibition, and inadequate physical soil conditions for injection treatment methods may affect MIDP treatment performance. The influencing mechanisms of these complexities need to be verified such that future field-scale MIDP treatment predictions are comprehensive. This study will focus on the development of a biogeochemical model to predict field-scale MIDP treatment considering natural soil characteristics and groundwater conditions.

Research Objectives and Scope

The primary objective of my work was to develop and test a biogeochemical model to consider biochemical effects on MIDP in soil susceptible to liquefaction. Though MIDP

has been shown to be effective in mitigating liquefaction in laboratory conditions (O'Donnell, 2016; Pham, 2017), little has been done to investigate up-scaling of this technology for real-world applications. Environmental conditions found in the source-water used to dilute the treatment substrate (often pumped from the subsurface and reintroduced during treatment) will introduce engineering challenges that affect process deployment and outcomes. Substrate composition and the interactions among biogeochemical properties have been investigated to develop a sound basis for improving MIDP application in the field. My overarching goals were to explore how MIDP may behave under field conditions through geotechnical and biogeochemical modeling to lead to a deeper understanding and accelerated application of MIDP.

The specific goals of my dissertation are:

1. Investigate MIDP biogenic gas production, distribution, and retention under centrifuge conditions. This will include the development of theoretical predictions of gas behavior and experimental result comparison.

2. Study and compare potential electron donors (e.g., acetate, glucose, molasses) for MIDP treatment.

3. Study and compare the effects of potential groundwater biochemical processes and characteristics (e.g., precipitation of other carbonates, potential inhibition by salinity) that may influence MIDP performance and feasibility in the field.

4. Conduct a preliminary techno-economic analysis comparing MIDP to permeation grouting, a currently used method for liquefaction mitigation.

The dissertation is organized into the following 8 chapters. Chapter 2 provides a critical review of the literature forming the basis for MIDP and the questions addressed in my research. Chapter 3 outlines a simplified biogeochemical model to predict biogenic gas behavior in the centrifuge. Chapter 4 details geotechnical centrifuge modeling experimentation and evaluation of MIDP's potential to mitigate liquefaction. Chapter 5 details the next generation biogeochemical model to predict MIDP product and by-product formation under natural conditions. Chapter 6 explores the impact of different source water conditions (i.e., groundwater and seawater) on MIDP using the model described in Chapter 5. Chapter 7 investigates the impact of different MIDP recipes by exploring three different potential electron donors (i.g., acetate, glucose, molasses) using the model detailed in Chapter 5. Chapter 8 uses information gained during modeling to establish a preliminary techno-economic analysis to compare MIDP to permeation grouting, a currently employed liquefaction mitigation technique. Chapter 9 details the major conclusions and take-home lessons from this work, followed by a separate chapter containing the references cited throughout this dissertation.

CHAPTER 2

APPLICATION OF MIDP FOR EARTHQUAKE-INDUCED LIQUEFACTION MITIGATION

In-situ, bio-based ground-improvement methods are gaining popularity due to their potential to be sustainable and cost-effective techniques to remediate soil under or around existing structures without disrupting existing structures and the community. Several different bio-based ground-improvement applications have been identified, including soil stabilization, groundwater remediation, and subsurface barriers (Phillips et al., 2013). A significant amount of research has focused on calcite precipitation via microbial or enzymatic urea hydrolysis through microbially induced calcium carbonate precipitation (MICP) or enzyme-induced calcium carbonate precipitation (EICP), respectively (Khodadadi et al., 2017; Umar et al., 2016). Both processes have an ammonium by-product, which can be harmful to the environment, as it is a source of nitrogenous biological oxygen demand and is potentially toxic to humans.

Microbially induced desaturation and precipitation via denitrification (MIDP) has been proposed as an alternative technology bio-based liquefaction mitigation solution. MIDP is a two-stage technique in which produced biogenic gas desaturates the soil rapidly, while calcium carbonate precipitation can mechanically strengthen the ground over the longer term (Lin et al., 2016; Martin et al., 2013; O'Donnell, 2016). Notably, MIDP is an anaerobic process and does not require introducing oxygen into the subsurface, though MIDP requires the introduction of aqueous substrates. For MIDP to be acceptable in the field, the substrate introduced into the soil must be completely converted to reduce potential harmful impacts

on the surrounding environment. For example, nitrate must be completely reduced to nitrogen gas, and an organic electron donor must be completely oxidized to bicarbonate.

Microbially Induced Calcium Carbonate Precipitation (MICP)

One of the primary bio-based ground-improvement processes that has been reported in the literature is Microbially Induced Carbonate Precipitation (MICP) via urea hydrolysis (DeJong et al., 2010). Urea hydrolysis is done by urease enzymes produced by certain microorganisms (e.g., *Sporosarcina pasteurii*), which then results in a release of ammonium (NH_4^+) and an increase of pH (DeJong et al., 2010). Increased pH leads to the production of CO_3^{2-}, facilitating the precipitation of $CaCO_3$ when dissolved calcium is available (Al Qabany et al., 2012). This relatively simple process can occur rather quickly (over hours to days) and has been shown to improve the mechanical soil properties from lab- to field-scale (Burbank et al., 2011; Cheng & Cord-Ruwisch, 2012; Gomez et al., 2018; Montoya et al., 2013; Pham, Nakano, et al., 2018; Pham, van Paassen, et al., 2018; van Paassen, Ghose, et al., 2010).

Despite initial successes, MICP faces many challenges. If the at-risk site does not have ureolytic bacteria that can be effectively biostimulated present, bioaugmentation is required (DeJong et al., 2010). Alternatively, Enzyme-induced Carbonate Precipitation (EICP), where bacteria are not needed due to the direct introduction of the enzyme, can be used to facilitate urea hydrolysis (Khodadadi et al., 2017). However, the cost for the required enzymes may render this impractical at large scale. Second, ammonium from the breakdown of urea and its complexes can be toxic, adds nitrogenous BOD, and can have a sharp odor, each of which may limit its applicability (van der Star et al., 2011).

Additionally, researchers have reported that additional environmental clean-up over four days was required to meet regulatory groundwater requirements (van der Star et al., 2011). MICP applied in the subsurface may be affected by limited oxygen availability at depth, and low dissolved oxygen may stifle urea hydrolysis by slowing or stopping microbial growth, even when sufficient decomposable organic material is available (Khodadadi et al., 2017; McCarty & Bremner, 1991; Mortensen et al., 2011; Yeomans et al., 1992). Finally, scaling EICP to field applications may be costly (ranging from \$100 to \$400 per m^3 of treated soil volume), which may limit its competitiveness with other technologies (Pham, Nakano, et al., 2018).

Microbially Induced Desaturation and Precipitation via Denitrification (MIDP) for Liquefaction Mitigation

One proposed bio-based ground-improvement process is Microbially Induced Desaturation and Precipitation (MIDP) via denitrification. MIDP is a two-stage ground-improvement process, in which biogenic gas desaturation and calcium carbonate ($CaCO_3$) precipitation can provide short-and long-term liquefaction resistance, respectively (O'Donnell, Kavazanjian, et al., 2017; O'Donnell, Rittmann, et al., 2017; O'Donnelli et al., 2019; Pham, van Paassen, et al., 2018; van Paassen, Daza, et al., 2010). MIDP influences the geochemical environment and the hydro-mechanical behavior of soils through biogenic gas production, precipitation of calcium carbonate, and biomass growth. Whereas biogenic gas can reduce pore pressure build-up during cyclic loading, calcium carbonate has the potential to improve soil strength and dilatancy. Biomass growth can also reduce the

available pore space for gas production and mineral precipitation, as well as reduce permeability.

All three components influence the biogeochemical environment and subsurface soil characteristics, thereby affecting the transport of substrates and subsequent product formation. The products of MIDP have shown potential to address mitigate liquefaction at the lab-scale, but field-scale application was untried up to now.

MIDP Stage 1: Biogenic Gas Desaturation

Desaturation by biogenic gas formation has shown promise to mitigate static liquefaction and earthquake-induced liquefaction, including nitrogen gas (N_2) from denitrification (He & Chu, 2014; He et al., 2013; O'Donnell, Rittmann, et al., 2017; Rebata-Landa & Santamarina, 2012). Even a small amount of gas has the capability to reduce pore pressure build-up during monotonic and cyclic shear strain loading in soils to reduce liquefaction triggering (He & Chu, 2014; He et al., 2013; Yegian et al., 2007). Since N_2 gas has low water solubility and is neither toxic nor a greenhouse gas, biogenic production of N_2 may be an attractive candidate for reducing the liquefaction triggering potential.

Denitrification, or dissimilatory reduction of nitrate (NO_3^-), is a natural biologically driven process during which nitrate is reduced to N_2 gas and dissolved organic carbon is oxidized. Since denitrifying bacteria are ubiquitous, stimulating indigenous bacteria for MIDP is very likely to be feasible at a project site, and there not require bioaugmentation. Additionally, as denitrification is an anaerobic process, deep soil profiles can be treated (Yeomans et al., 1992).

8

To evaluate the potential use of desaturation via biogenic gas and estimate subsequent hydro-mechanical effects in geotechnical applications, it is essential to be able to predict the amount, composition, and distribution of produced gas (Kavazanjian et al., 2015; O'Donnell, Rittmann, et al., 2017; Pham, Nakano, et al., 2018; Pham, van Paassen, et al., 2018). Various organic substrates can be used to induce denitrification, but many studies have used a solution containing calcium acetate and calcium nitrate (Kavazanjian et al., 2015; O'Donnell, Rittmann, et al., 2017; Pham, Nakano, et al., 2018; Pham, van Paassen, et al., 2018). To promote the efficient and full reduction of nitrate to N_2 gas, without leaving an excess of organic substrate, selecting the right substrate composition is essential. Variations of the substrate composition on the thermodynamics and stoichiometry of this process should be considered when making MIDP outcome and process predictions. Illustrated in Eq. 1 and Eq. 2 are the expected catabolic N_2 gas productions for equal molar amounts of introduced acetate and formate, respectively.

$$8NO_3^- + 5C_2H_3O_2^- + 8H^+ \rightarrow 9H_2O + 4N_2 + 5CO_2 + 5HCO_3^- \qquad \text{Eq. 1}$$

$$2NO_3^- + 5HCO_2^- + 2H^+ \rightarrow H_2O + N_2 + 5HCO_3^- \qquad \text{Eq. 2}$$
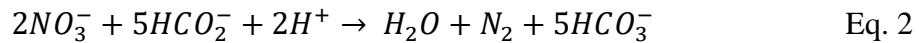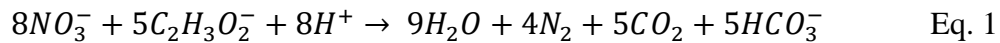
The amount of donor substrate available at a location will also influence the denitrification process. So, accounting for subsurface heterogeneity in the flow and delivery of substrate should be considered. Further, since even a small amount of subsurface gas production (i.e., gas-phase N_2 and CO_2) can reduce the hydraulic conductivity of soils, the resulting distribution of substrate and products may change during MIDP (Baird & Waldron, 2003; Mahabadi et al., 2016; Mahabadi & Jang, 2014).

Potential by-products and intermediates may form and accumulate, and they should be considered for process optimization and to evaluate the potential for adverse environmental products to be produced. The reduction of NO_3^- to N_2 gas proceeds through several nitrogen-containing intermediates: nitrite (NO_2^-), nitrous oxide (N_2O), and nitric oxide (NO). When employing denitrification for engineering purposes via MIDP, accumulation of these intermediates should be avoided because they have the potential to inhibit microbial growth, are potentially toxic to humans, and may contribute to greenhouse gas emissions (Rittmann et al., 2001; Zumft, 1997). As long as the NO_3^- is completely reduced to N_2, N-containing intermediates are avoided and environmental clean-up should not be required (van Paassen, Daza, et al., 2010). Complete denitrification can be assessed by measuring NO_2^-, HNO_2, NO, and N_2O in water and gas sampling. In typical soil environments, nitrate reduction is expected to be the primary consumer of substrate due to its favorable redox potential, though this is not always true (Achtnich et al., 1995; Grigoryan et al., 2008). For MIDP to be more widely considered, additional insight is required to reduce the production of potentially harmful species, such as intermediates from incomplete denitrification or the production of H_2S from SO_4^{2-} reduction. This can be done by adding in additional electron donor substrate, but a residual of organic substrate should be avoided to reduce its environmental impact and economic costs.

Denitrification involves the oxidation of organic matter, which generates dissolved inorganic carbon (DIC). DIC can exist as dissolved carbon dioxide ($CO_{2(aq)}$), carbonic acid (H_2CO_3), bicarbonate (HCO_3^-), and carbonate (CO_3^{2-}). Depending on the environmental

pH and pore pressure, produced $CO_{2(aq)}$ may partition to the gas phase. As a result, gas composition and products available for $CaCO_3$ precipitation may change.

MIDP Stage 1: Calcium Carbonate Precipitation

DIC produced during denitrification, which usually exists as HCO_3^- in neutral-pH environments, can precipitate with dissolved calcium to form $CaCO_3$ minerals. $CaCO_3$ precipitation not only provides mechanical strength benefits but also provides a self-buffering pH system through alkalinity consumption (O'Donnell, Kavazanjian, et al., 2017). pH stability is crucial to ensure ideal microbial growth conditions and reduce the potential for incomplete denitrification, which may lead to a reduction in products and an increase of intermediate accumulation (O'Donnelli et al., 2019; Pham, Nakano, et al., 2018). While $CaCO_3$ formation by MIDP via denitrification is a time-intensive process that can take from weeks to months and requires a higher amount of substrate than is required for soil desaturation, long-term soil improvement is provided (O'Donnell, Kavazanjian, et al., 2017; Pham, Nakano, et al., 2018; van Paassen, Daza, et al., 2010). Precipitation rates during MIDP are markedly slower than MICP, in which the necessary time for enough precipitation to achieve liquefaction mitigation is on the order of days (DeJong et al., 2010). Hence, MIDP can be considered a two-stage ground-improvement method: in the short-term, mitigating liquefaction by gas formation and, in the long-term, calcium carbonate precipitation to strengthen the soil matrix (Kavazanjian et al., 2015; Khodadadi et al., 2017; O'Donnell, Kavazanjian, et al., 2017; O'Donnell, Rittmann, et al., 2017; van Paassen, Daza, et al., 2010).

Like biogenic gas production, $CaCO_3$ formation is influenced by substrate availability. Depending on the organic electron-donor substrate introduced, the available DIC for $CaCO_3$ precipitation is stoichiometrically altered. As demonstrated in Eq. 1 and Eq. 2, the amount of required amount of organic substrate to achieve equal amounts of available DIC and base for $CaCO_3$ precipitation varies widely between organic electron donors. Optimizing the process for $CaCO_3$ production or N_2 production will be required to reduce any build-up of residuals or intermediates during MIDP, along with minimizing competing biochemical processes in the subsurface, and will vary by environment or experimental condition.

Denitrification rates will depend on the choice of organic substrate, indigenous species, and environmental conditions (e.g., temperature, salinity). Because diverse microbial species are abundant in the subsurface, competition for the electron donor is possible (Mortensen et al., 2011; Rittmann et al., 2001). Electron donor competition during the different stages of denitrification has also been reported (Pan et al., 2019). It is expected that the main competition from non-denitrifying bacteria is sulfate reduction and iron reduction. This may result in reduced carbonate species availability for $CaCO_3$ precipitation. Furthermore, the production of other carbonate solids, like iron(II) carbonate, reduces the available inorganic carbon for precipitation with calcium. Methanogenesis may not be of concern for MIDP product formation because methanogenesis was significantly inhibited in the presence of nitrate when competing for electron donor and its comparatively slow growth rate (Rittmann et al., 2001; Scholten et al., 2002).

The environment is also a significant factor for complete denitrification. Many studies have noted that denitrification rates are significantly reduced in temperatures below 5°C (Sirivedhin & Gray, 2006) and pH below 7 (Glass & Silverstein, 1998; Glass et al., 1997). Researchers have reported a significant reduction in denitrification rates from tidal freshwater to more saline water (Bongoua-Devisme et al., 2012; Craft et al., 2009; Glass et al., 1997; Martin et al., 2013; Marton et al., 2012; Singurindy et al., 2004; Weston et al., 2011). However, others have reported salinity effects to be less severe when a population had acclimated to higher salt concentrations when investigating denitrification in wastewater treatment systems (Zhu, 2017). As a result, the environment is expected to influence the rate and effectiveness of MIDP, which should be considered when designing field-scale trials to maximize treatment expectations.

The dominant biogeochemical pathways that lead to or compete with $CaCO_3$ precipitation may change depending on environmental conditions and dominant biochemical processes, due to changes in thermodynamic favourability (S. et al., 2000; Zarga et al., 2013). Abiotic carbonate precipitation can occur, though it is limited by naturally available carbonate species, including amounts released during the breakdown of existing minerals from pH increase, and the ionic strength of solutions (Zhu, 2017). Biotic carbonate precipitation by heterotrophic microorganisms is also possible either actively, when carbonate is released by ionic exchanges through the cell membrane, or passively, when microorganisms produce carbonate species that promote an alkaline environment (Zhu, 2017). Many microorganisms are able to do both processes, though the focus herein is on passive precipitation mechanisms. Passive precipitation can occur in the nitrogen

cycle as carbonate species are produced during denitrification, ammonification, and ureolysis, promoting carbonate species availability for precipitation by available cation and metal species (Achal et al., 2012; Al Qabany et al., 2012; Anbu et al., 2016; Zarga et al., 2013). Alternate biogeochemical pathways (e.g., sulfate reduction) may also result in by-product $CaCO_3$ precipitation, as pH increases when H_2S is formed and discharged (Castanier et al., 2000). Co-precipitation of different minerals is also possible and may influence $CaCO_3$ precipitation. In wastewater treatment, where calcium, sulfate, and carbonate species were present, $CaSO_4 \cdot 2H_2O$ (gypsum) was the dominant precipitate, while calcite and other species were less dominant (Zarga et al., 2013). They also found that the formation of other minerals promoted calcite precipitation over other $CaCO_3$ forms (Zarga et al., 2013). The presence of $CaSO_4$ has also indicated a reduced amount of $CaCO_3$ precipitation in batch experiments and that first-order precipitation kinetics for pure salt could not be applied to the solution, indicating a complicated interaction (Chong & Sheikholeslami, 2001).

Lab-Scale Experimentation of MIDP

MIDP has been shown at the lab-scale to be effective for liquefaction mitigation (He & Chu, 2014; He et al., 2013; O'Donnell, Rittmann, et al., 2017; Pham, Nakano, et al., 2018). Treatment is done in two stages: desaturation by biogenic gas in the short-term and calcium carbonate formation in the long-term. 1-D column tests have shown that MIDP can provide enough gas to reduce the potential for liquefaction triggering in a relatively short amount of time, on the order of days (Pham, Nakano, et al., 2018). Liquefaction triggering was sufficiently reduced when the degree of saturation was as high as 95% (O'Donnell, Rittmann, et al., 2017; Pham, Nakano, et al., 2018). When immediate liquefaction mitigation is required, biogenic gas production is particularly attractive, because calcium carbonate precipitation via MIDP requires more time to achieve target levels for liquefaction triggering reduction (O'Donnell, Rittmann, et al., 2017; Pham, Nakano, et al., 2018). However, gas production, retention, and transport to improve cyclic resistance are strongly influenced by microbial production rates, pore pressure, and soil conditions (Okamura & Soga, 2006; Pham, Nakano, et al., 2018; Rebata-Landa & Santamarina, 2012). Scaling up from lab- to field-scale should consider these aspects while determining expected liquefaction mitigation by biogenic gas via MIDP.

Calcium carbonate precipitation is the second stage of the two-stage MIDP treatment process due to its longer time requirement to provide soil improvement, on the order of weeks (Khodadadi et al., 2017; O'Donnell, Kavazanjian, et al., 2017). Calcium carbonate precipitation via MIDP is also more time-intensive than by MICP via ureolysis in column-scale tests. However, minimal calcium carbonate precipitation (0.1%) by MIDP

can result in significant soil improvements (O'Donnell, Kavazanjian, et al., 2017). They expect that these soil improvements are influenced by the slower precipitation rate of MIDP, resulting in a large, discrete calcium carbonate morphology. This slower precipitation rate could be subsequently due to the slower rate of denitrification or the reduced availability of reactants to form $CaCO_3$. However, consideration must be given for the more time-intensive process of calcium carbonate formation, as well as environmental characteristics or biogeochemical processes that may impede formation (i.e., low pH).

Modeling of MIDP

The current generation of MIDP models consider batch reactor conditions have not yet explored the impact of natural environmental conditions when used as the source-water to dilute the substrate recipe, the use different electron donors, chemical speciation, competing microbial processes, and phase kinetics together (O'Donnell et al., 2019; Pham, 2017). By using an established modelling toolbox (van Turnhout et al., 2016), all of these processes can be implemented to better understand how MIDP may behave in the field. This model included multiple potential by-product complexes that could be found during the treatment process using ORCHESTRA and the *minteq.v4.dat* thermodynamic database (Meeussen, 2003; van Turnhout et al., 2016; Vink & Meeussen, 2007). Kinetic reactions can also be implemented into this toolbox as individual reactions and protonation/deprotonation speciation mechanisms. Others have modelled MIDP using a mechanistic batch-condition model with more biochemical metabolic processes considered (i.e., denitrification, sulfate reduction, and biomass decay), though with fewer potential by-

16

products estimated (O'Donnell et al., 2019). The reaction parameters were initially derived from the literature and then modified, within reported values in the literature, to provide visual best fit (O'Donnell et al., 2019). These established models, in their current state, may be too simplistic. Prior to establishing field-scale models for MIDP, 1-D modeling may be done to identify the expected distribution of MIDP products. The behavior of biogenic gas will be particularly impacted by increasing pressures at field-scale depth and transport of aqueous products and reactants.

Microbial conversion of NO_3^- to N_2 gas is the primary mechanism of biogenic gas production via MIDP, although CO_2 generation also can be a factor for permeability reduction. While production of biogenic gas is desirable for liquefaction mitigation, biogas accumulation may limit substrate distribution in the subsurface. Up to now, MIDP gas production has been modeled such that production depends on active biomass and substrate availabilities (O'Donnell et al., 2019; Pham, 2017). The phase-transfer process controlling the rate and amount of out-gassing has been modeled to depend on pore pressure (C. Hall et al., 2018; C. A. Hall et al., 2018; Pham, 2017; van Turnhout et al., 2016). However, these efforts have not considered gas transport. Many models assume that there is no gas transport, but these are likely oversimplifications when considering the mechanical response of an earthquake. Gas escape has also been observed when the degree of saturation reaches a certain threshold (C. A. Hall et al., 2018; Pham, 2017). This threshold ultimately depends on soil characteristics but is around 80% for fine grained clean sands (Pham, 2017).

Additional by-products may also form, including the precipitation of other species. During MICP via ureolysis, researchers have been able to co-precipitate multiple types of heavy metals and compounds (Achal et al., 2012; Anbu et al., 2016). This potential for co-precipitation should be considered during the design of MIDP treatment to ensure that natural species do not reduce calcium carbonate precipitation needed for ground stabilization.

MIDP also has the potential to co-precipitate metals and other compounds, but these may also inhibit denitrification (Ramirez et al., 2018). Low pH metallurgic wastewater, containing high amounts of nitrate and heavy metals (e.g., iron, nickel, chromium), led to inhibition and the accumulation of intermediates (Ramirez et al., 2018). These factors need to be addressed to ensure that MIDP treatment is applied in the intended locations and that the input substrate does not facilitate unwanted biochemical reactions or intermediate reaction. Within this work, I focus on mineral and metal concentrations expected in drinking water, groundwater, and sea water, rather than extreme environments. Accurate prediction of MIDP behavior in the field is critical for treatment design.

CHAPTER 3

PREDICTING DESATURATION BY BIOGENIC GAS FORMATION DURING CENTRIFUGAL LOADING USING A SIMPLIFIED MODEL

Published in part as Hall, C.A., van Paassen, L.A., Rittmann, B.E., Kavazanjian, E., DeJong, J.T., and Wilson, D.W. (2018). Predicting Desaturation by Biogenic Gas Formation via Denitrification During Centrifugal Loading. 7th International Conference on Unsaturated Soil Mechanics. Hong Kong: ISSMGE. 1-6.

Saturated, cohesionless soils are at risk of liquefying due to earthquake events, and that may lead to significant infrastructure damage. The primary mechanism leading to earthquake-induced liquefaction is the build-up of excess pore water pressure resulting from seismic loading, which reduces the effective stress and causes a loss of soil strength (Vaid & Sivathayalan, 2000). Biologically driven ground improvement through microbially induced carbonate precipitation by urea hydrolyzing bacteria has been proposed and shown to successfully improve the soil's mechanical properties at lab- and field-scale (DeJong et al., 2010; van Paassen, Daza, et al., 2010). However, the process is still costly, and by-products from this process are potentially harmful.

An alternative bio-based solution to reduce liquefaction is microbially induced desaturation and precipitation (MIDP) by dissimilatory nitrate reduction, or denitrification. MIDP results in generation of biogenic di-nitrogen gas (N_2) and calcium carbonate ($CaCO_3$) precipitation. N_2 gas has the potential to reduce liquefaction by decreasing the ratio of water volume to voids volume, or the degree of saturation, of the soil; $CaCO_3$ precipitation can increase the soil's mechanical strengthen (DeJong et al., 2010; O'Donnell,

19

Kavazanjian, et al., 2017; O'Donnell, Rittmann, et al., 2017; Pham, Nakano, et al., 2018; Pham, van Paassen, et al., 2018). The biocementation component of denitrification can take time, but biogenic gas production can act quickly to dampen pore pressure rise during seismic loading by increasing the compressibility of the pore space, thereby reducing the potential for liquefaction triggering (He & Chu, 2014; He et al., 2013; O'Donnell, Kavazanjian, et al., 2017; O'Donnell, Rittmann, et al., 2017; Pham, Nakano, et al., 2018; Rebata-Landa & Santamarina, 2012).

The primary biogenic gas generated by denitrification is N_2, as it is the most abundantly produced biogenic gas compared to other gas by-products (e.g., CO_2) and has low water solubility. Laboratory experiments have shown that even minimal desaturation by N_2 can significantly increase the undrained shear strength and liquefaction resistance of the soil (He & Chu, 2014; He et al., 2013; Rebata-Landa & Santamarina, 2012). However, due to the low pressure of most lab-scale specimens, the gas pressure produced by the microbial metabolism may exceed the overburden pressure. This can result in formation of gas pockets or gas lenses, and result in soil heave, as shown in Figure 1.

The goal was to gain knowledge regarding the production, migration, and retention of biogenic gas and treatment effectiveness relevant at depths more realistic for field applications. We used a simplified numerical model to evaluate the scaling effects on pressures and stresses between the centrifuge model (hereafter, referred to as model) and simulated field-scale pressures under centrifugal loading (hereafter, referred to as prototype), as well as to interpret the centrifuge model results. Detailed herein are the

simplified numerical model developed to predict biogenic gas behavior and characteristics in the model and prototype environment.
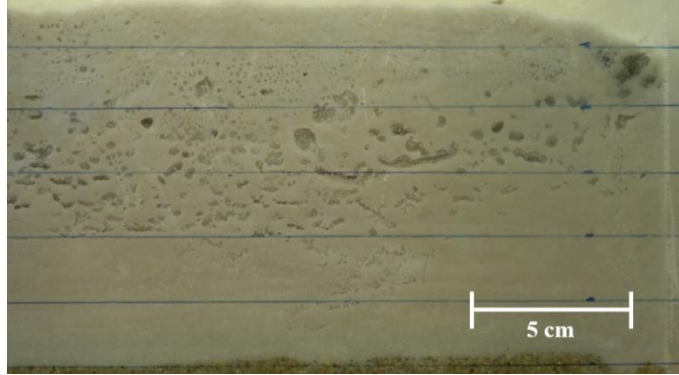
Figure 1. Biogenic Gas Pockets in a 1-g Experiment, 10 Days after MIDP via Denitrification Treatment.

Theoretical Predictions of the Volume of Biogenic Gas During Centrifugal Loading

In the simplified numerical model, N_2 was the only gas considered. While CO_2 also is a product of denitrification and biomass decay, we assumed that desaturation resulting from CO_2 is negligible due to the high solubility of CO_2 at prototype depth and with the water's prevailing alkalinity. We also assumed that the soil profile is a closed system and NO_3^- (provided as one substrate) undergoes complete reduction to N_2. The effects of vapor barriers at the inter-particle soil contacts are neglected.

Based on established methods (Pham, 2017), Eq. 3 estimates the required concentration of consumed NO_3^- ($[NO_3^-]_{con}$, mol m^{-3}) by microbes to achieve desired gas volume (V_g) in the total pore volume (V_P), which is defined by the fractional degree of gas saturation (S_g, dimensionless) at 1 g.

$$[NO_3^-]_{con} = \frac{Y_{NO_3^-} P_{N2,m}}{Y_{N_2}} \left(\frac{S_g}{RT} + K_{H,N2} \right) \qquad \text{Eq. 3}$$

21

where Y_{N2} and Y_{NO3-} are the stoichiometric coefficients of N_2 and NO_3^- during denitrification, respectively; $P_{N2,m}$ (atm) is the partial pressure of the model and is assumed to be equal to the hydraulic pressure in the saturated soil environment; T (K) is the system temperature; R (atm L K^{-1} mol^{-1}) is the universal gas constant; and $K_{H,N2}$ is Henry's constant for N_2 at standard temperature (mol L^{-1} atm^{-1}). The initial soil condition is fully water saturated at $P_{N2,m}$, which is equal to the hydrostatic pressure that is a function of specific weight of water (γ_w, kN m^{-3}) and the depth below the phreatic surface of the model.

The desaturation capacity is limited by what can be achieved at 1 atm and does not vary significantly across the shallow depth of the test set-up. The gas percolation threshold at ambient temperature and pressure occurring at approximately 80% saturation has been experimentally determined (Pham, 2017). Gas venting was observed when this threshold was exceeded, and the degree of saturation did not continue to decrease with additional production of N_2 from denitrification. From these observations, our theoretical target for the initial degree of saturation was 80% at 1 g conditions (without centrifugal force from spinning). To determine Y_{NO3} and Y_{N2}, we considered catabolism and anabolism for estimating the maximum synthesis yield:

$$1.21 C_2H_4O_2 + 0.97 NO_3^- + 0.97 H^+$$

$$\rightarrow CH_{1.8}O_{0.8}N_{0.2} + 1.41 H_2CO_3 + 0.39 N_2 + 0.59 H_2O$$
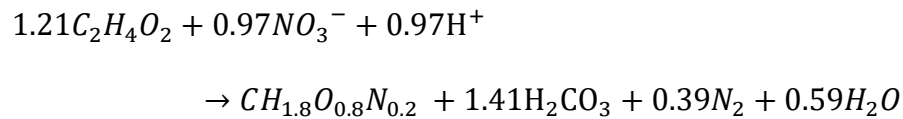
Modeling Gas Production and Distribution in the Centrifuge

Eq. 4 was used to estimate the production rate of N_2 gas in the pore space (r_{N2}, mol h^{-1}) via single-step denitrification according to Monod kinetics,

22

$$r_{N2} = 0.5 q_S C_X \left(\frac{C_{NO3}}{K_{NO3} + C_{NO3}} \right) \left(\frac{V_P}{V_T} \right)$$ Eq. 4

where 0.5 is the stoichiometric ratio of N for NO_3^- and N_2 gas, q_S (mol g^{-1} of biomass h^{-1}) is the maximum substrate utilization rate, C_X (mol biomass m^{-3}) is the amount of active biomass, C_{NO3} (mol m^{-3}) is the concentration of NO_3^-, K_{NO3} (mol m^{-3}) is the half-maximum-rate concentration for the substrate, V_P (m^3) is the pore volume, and V_T (m^3) is the total volume of soil and pore space. q_S is defined by Eq. 5 as

$$q_S = \mu_{max}/Y_{SX}$$ Eq. 5

where μ_{max} (h^{-1}) is the maximum theoretical microbial growth rate and Y_{SX} (mol biomass mol NO_3^--N^{-1}) is the stoichiometric ratio of nitrate in the substrate to biomass production at the maximum growth rate. V_P was estimated using Eq. 6, based on relative density and the volume of solids in the total space.

$$V_P = \left(\frac{V_T \left(e_{max} - D_R (e_{max} - e_{min}) \right)}{1 + e_{max} - D_R (e_{max} - e_{min})} \right)$$ Eq. 6

where e_{max} (dimensionless) is the soil void ratio in its loosest state, D_R (g m^{-3}) is the relative soil density, and e_{min} (dimensionless) is the soil void ratio in its densest state.

The rate at which N_2 gas is produced is proportional to the rate of microbial metabolism and the concentration of active biomass (C_x). During experiments, a rate of N_2 production at bench-scale conditions at 1 g of 0.085 mol N_2 h^{-1} with the initial NO_3^- concentrations of 22 mol m^{-3} and an assumed K_{NO3} to be 0.1 mol NO_3^- m^{-3} has been experimentally observed (Pham, Nakano, et al., 2018). However, this is one magnitude higher than other reported values (Abdul-Talib et al., 2002; Henze et al., 1999). It should

23

be noted that the reaction rate declines as substrate is consumed but increases as more biomass accumulates. For this simplified model, biomass accumulation was assumed to be constant.

The pressure increase upon loading directly influences gas solubility, and the resulting estimated amount of $N_{2,(g)}$ in the gas phase is given by Eq. 7.

$$N_{2(g),P} = \frac{\left(r_{N2}\, t - c_{N_{2(aq)}}\right) RT}{P_{N_2,P}}$$

Eq. 7

where t (h^{-1}) is the reaction duration, and $c_{N2(aq)}$ (mol m^{-3}) is the concentration of aqueous $N_{2,(g)}$ gas in equilibrium as determined by Henry's law, and $P_{N2,P}$ (atm) is the simulated prototype pressure of the environment during centrifugal loading, and was assumed to be the hydrostatic pressure of the pore fluid during centrifuge operation. Based on pressure-scaling laws under centrifugal loading, the prototype hydrostatic pressure ($P_{N2,P}$, atm) and the depth scale are linearly related by the gravity acceleration factor induced on the soil in the model, g (Caicedo & Thorel, 2014; Garnier et al., 2007; Kutter, 2013).

Influences on the pore volume, such as relative density and grain size, must be calculated, because these factors put physical limitations on the amount of pore space available for pore fluid to occupy and gas to form. For example, samples with higher relative densities will have more densely packed soil in a given volume than samples with lower relative densities, resulting in a reduced amount of available pore space. Further, poorly graded soils with a large grain size will have higher available pore space than soils that are well graded with a small grain size because smaller soil grains will be able to occupy the space between large grains.

24

In the centrifuge model, soil particles homogenously sized. For the results described here, sand ($D_{50} = 0.2$ mm) at 40% relative density was used, resulting in Vp values of 0.41 m^3 per m^3 of soil. Additionally, the initial pore fluid composition was well-mixed and uniform throughout the soil but was subject to diffusive transport and phase transfer beyond $t = 0$.

One of the limitations of centrifuge testing is that the reaction rate does not scale with g, unlike stress and pressure. Aqueous gas diffusion in the model is scaled by the squared gravitational constant, g^{-2}, to model the expected diffusion behavior in the field-scale prototype (Garnier et al., 2007; Kutter, 2013). Consequently, diffusive fluxes are expected to be relatively greater in the model than for the prototype. This leads to the question of whether the gas distribution in the centrifuge model is representative of the gas distribution in the field-scale prototype. Alternatively, gas distribution would be different as a result of the increased diffusive flux in the model due to its scaling of g^2 from centrifugal loading.

The equation for diffusive flux in the prototype at a depth node i ($J_{P,i}$, mol m h^{-1}) is Eq. 8.

$$J_{P,i} = -D_{N2,aq} \frac{\partial c_{N2}}{\partial x_P} \qquad \text{Eq. 8}$$

where $D_{N2,aq}$ (m^2 h^{-1}) is the diffusion coefficient of aqueous $N_{2,(aq)}$ in water and x_P (m) is the distance in the field-scale prototype. The equation for diffusive flux ($J_{m,i}$, mol m h^{-1}) at a depth layer (i) in the centrifuge model scale is defined in Eq. 9.

$$J_{m,i} = -D_{N2,aq} g^2 \frac{\partial c_{N2}}{\partial x_m} \qquad \text{Eq. 9}$$

where x_m (m) is the 1-D distance from the point of production to the next layer in the model.

When considering diffusive flux between the soil layers, additional kinetic and friction factors was neglected and assumed $D_{N2,aq}$ to be 7.2×10^{-6} m^2 h^{-1} at 298 K and independent of pressure effects (Cadogan et al., 2016).

The flux of aqueous $N_{2,(aq)}$ was determined by considering diffusion between the soil layers, gaseous $N_{2,(g)}$ formation, and the N_2-production rate was used to estimate the aqueous $N_{2,(g)}$ gas concentration at simulated prototype depth. Eq. 10 details the aqueous $N_{2,(aq)}$ concentration flux at a given i and t.

$$\frac{dN_{2(aq),P}}{dt} = r_{N2} - c_{N_{2(g)}} + \frac{J_{P,i-1} - J_{P,i}}{w_p} \qquad \text{Eq. 10}$$

where $c_{N2(g)}$ (mol h^{-1}) is the total amount of N_2 transferring from the liquid to the gas phase at each node and w_p is the width of each node layer (m). Since equilibrium was assumed, the transition of N_2 from the liquid to the gas phase is instantaneous. This was likely an oversimplification, and future modeling efforts should consider the difference between the aqueous-phase gas concentration and gas-phase gas concentration in equilibrium (i.e. the mass transfer coefficient k_La). As a result, $c_{N2(g)}$ is based on total N_2 that transferred from aqueous to gas from r_{N2} and diffusion transport at t.

To identify the significance of diffusion on the concentration of soluble $N_{2,(aq)}$, the second Damköhler number, which relates the rate of complete denitrification and diffusion, was determined for the field-scale prototype ($Da_{II,P}$, dimensionless) and centrifuge model scale ($Da_{II,m}$, dimensionless) in Eq. 11 and Eq. 12, respectively (Connolly et al., 2015).

$$Da_{II,P} = \frac{r_{N2}}{J_{P,i}} \qquad \text{Eq. 11}$$

$$Da_{II,m} = \frac{r_{N2}}{J_{m,i}} \qquad \text{Eq. 12}$$

Results and Discussion

Figure 2 illustrates the concentration of aqueous N_2 for prototype and model-scale conditions, considering aqueous $N_{2,(aq)}$ diffusion between the soil layers, gaseous $N_{2,(g)}$ formation at a constant production rate from microbial nitrate reduction, gas/liquid-phase equilibrium for N_2, and no advective flux of biogenic gas. Soluble $N_{2(aq)}$ saturation was achieved at upper levels shortly after 6 hours at both scales. After 12 hours, equilibrium was reached over the total depth in both scales, and all additional produced biogenic N_2 entered the gas phase. Prototype and model conditions showed little difference for the soluble $N_{2,(aq)}$ concentration during the modeled time period, which implies that the dominating mechanisms scale linearly with centrifuge loading. Once liquid-gas phase equilibrium was reached, the soluble $N_{2,(aq)}$ concentration gradient varied linearly with depth.
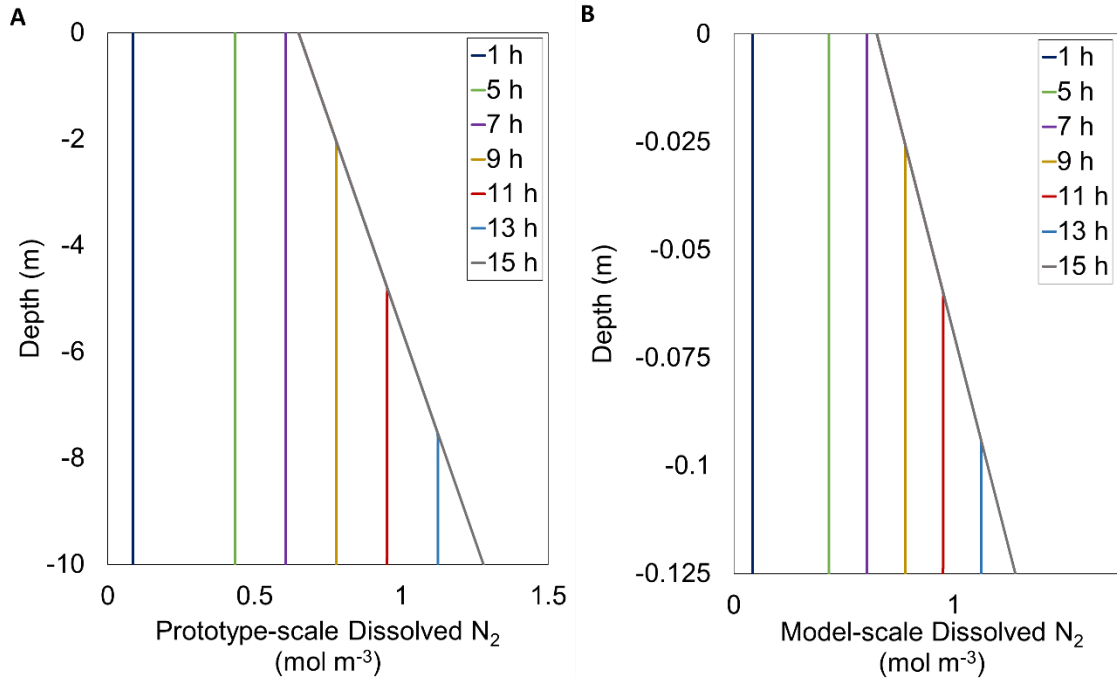
Figure 2. Time series showing soluble N_2 ($c_{N2(aq)}$) at Equilibrium Considering Biogenic N_2 Production (r_{N2}), Aqueous $N_{2,(aq)}$ Diffusion Between the Layers ($J_{P,i}$ and $J_{P,i-1}$), and Liquid-gas Transfer ($c_{N2(g)}$) in Ottawa F-65 Sand at 40% Relative Density for Simulated [A] Prototype and [B] Model-scale Conditions from t = 1 to 15 Hours.

Figure 3 shows the diffusive flux from the lower level, *i-1*, to the upper level, *i* ($J_{P,i-1}$). As the reaction rate was constant over depth, diffusion was zero until shortly after 6 hours, when the liquid-gas phase threshold was met at the surface. After that, diffusive flux changed step-wise over time in both scales. As the solubility changed linearly with depth, saturation was achieved at increasing depths as a linear function of time. Since diffusion scales by g^2, unlike linear scaling for pressure and stress, diffusive flux was much greater in the model scale than at the prototype scale.
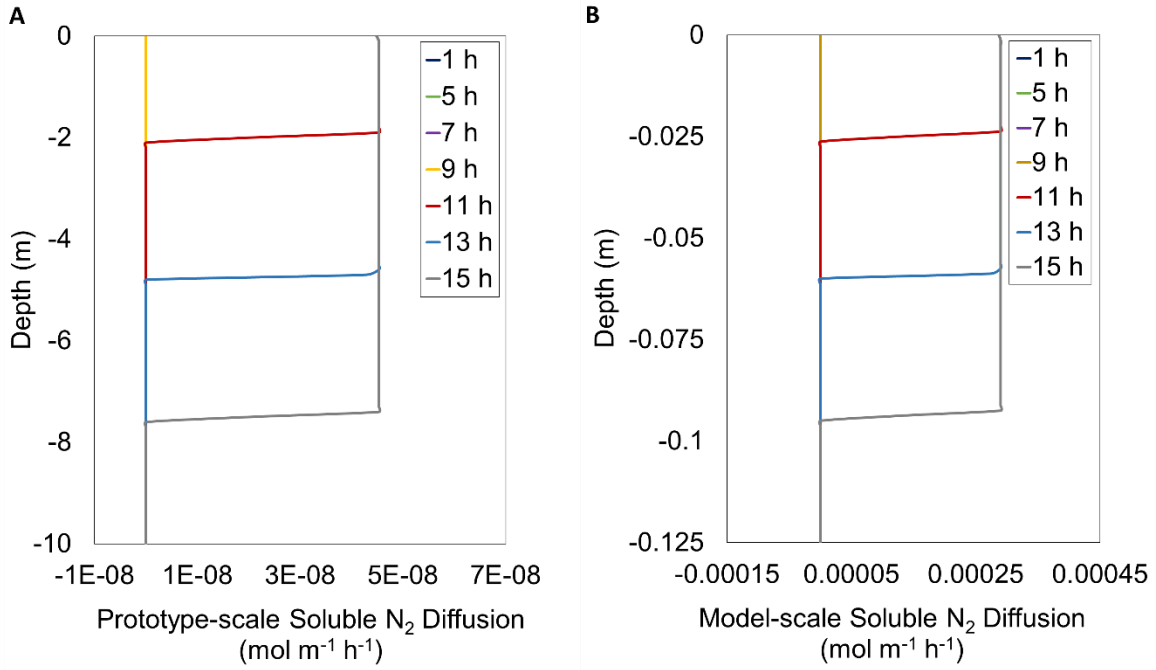
Figure 3. Diffusion Rate of Liquid-phase $N_{2,(aq)}$ ($J_{P,i-1}$) Going into Each Discretized Layer in Ottawa F-65 Sand at 40% Relative Density at [A] Simulated Prototype and [B] Model scale Conditions from t = 1 to 15 Hours.

For the cases illustrated in Figure 3, $Da_{(II),P}$ and $Da_{(II),m}$ were calculated to be 2,360,000 and 369, respectively. As the Damköhler numbers for both scales was greater than 10, the diffusion rate was insignificant compared to the reaction rate, which implies that the nitrate was immediately converted (Folger, 2011). Therefore, diffusion did not have a significant effect during this time period. However, in field conditions the Damköhler number may decrease as the reaction rate decreases, and diffusion may play a more significant role in substrate transport than modeled here.

In the current model, the diffusive fluxes in and out of each layer are equal, except for the bottom and the top layer, resulting in a relatively constant diffusion over the domain between layers and a net diffusion balance of approximately zero. As a consequence, the transfer of N_2 from the solute phase to the gas phase in each layer was unaffected by the

29

diffusive flux; once the liquid-gas equilibrium concentration was reached, the transfer of N_2 from the solute phase to the gas phase was equal to the reaction rate.

The accumulated $N_{2,(g)}$ gas content in the prototype, considering soluble $N_{2,(aq)}$ production, diffusion, and phase equilibrium, is shown in Figure 4. Gas produced at varying depths over time was fixed, was evenly distributed horizontally, and did not diffuse through the soil. Figure 4 illustrates the overall $N_{2,(g)}$ at each layer, assuming pore-level and distribution effects are negligible.

Figure 4A shows concentration accumulation of N_2 gas resulting from biological production and transfer to the gas phase. Figure 4B and Figure 4Figure 5C show that the upper layers of sand experienced much lower degrees of saturation because of a higher level of N_2 gas volume accumulation, though the trends are not linearly distributed. This trend makes sense considering the volume of the gas, calculated using the ideal gas law, is proportional to the pressure, which declines in the upper layers. Figure 4C directly corresponds with the amount of gas in the pore space that will reduce the soil liquefaction triggering potential at each layer. As a further result of a changing profile in the degree of saturation over the depth, the hydraulic conductivity of the upper layers of soil was expected to be less than soil at depth.
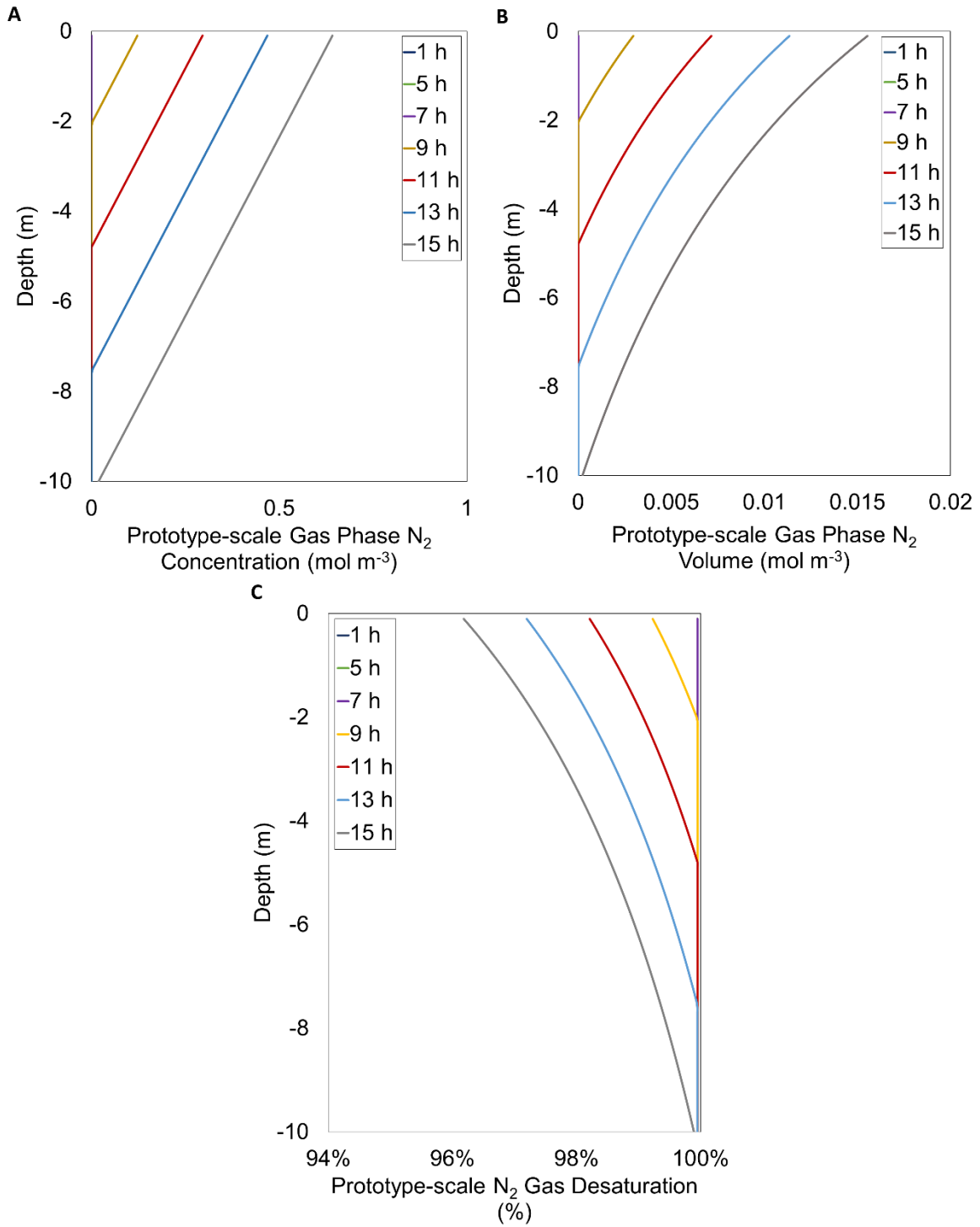
Figure 4. Gaseous $N_{2,(g)}$ ($N_{2(g),p}$) Production over 15 hours at Simulated Prototype Depth Conditions at Equilibrium Considering Biogenic N_2 Production (r_{N2}), Aqueous $N_{2,(aq)}$ Diffusion Between the Layers ($J_{P,i}$ and $J_{P,i-1}$), and Liquid-gas Transfer ($c_{N2(g)}$) in Ottawa F-65 Sand at 40% Relative Density by [A] mol, [B] Volume, and [C] Percent Desaturation.

Although the model seems to indicate that diffusion did not significantly influence the gas distribution and resulting development of gas saturation in time, other pore-scale influences and mixing from liquid-gas transfer and transport were not considered in this simplified model. For example, substrate limitation may also occur when the saturation drops and some of the denitrifying bacteria lose contact with the liquid phase or due to diffusion limitations at the pore scale. These other factors may influence the gas and aqueous N_2 concentrations, the gas distribution at the pore scale, and ultimately the resulting degree of saturation.

Future model enhancements should be added to resolve the differences between the model and prototype scale during centrifuge testing for prediction of biogenic gas production. Current iterations of this and established MIDP models only consider 1-D and assume that each layer is completely mixed. However, transport and product formation will be a function of depth and length, especially when investigating field applications. Modeling transport of the gas phase will improve the ability to predict the distribution and migration of the gas and the potential change in the soil hydraulic conductivity. Since only single-step denitrification was considered here, considering at least two-step denitrification, the reduction of NO_3^- to NO_2^- and NO_2^- to N_2 gas, is recommended. Expanding the model to consider intermediate steps is critical because of potential inhibition from intermediate accumulation, especially NO_2^- and subsequently HNO_2 .(Almeida et al., 1995) Furthermore, other biogeochemical processes may be in competition with the provided electron donor and should be considered, including SO_4^{2-} reduction. These improvements will enhance interpretation of the physical model results

and provide insight on the potential future challenges when applying MIDP via denitrification to mitigate liquefaction risk at the field-scale. Soil characteristics, like permeability and suction, resulting from biogenic gas production are influenced by the distribution and movement of gas pre- and post-liquefaction and will likely need to be evaluated on a case-by-case basis as soil type and structure changes.

Model Conclusions and Proposed Model Enhancements

Desaturation by biogenic gas production via denitrification has been proposed as a method for liquefaction mitigation. Preliminary lab-scale tests indicate that at shallow depth gas pockets may occur as a result of limited overburden pressure. Centrifuge tests can be performed to evaluate the performance of the process at field pressure conditions prior to scale up to the field. As reactive transport processes scale differently with centrifuge-pressure conditions compared to the field, the N_2-gas distribution in the centrifuge is expected would differ from the expected distribution in the field. Therefore, a simplified numerical model was developed and used to simulate the process at model and field scales. The results presented here indicate that diffusion of soluble $N_{2,(aq)}$ was negligible at both scales for the simulated reaction rate. Consequently, the degrees of saturation between model and field scales were similar, implying that centrifuge testing has the potential to adequately simulate field conditions. However, the simplified model does not consider important pore-scale influences, such as the change in porosity and the distribution of active biomass and substrate. It also does not consider how changes in permeability can affect gas stability and how mixing is enhanced by liquid-gas transfer and transport.

Therefore, the model needs to be enhanced to adequately consider all important parameters to predict MIDP at centrifuge or field scale.

CHAPTER 4

CENTRIFUGE MODEL TESTING OF LIQUEFACTION MITIGATION VIA DENITRIFICATION-INDUCED DESATURATION

The first of several planned centrifuge-model tests was conducted to investigate desaturation via biogenic gas production and retention as a means of mitigating the potential for earthquake-induced soil liquefaction. Microbially induced desaturation and precipitation (MIDP) has the potential to reduce the liquefaction potential of saturated cohesionless soils by desaturating and mechanically strengthening the soil (Karatas et al., 2008; O'Donnell, Kavazanjian, et al., 2017; O'Donnell, Rittmann, et al., 2017; Pham, Nakano, et al., 2018; Pham, van Paassen, et al., 2018). The non-disruptive nature of MIDP and the ubiquitous nature of denitrifying microorganisms offers the potential for cost-effective mitigation of the risk posed by liquefaction to infrastructure world-wide. Liquefaction mitigation via MIDP is a two-stage process wherein the reduction of nitrate (NO_3^-) by denitrifying bacteria produces dinitrogen gas (N_2), leading to desaturation, and dissolved inorganic carbon (DIC), leading to carbonate precipitation. Soil desaturation via N_2 production in the first stage of MIDP of desaturates the soil, providing rapid but possibly limited duration reduction of liquefaction potential. In the second stage of MIDP, the DIC combines with calcium ions to form calcium carbonate (preferably as calcite) which then

precipitates to mechanically strengthen the soil and provide long-term mitigation of liquefaction potential.

A significant amount of research has focused on the phase in which calcium carbonate is produced in bio-based processes, including MIDP (Martin et al., 2013; O'Donnell, Kavazanjian, et al., 2017; Pham, van Paassen, et al., 2018). Since calcium carbonate precipitation by MIDP can be time intensive, interest in biogenic gas production by denitrification (He & Chu, 2014; Kavazanjian et al., 2015; O'Donnell, Rittmann, et al., 2017; Pham, Nakano, et al., 2018) has increased due to the potential to increase the liquefaction resistance of soil by desaturation (Okamura & Soga, 2006; Rebata-Landa & Santamarina, 2012; Yegian et al., 2007) in the short term in a relatively rapid manner while calcium carbonate precipitates to provide long-term resistance.

Denitrification produces significant amounts of N_2 and carbon dioxide (CO_2) gases. The primary gas of interest with respect to desaturation by denitrification is the N_2 gas, due to its abundance and relatively low solubility compared to CO_2. Laboratory column tests have shown that as little as 5% desaturation by denitrification can increase the undrained shear strength and cyclic shear resistance of a soil significantly (He & Chu, 2014; O'Donnell, Rittmann, et al., 2017). However, knowledge regarding the production, migration, and retention of biogenic gas at depth is limited for field-scale stress conditions and subsequent to earthquake shaking. Centrifuge modelling can provide insight into behavior and treatment effectiveness at depth both before and after an earthquake event. In the work reported herein, the initial centrifuge model test of a planned series of centrifuge tests was conducted to investigate the biogenic gas production due to

36

denitrification as a means of mitigating the potential for liquefaction triggering at field depth.

Centrifuge Experimentation Set-Up

Centrifuge testing was performed using the 1-m radius centrifuge at the UC Davis Center for Geotechnical Modeling. A model consisting of uniform, level F-65 Ottawa sand ($D50$ = 0.20 mm, Cu = 1.61, Cc = 0.96, e_{min} = 0.51, e_{max} = 0.83) was constructed in a flexible shear beam container to the dimensions provided in Figure 5. The F-65 Ottawa sand was placed at an initial relative density of approximately 40% in a series of 2-cm lifts using dry pluviation. A 3-cm layer of coarse Monterey sand and gravel was placed below the Ottawa sand layer to facilitate uniform saturation. The model was saturated under vacuum with deionized (DI), de-aired water. Geotechnical centrifuge modeling has an inherent discrepancy in scaling the model to the prototype for different parameters. For example, length scales from the centrifuge model to the field-scale prototype by g, whereas and diffusion time scales by g^2 (Adamidis & Madabhushi, 2015; Adamidis & Madabhushi, 2018). This results in the soil in the centrifuge model being more permeable (by a factor of g) than the prototype. In principle, this discrepancy can be resolved by reducing the soil grain size or by increasing the viscosity of the pore fluid in the centrifuge model, although changing the grain size may affect the stress-strain behavior of the soil (Adamidis & Madabhushi, 2015). Therefore, the pore fluid often is made more viscous by adding a compound such as methyl cellulose (Darby et al., 2017; Darby et al., 2019). In this test, the viscosity of the DI water was not scaled for g-level due to concerns about altering the

microbial denitrification process, including microbial N_2 formation. The lack of viscosity

scaling complicates some aspects of the interpretation of transient pore-pressure data.
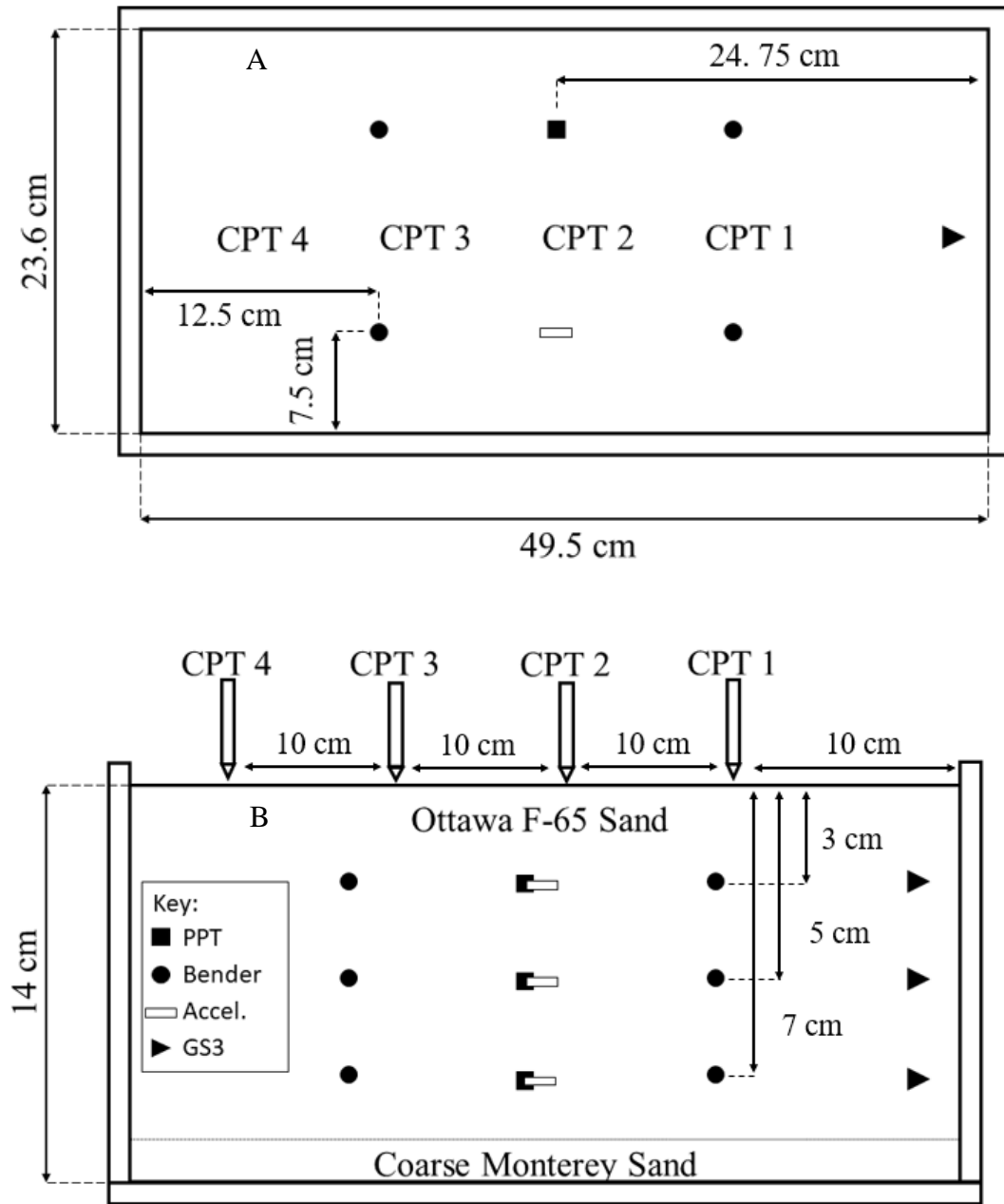
Figure 5. [A] Plan and [B] Side View of Centrifuge Container Dimensions and Sensor Layout.

After saturation, two pore volumes (10 L) of a treatment fluid containing the substrates required for denitrification and a mixed microbial culture of denitrifying bacteria, enriched from locally available organic soil, were flushed through the model from the bottom up via six 2-mm-diameter inlet ports. The active denitrifying culture was added to the soil to increase the rate of desaturation during the experiment. Displaced liquid was drained through a port in the top of the FSB container. The treatment solution contained calcium acetate hydrate and calcium nitrate tetrahydrate at concentrations of 4.75 and 5.67 g/L, respectively, giving an acetate:nitrate molar ratio of 1.25:1. This molar ratio has been shown to be self-buffering and sufficient to facilitate complete nitrate reduction with a relatively small accumulation of intermediates (O'Donnell, Rittmann, et al., 2017; Pham, Nakano, et al., 2018). The small amount of calcium carbonate precipitated during the short-term (2 days) experiment should not have influenced soil behavior, because significant carbonate precipitation occurs on a much longer time scale, i.e., on the order of weeks or months (O'Donnell, Kavazanjian, et al., 2017).

The model was instrumented with 3 soil-moisture and electrical-conductivity sensors (GS3, Meter Group), 6 p-wave (compressional) bender disk pairs (Piezo Sytsems), 3 pore-pressure transducers (PPTs), 3 accelerometers, and a linear potentiometer (LP). The degree of saturation (S_m) was monitored by soil-moisture sensors. Figure 5 illustrates approximate sensor placement in the model, except the LP, which is placed on the surface of the soil model during shaking events. The GS3 sensors were used to track desaturation by biogenic gas generation (based upon moisture content) and substrate utilization (based upon electrical conductivity).

Spinning was initiated when moisture-content measurements indicated that the degree of saturation of the soil within the model was equal to or less than 90%. Acceleration data were processed using a fourth-order Butterworth bandpass filter with 0.15 Hz and 0.75 Hz corner frequencies. A 50-mm stroke LP was mounted on an instrument rack to monitor surface settlement of the soil. A cone-penetration test (CPT) was performed to measure the liquefaction resistance of the soils by using a 6 mm-diameter cone and a hydraulic actuator that advanced the cone at 1 cm/sec. CPT tests were conducted at locations shown in Figure 5 at select times during model testing to evaluate the effect of desaturation on penetration resistance (q_c).

Centrifuge Testing Procedure

Upon reaching the target degree of saturation of approximately 90% at 1 g conditions (no spinning), the model was spun to a gravity acceleration of 80 g applied to the upper surface of the centrifuge model. For the remainder of this chapter, all dimensions are in prototype units, i.e., length, diffusion, pressure, stress dimensions scaled by 80 g using appropriate scaling laws (Garnier et al., 2007), unless otherwise noted. The difference between the degree of saturation at 1 g and the degree of saturation at 80 g provides a measure of the effect of the increase in steady-state pore pressure (due to centrifuge acceleration) upon the degree of saturation. Once the degree of saturation at the approximate depths of 2.4 m, 4.0 m, and 5.6 m had equilibrated at an acceleration of 80 g, the hydraulic actuator pushed the CPT cone into the soil, the model was spun back down to 1 g, and the cone penetrometer chassis was removed to prepare for shaking tests to investigate liquefaction triggering. Equipment constraints necessitated a spin down/spin up between a cone push and shaking;

the influence of spin down/spin up on degree of saturation is discussed later. For the first shaking sequence, the model was spun back up to 80 g and subjected to nine shaking events consisting of 15 cycles of a uniform amplitude 1 Hz frequency sine wave. Acceleration amplitudes of each shaking event were progressively increased until liquefaction was triggered as indicated by an excess pore pressure ratio, r_u ($r_u = u_e/\sigma'_{vo}$) of 0.95. After achieving a value of $r_u = 0.95$, the model was spun down and then spun up again for a second cone push to complete the first day of centrifuge testing.

Since centrifuge testing was performed over two days, the model was covered to limit oxygen intrusion that may inhibit microbial denitrification after the second cone push. The model was left to sit overnight at 1 g. During this rest period, the denitrifying bacteria were still active, as evidenced by the continued decrease in the degree of saturation value.

The next day, a third cone was pushed to evaluate the effect of continued desaturation on the cone penetration resistances (q_c). The model was then subjected to another six shaking events of progressively increasing amplitudes of seismic acceleration to a maximum of 0.70 g, in which the equipment maximum was reached. The first shaking event with a seismic acceleration of 0.70 g generated r_u values of 0.05, 0.06, and 0.16 at prototype depths 2.4 m, 4.0 m, and 5.6 m, respectively, indicating that liquefaction was not triggered. The model was then subjected to three additional shaking events of 15, 30, and 45 cycles, respectively, at the 0.70 g target acceleration level. At the conclusion of this intense shaking sequence, soil densification was expected because the r_u values continued to increase each shaking event, without indicating that liquefaction had been triggered at the mid-depth pore pressure sensor location (in which, $r_u \geq 0.95$). The model was spun

41

down to 1 g, and set-up with the CPT chassis for a fourth and final CPT cone push. After the final CPT cone push, the model was spun down in in 20 g increments to evaluate the effect of g-level on desaturation.

Experimental Results and Discussion

The target and achieved amplitudes for each sinusoidal shaking event are detailed in Table 1. Figure 6 shows the desaturation over the total experiment. In some cases, the target amplitude was not equal to the achieved amplitude measured by accelerometers placed at the base of the model. As a result, it was not able to be confirmed that a higher amplitude of seismic acceleration was achieved to deeply investigate liquefaction trigger potential. Figure 7 shows the effect of the achieved g-level on the degree of saturation based upon the soil moisture content measured by the GS3 sensors at three different elevations in the model. Excluding the periods of gas venting, desaturation from denitrification occurred at a relatively consistent rate from initial treatment to shortly before the first spin sequence. Several episodes of gas venting occurred during model placement on the arm and model balancing, suggesting that agitation of the model led to the formation of gas channels, leading to a loss of gas in the soil and an increase in saturation. Gas venting was visually observed to occur most commonly at the sensor-soil and soil-container boundaries. These observations indicated loss of desaturation prior to centrifugal loading in the model. This poor gas retention is believed to be due to the low sand relative density and the low overburden pressure in the model at 1 g. However, the degree of desaturation was retained was still sufficient to provide substantial mitigation of liquefaction triggering.
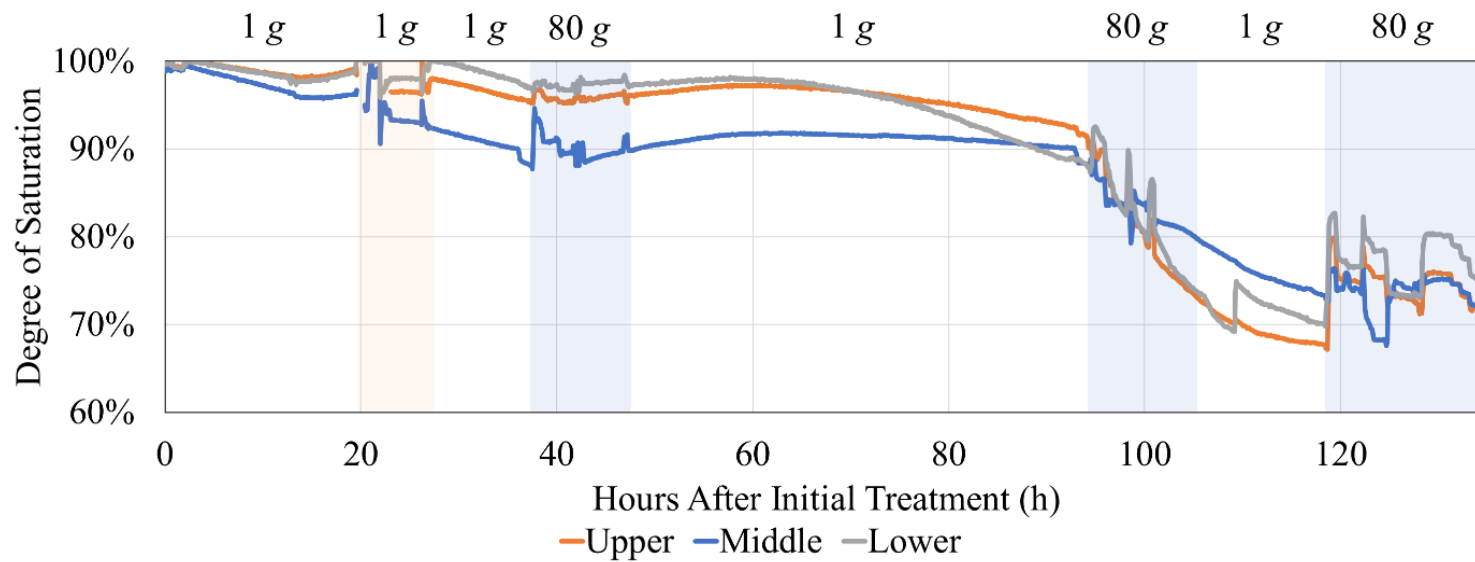
Figure 6. Monitored Saturation Level During Entire Centrifuge Experiment.

Table 1. Shaking Sequences of Uniform Sinusoidal Cyclic Loading During Spin-up to 80g

Spin Sequence 1			
Shake Number	Target Amplitude (*g*)	Achieved Amplitude at Model Base (*g*)	Number of Cycles
1	0.04	0.025	15
2	0.06	0.044	15
3	0.09	0.054	15
4	0.12	0.074	15
5	0.15	0.10	15
6	0.20	0.14	15
7	0.25	0.20	15
8	0.35	0.26	15
9*	0.40	0.36	15
Spin Sequence 2			
Shake Number	Target Amplitude (*g*)	Achieved Amplitude at Model Base (*g*)	Number of Cycles
10	0.40	0.34	15
11	0.45	0.34	15
12	0.50	0.38	15
13	0.50	0.35	15
14	0.50	0.41	15
15	0.60	0.40	15
16	0.7	0.44	15
17	0.7	0.44	15
18	0.7	0.45	30
19	0.7	0.41	45

*Liquefaction triggered at 2.4 m prototype depth (0.03 m model depth), as determined by PPT readings ($r_u \geq 0.95$) during spinning.
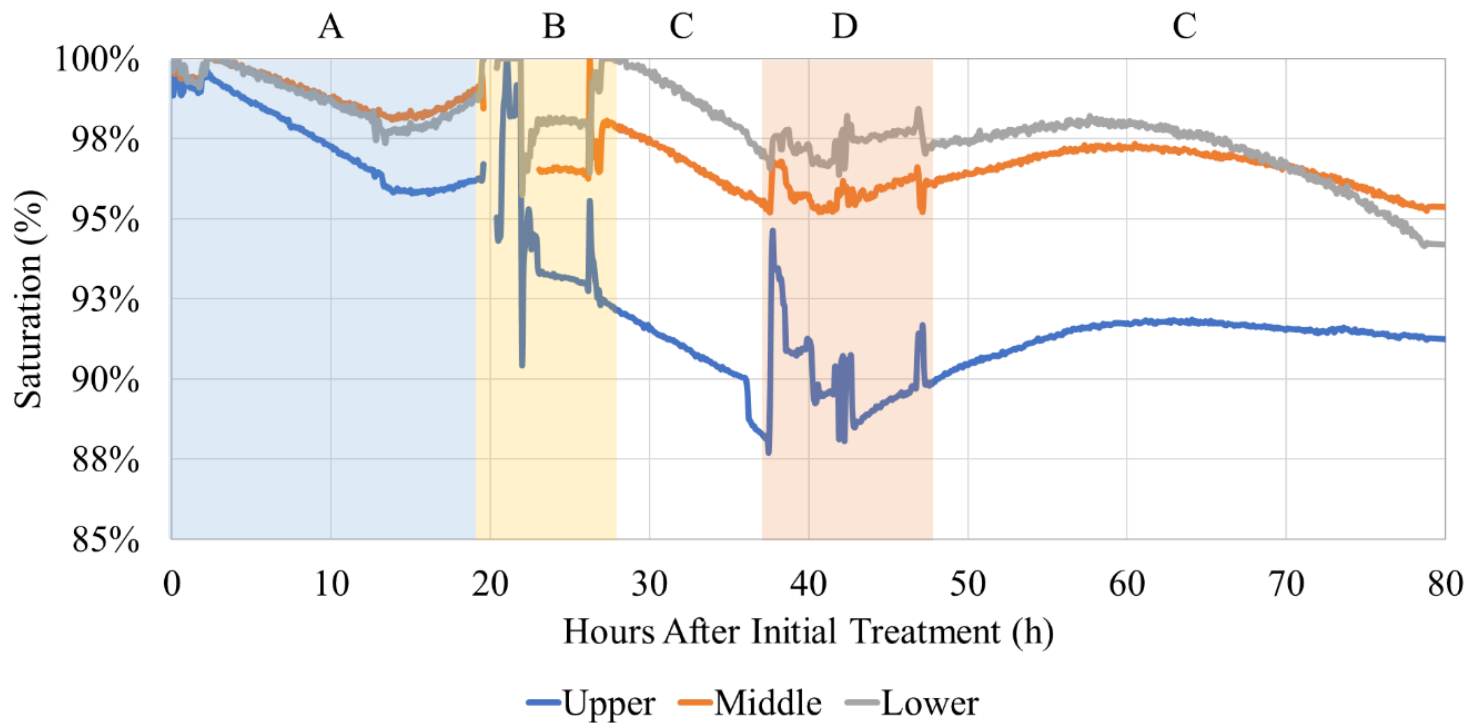
Figure 7. Monitored Saturation Level During: [A] Initial Treatment Period; [B] Placement on Arm; [C] Model at 1 g; and [D] During Spinning up to 80 g for Centrifuge Balancing.

Between hours 80 and 97, the box remained at 1 g, and desaturation in the soil reached equilibrium. After approximately 60 hours following the commencement of treatment at 1 g, a degree of saturation less than the target saturation of 90% was reached at all layers, as shown in Figure 7. The 90% saturation target level was established based upon the previous findings (He & Chu, 2014), who reported that 95% soil saturation significantly reduced liquefaction triggering in monotonic triaxial testing and the desire to provide a margin of safety to account for a reduction in desaturation during loading the model on the centrifuge and spin up of the model.

Figure 8A and Figure 8B show the prototype settlement and r_u resulting from each shake during the first and second shaking sequences. Shakes 1 through 9 resulted in 476 mm of settlement and 1695 mm at the conclusion of Shake 19. The height of the soil had visibly heaved overnight due to biogenic gas production, but the height change was not monitored. Shake 10 resulted in the most significant settlement, which was expected to have occurred during gas accumulation in the uppermost layers of the soil from overnight gas production and transport of gas during the third CPT spin up and down sequence, and the initial spin up at the beginning of the second shaking sequence. The r_u values increased when the target shake amplitude increased, until during shake 9, resulting from experimental error in which the shaking sequence was performed twice. The pre-processed data read during the spin experimentation indicated that the top layer liquefied during Shake 9, and spinning was stopped until the next day. Shake 10 (or the first during the second spin sequence) indicated liquefaction in the uppermost layer. Due to experimental set-up concerns, including a sudden release of trapped gas accumulated during overnight

generation and transport during spin up and down, this initial shake is potentially unreliable due to several interacting mechanisms.
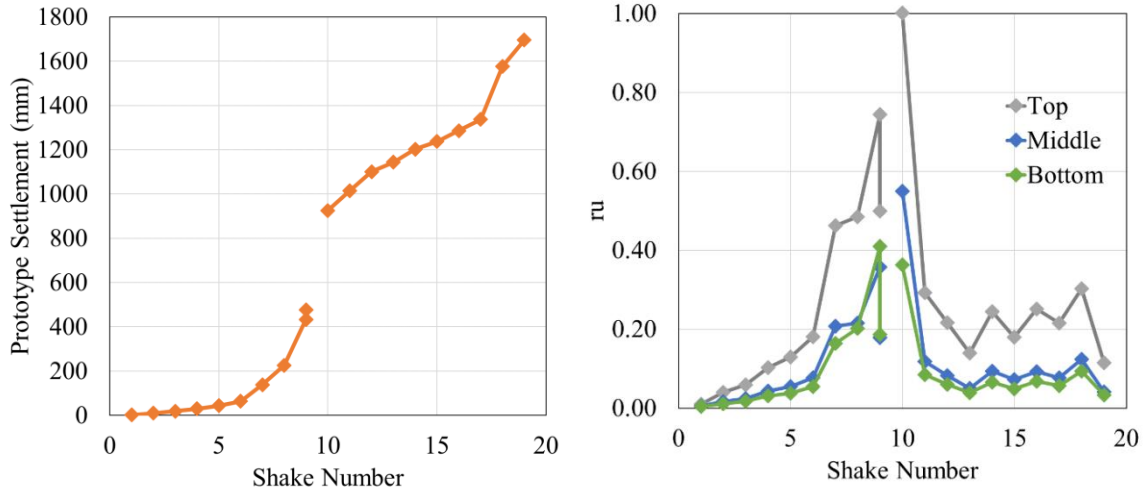
Figure 8. Monitored [A] Accumulated Prototype Settlement and [B] r_u During Each Shaking Event.

The saturation level increased upon spinning at all levels by 1-5%, depending on depth within the model, with the most notable increase at the middle and lower sensor levels, where the steady-state pore pressure and effective overburden stress was greater than in the shallow sensor level. This increase in saturation during spinning was expected based upon two mechanisms. First, based upon ideal gas law properties, dissolution of biogenic gas into the pore fluid and a reduction in bubble size are likely as the steady- state pore pressure increased by a factor of 80 (due to the body force acceleration increasing from 1 g to 80 g). Second, the biogenic gas tends to migrate upwards due to the low relative density of the sand (as observed during treatment at 1 g). The rapid increase in desaturation during the first shaking event shown in Figure 9 is expected to have occurred due to agitation of the soil, causing gas to travel through the upper layers and move from the aqueous phase to the gaseous phase. The desaturation readings also show that a venting occurred at the end

47

of the shaking sequence and during spin down. This was also observed during experimentation. The desaturation measurements taken during the second CPT test at 80 g, shown in Figure 9 (zone C), indicate that the gas-aqueous phase transfer equilibrium was reached in all layers approximately half-way through the spin cycle.

Cone-penetration resistances were obtained 1) before any shaking, 2) after initial liquefaction triggering (9 shaking events), 3) after overnight gas generation, and 4) at the end of all shaking (17 shaking events). Profiles of normalized cone penetration resistance (q_{c1N}) are shown in Figure 10. Measured penetration resistances are normalized and corrected for overburden using the modified q_{c1N}-D_R relationship described in literature (Darby et al., 2017). Cone penetration resistance slightly increased after reaching an $r_u = 0.95$ at 2.4 m, though this increase is primarily located below 4.5 m depth.
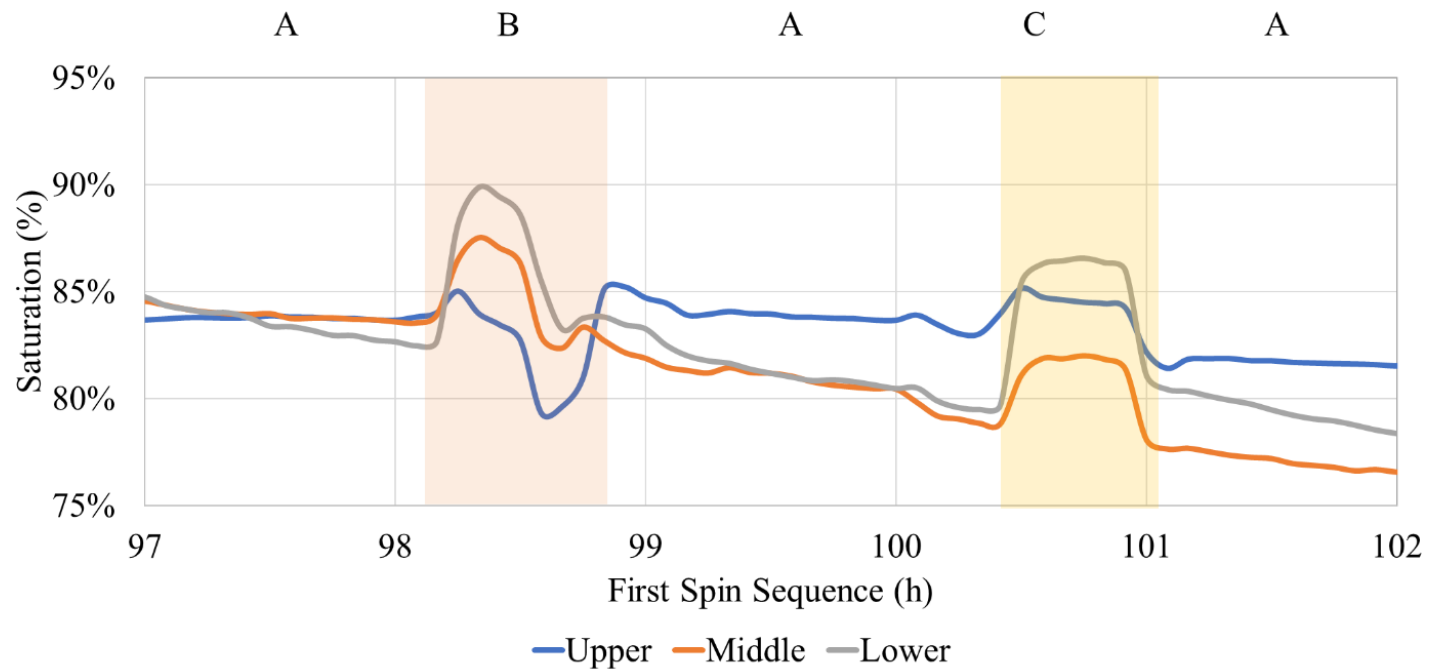
Figure 9. Monitored Saturation Level: [A] Continued Desaturation by Biogenic Gas Generation; [B] First Shake Sequence; and [C] Second Cone During First Spin Sequence.
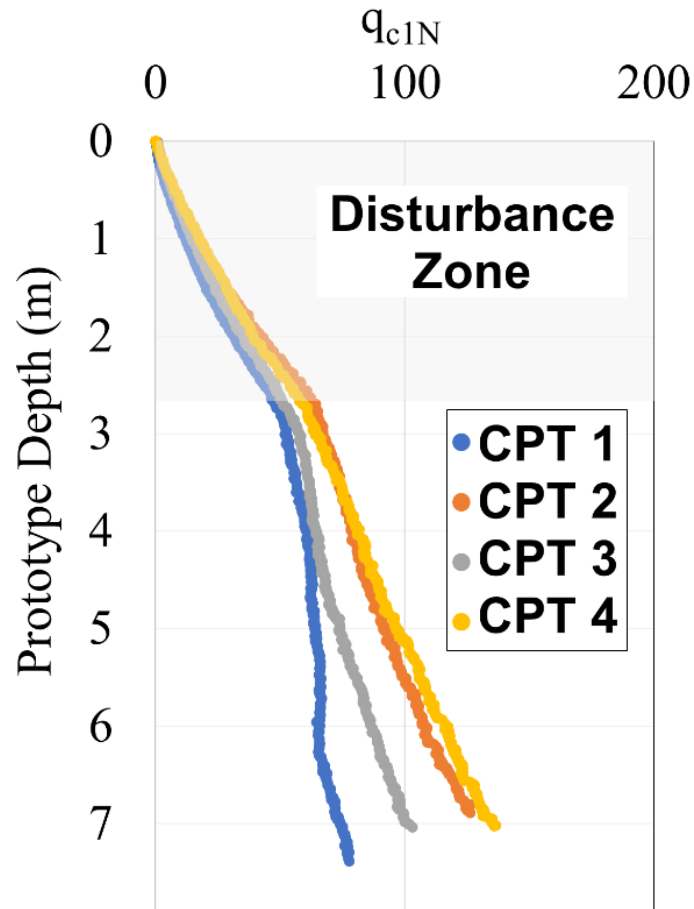
Figure 10. CPT Tip Resistance for Both Spin Sequences.

Cone-penetration resistances appear to have been affected by gas production, as shown by the difference in Cone 2 and 3, and the shaking events, as shown by comparing the difference in q_{c1N} values of Cones 1 and 2, and Cones 3 and 4. The first shaking event resulted in a significant increase in penetration resistance followed by a decrease in penetration resistance from Cone 2 (after spin down during the first day of testing) to Cone 3 (on the second day of testing, after the model was left overnight, during which significant additional gas was generated, and the model was spun up to 80 g again). The penetration resistances were greater following shaking (Cones 2 and 4) than prior to shaking (Cones 1

and 3), which may indicate settlement during shaking or during the pressure changes during spin up and down between shaking sequences and CPTs that resulted in gas venting.

As indicated by the degree of saturation in Figure 6, all shaking events induced some gas venting. The increase in saturation accompanying gas venting may have been the cause of the changes in CPT resistance between tests CPT 1 and 2, but settlement from shaking also was likely to have been a considerable factor on the change in q_{C1N}. While an increase in desaturation (a decrease in saturation) was observed in all layers after liquefaction was induced in the upper layer, it occurred most notably in the upper soil layer. This observation can be attributed to biogenic gas migration upwards through the model due to the shaking. Even if the mass of gas flowing into the upper layer was later balanced by gas flowing out of the upper layer, the gas volume expands as pore water travels upward due to the pore water pressure gradient, resulting in additional desaturation in the upper layers of the soil profile. During the final shaking sequence on the second day of spinning, the inability to generate high excess pore pressure below 2.4 m depth may have been influenced by both the low degree of saturation (the degree of saturation dropped below 75% by the beginning of the second sequence of shaking vents) and the use of unscaled pore fluid. Further investigation is needed to isolate the effect of shaking on q_{c1N} and the changes in saturation due to biogenic gas formation during treatment and testing.

The final spin-down was performed in 20-*g* increments to observe the effect of *g*-level (from overburden in the field) on equilibrium degree of saturation at the different sensor depths. This effect is illustrated in Figure 11. Measurements taken in the upper and middle layers of soil during the spin up and spin down process show a difference in

saturation between the layers of only approximately 1%. This suggests either that the degree of saturation at those depths was independent of overburden pressure and steady state pore pressure, that gas was trapped around the sensors overlapping sphere of measurement, or that the difference in overburden between the upper and middle sensors may not be significantly different due to sensor movement. However, this saturation difference further reduced upon incremental spin down, during which the difference in overburden pressure and steady state pore pressure induced by spinning decreases, suggesting that the degree of saturation is not entirely independent of overburden pressure and steady state pore pressure.

At the end of spin down, an equilibrium saturation of approximately 72% was reached at all layers at all depths. In denitrification tests, a maximum desaturation of 76-80% was reported using similar calcium nitrate to calcium acetate substrate concentrations in fine grained, loose sand (Pham, 2017). It was expected that the high desaturation rate was achieved due to migration of aqueous N_2 during spinning that transferred to the gaseous phase when the physical model was spun down. This would not occur in field conditions, where the pressure remains constant during MIDP treatment.

Surface settlement measured at the end of the second spin sequence was most significant at the center of the soil model (a settlement of approximately 0.75 cm on the model scale). In addition, model deconstruction showed some movement of the sensors during testing, likely resulting from spin up/spin down and shaking events.
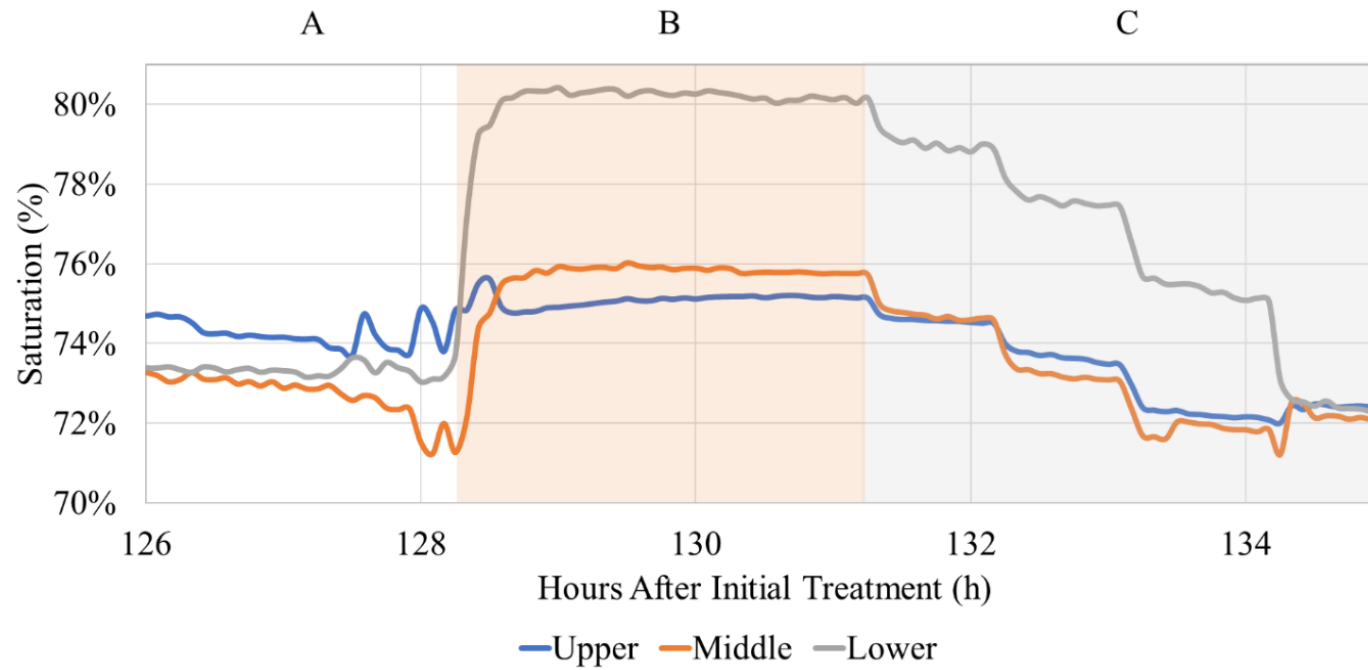
Figure 11. Monitored Saturation Level During the Final CPT Test During the Second Spin Sequence: [A] Biogenic Gas Generation at 1 g Following Shaking During the Second Spin Sequence; [B] Centrifuge Spinning up to 80 g; and [C] Incremental Spin Down from 80 to 1 g

Experiment Conclusions

Mitigation of the potential for triggering liquefaction by desaturation via biogenic gas production from denitrification was demonstrated on a systems level in a centrifuge model test. Centrifuge testing also provided insight on the effect of steady-state pore pressure on desaturation level. An increase in saturation as the model was spun up from 1 g to 80 g showed the potential for compression and dissolution of biogenic gas due to an increase in steady-state pore pressure. Soil desaturation to a degree of saturation of 90 – 95% due to biogenic gas production did not prevent soil at a relative density of 40% from liquefying ($r_u < 0.95$), as measured by pore pressure sensors in the soil model, when 15 uniform cycles of loading with target amplitude of 0.35 g (actual 0.36 g, calculated during post-processing) was applied to the model. However, the cyclic resistance of the soil at this degree of saturation was still greater than what would be expected if the soil were saturated, because the cyclic resistance of the soil increases as saturation decreased. When soil desaturation approached a degree of saturation of 70%, liquefaction was not triggered even after 45 cycles of loading with a target amplitude of 0.70 g (actual 0.44 g due to physical equipment limitations, calculated during post-processing), though this observation is tempered by the fact that an unscaled pore fluid. This lack of liquefaction is expected to be a result of significant pore-pressure dampening during cyclic loading by the biogenic gas in the soil. The use of an unscaled pore fluid resulted in an increased rate of pore pressure dissipation, and, thus, the soil may not have behaved in a truly undrained manner during cyclic loading and may have changed the mechanical behavior of the soil.

To prevent potential gas escape and soil disturbance, spinning the model up and down should be limited because gas that remains in solution during centrifugal loading may escape under normal conditions. Ideally, the soil should be under simulated field conditions as soon as possible and should remain "in flight" until cyclic loading trials are complete. However, this would limit the ability to conduct cone penetration tests and alternatives may need to be explored.

In future experimentation, different sensors should also be explored; namely, alternative p-wave sensors and soil moisture content sensors should be chosen. Since the p-wave bender disks were very small, they had to be placed in the soil close together in order to send/receive signal. In the future, the disks should be larger to allow for placement further from the center of the box. Then, the GS3 sensors were large relative to the size of the soil volume and likely influenced the treatment behavior in the surrounding area, particularly on the sides of the box where the bulk of the sensor was fixed.

CHAPTER 5

MULTIPHASE BIOGEOCHEMICAL MODEL FOR MIDP

Denitrifying bacteria are ubiquitous in most subsurface environments, and denitrification is a common process in anaerobic environments. Since denitrification is feasible in a wide range of locations, MIDP has widespread potential for liquefaction mitigation based on current understanding from laboratory-scale experimentation (O'Donnell, Kavazanjian, et al., 2017; O'Donnell, Rittmann, et al., 2017; Pham, van Paassen, et al., 2018). However, the effect of variable subsurface biogeochemical conditions that may influence *in-situ* MIDP treatment has not been extensively explored.

My goal was to develop a biogeochemical model to consider how other biochemical processes and natural conditions may affect soil treatment by MIDP. Using locally extracted water as the source-water solute to prepare the MIDP treatment solution is a logical choice from an environmental and economical perspective to maintain a closed water balance. However, natural constituents in the source-water may inhibit the denitrification process or stimulate processes which compete for the available nutrients. Competing *in-situ* biochemical processes may consume the provided electron donor (herein, acetate), leading to incomplete denitrification and the accumulation of intermediates. Electron donors consumed by microorganisms other than denitrifiers, like sulfate reducers, and may result in precipitation of other minerals and unwanted by-products. For MIDP to be successful in the field, I want to promote liquefaction mitigation products (i.e., nitrogen gas for desaturation and mineral precipitates that improve soil strength) by promoting full denitrification, while limiting toxic by-products. Potential

consequences of denitrification in a complex biogeochemical environment in the field also may be biogeochemical changes (e.g., pH) that alter kinetics and final multi-phase products.

Previous work has been done on biogeotechnical modeling of MIDP (O'Donnell et al., 2019; Pham, 2017), but these efforts did not consider the impact of MIDP on the environment and vice versa. My next-generation MIDP biogeochemical model could become unnecessarily complex if all possible biogeochemical reactions were to be included. Therefore, I include only the essential processes based on natural water constituents and are commonly observed in the natural environment: the processes that consume electron donor, significantly impact the pH and critical environmental characteristics, and lead to desaturation and precipitation. Since I anticipate that MIDP will often be deployed in coastal areas (due to the prevalence of liquefiable soil deposits in this environment), I include processes and compounds that are typical for coastal seawater conditions in my model to consider the impact of saltwater intrusion. Herein, I detail the biogeochemical processes that I have determined to be critical for understanding the behavior of MIDP in a generic coastal environment and their incorporation in a publicly accessible model.

Model Implementation

To identify the potential impact of natural biogeochemical conditions on MIDP-product formation and reaction rates, the model builds upon previous modeling work (O'Donnell et al., 2019; Pham, 2017). While these earlier models considered certain biogeochemical conditions of the following, my model considers a broader range of components: microbial

57

growth and decay, alternative microbial metabolic processes, gas production, mineral

production, pH, and microbial inhibition. The comparison between the two earlier MIDP

models and this one is shown in

Table 2. Going beyond those earlier models, my model considers additional biochemical

inhibition mechanisms, mineral kinetics, additional gas generation, microbial electron

donor competition, and desaturation and precipitation metrics in a coastal field

environment. The model was built using the biogeochemical modeling toolbox (van

Turnhout et al., 2016), hereafter referred to at the van Turnhout Toolbox.

Table 2. Comparison of Existing MIDP Models and the Presented Next Generation MIDP
Model

Modeling Component	O'Donnell et al., 2019	Pham, 2017	Next Generation Model
Baseline Substrate Recipe Estimation for Desaturation		X	X
Baseline Substrate Recipe Estimation for Precipitation			X
Complex Acid Base Equilibrium		X	X
Denitrifier Growth and Decay	X	X	X
Other Microbial Growth and Decay			X
Microbial Electron Donor Competition			X
Nitrous Acid Inhibition	X	X	X
Alternative MIDP Inhibition			X
Other Microbial Inhibition			X
pH Calculation	X	X	X
$CaCO_3$ Mineral Formation	X	X	X
Other Mineral Equilibrium			X
Mineral Precipitation and Dissolution Kinetics			X
N_2 Phase Transfer Kinetics		X	X
Other Gas Production and Phase Transfer Kinetics			X
Ground Improvement Metric Calculations (i.e., desaturation and % precipitation)			X

The model was constructed in Matlab and is publicly available online at Github, though Matlab is required to use the code (https://github.com/caitlynahall/Biogeochemical-Model-for-MIDP/). The modeling equations (e.g., microbial growth, calcium carbonate precipitation, and biogenic gas evolution) are programmed within the original, generic-form van Turnhout Toolbox (also publicly accessible), while the biogeochemical model components (i.e., stoichiometry, type of inhibition and kinetics, potential chemical species) are specified in the input spreadsheet that the program accesses. The degree of saturation and percent biocementation are calculated outside of the van Turnhout Toolbox using model results, as discussed later in this chapter.

Model Principles

Denitrification is a multi-step process of nitrogen-species reduction, as detailed below. During each reduction step, energy and biomass are produced when paired with oxidation of an electron donor that produces a thermodynamically favorable reduction-oxidation (redox) reaction. As a result of this process, the surrounding environment's characteristics (e.g., alkalinity and pH) are changed.

The four steps of nitrogen reduction in denitrification conform to the following reduction half reactions, each consuming one electron equivalent (e^-):

<div align="center">

Nitrate Reduction to Nitrite

$$0.5NO_3^- + H^+ + e^- \rightarrow 0.5NO_2^- + 0.5H_2O$$
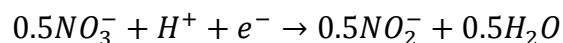
Nitrite Reduction to Nitric Oxide

</div>

$$NO_2^- + 2H^+ + e^- \rightarrow NO + H_2O$$
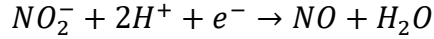
Nitric Oxide Reduction to Nitrous Oxide

$$NO + H^+ + e^- \rightarrow 0.5N_2O + 0.5H_2O$$
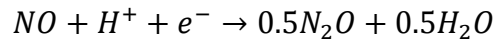
Nitrous Oxide Reduction to Dinitrogen

$$0.5N_2O + H^+ + e^- \rightarrow 0.5N_2 + 0.5H_2O$$
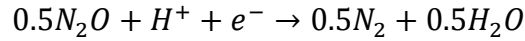
In the model, the four-step reaction was simplified to a two-step process, nitrate to nitrite and nitrite to dinitrogen gas, because the accumulation of nitric oxide and nitrous oxide normally is minimal. In contrast, the accumulation of NO_2^- (and, subsequently, HNO_2) must be considered explicitly, because nitrite can accumulate, presents risks to human health, and can inhibit the denitrifying bacteria. It should be noted that this is a batch model that assumes that the environment is well-mixed and no compounds are not available due to sorption.

Environmental Conditions and Species

The van Turnhout toolbox is flexible and can consider all relevant compounds that influence or are a result of denitrification. The van Turnhout Toolbox simulates chemical speciation with ORCHESTRA (Meeussen, 2003), which has an extensive database of established geochemical equilibria. The following aqueous species are included in my MIDP model:

NO_3^-, NO_2^-, HNO_2, NH_4^+, NH_3, $C_2H_3O_2^-$, $C_2H_4O_2$, H_2CO_3, HCO_3^-, CO_3^{2-}, CO_2, Ca^{2+}, $CaSO_4 \cdot 2H_2O$, $CaHCO_3^+$, $CaOH^+$, $CaC_2H_3O_2^+$, SO_4^{2-}, HSO_4^-, H_2S, HS^-, Fe^{3+}, Fe^{2+}, $FeOH^+$, $Fe(OH)_2$, $Fe(OH)_2^+$, $Fe(OH)_3$, $FeCO_3$, H^+, OH^-, and H_2O.

pH has a profound impact on speciation of dissolved inorganic carbon (DIC). For carbonate systems, including $CaCO_3$. These equilibriums and others driven by acid-base

speciation are automatically calculated within the model using Orchestra, which is discussed later when describing pH.

<p align="center">*Microbial Metabolism, Growth, and Decay*</p>

Based on Monod kinetics and using multiplicative dual-substrate limitation, Eq. 13 governs the most basic microbial metabolic process, oxidation of the electron-donor substrate (Bae & Rittmann, 1996; O'Donnell et al., 2019).

$$\frac{dC_d}{dt} = -\hat{q}X_a \frac{C_d}{K_d + C_d} \cdot \frac{C_a}{K_a + C_a} I_i \qquad \text{Eq. 13}$$

where $\hat{q}$ is the maximum specific rate of electron-donor utilization (mol electron donor mol^{-1} biomass d^{-1}), X_a is the concentration of active biomass (mol L^{-1}), C_d is the concentration of the electron donor (mol L^{-1}), K_d is the half-maximum-rate concentration of the electron donor (mol L^{-1}), C_a is the concentration of the electron acceptor (mol L^{-1}), and K_a is the half-maximum substrate concentration of the electron acceptor (mol L^{-1}), and I_i is the inhibition factor ($0 < I_i < 1$) to give the inhibited rate, detailed below. I assumed an initial denitrifier biomass concentration of 0.5 mmol L^{-1} and sulfate reduce biomass concentration of 0.25 mmol L^{-1}. The kinetic type (Monod in this case) is specified within the input spreadsheet. C_d and C_a are dependent on the biochemical transformation of substrate through microbial processes, speciation based on pH, mineralization, and phase transfer to gas. Many of the constants used in this model can be found in Appendix A.

$\hat{q}$ (mol electron donor mol^{-1} biomass d^{-1}) was estimated using Eq. 14 (Rittmann & McCarty, 2020).

<p align="center">61</p>

$$\hat{q} = \frac{\hat{q}_e e_d^-}{f_e^0} \qquad \text{Eq. 14}$$

where $\hat{q}_e$ is the maximum electron flow from the donor to the acceptor for energy production (acceptor e⁻ eq mol⁻¹ biomass d⁻¹), f_e^0 is the fraction of donor electrons used for energy production (acceptor e⁻ eq (donor e⁻ eq)⁻¹), and e_d^- is the amount of donor per electron equivalent (mol electron donor (donor e⁻ equivalent)⁻¹). The molecular formula for biomass was taken as $CH_{1.8}O_{0.5}N_{0.2}$, and the resulting $\hat{q}_e$ is 24.6 e⁻ eq mol⁻¹ biomass d⁻¹. For acetate, e_d^- is 0.13 mol electron donor e⁻ equivalent⁻¹. f_e^0 was determined using Eq. 15 (Rittmann & McCarty, 2020).

$$f_e^0 = 1 - \frac{1}{-\left(\dfrac{\dfrac{30.09 - \Delta G_c^{0\prime}}{\varepsilon^n} + \dfrac{\Delta G_{pc}}{\varepsilon}}{\varepsilon(\Delta G_a^{0\prime} - \Delta G_d^{0\prime})}\right) + 1} \qquad \text{Eq. 15}$$

where 30.09 is the amount of energy required to form the representative intermediate during synthesis, acetate (acetyl-CoA) (kJ e⁻ eq), $\Delta G_c^{0\prime}$ is the energy required to convert the carbon source to forms useful in synthesis (in this case, the carbon source is also the electron donor) (kJ e⁻ eq⁻¹), ε is the energy transfer efficiency term ($\varepsilon = 0.6$), n is used to consider energy efficiency when the reaction is thermodynamically positive ($n = -1$) or negative ($n = -1$), ΔG_{pc} is the energy required to convert the carbon source (acetate in this case) to carbon used for biomass synthesis, depending on the nitrogen source (kJ e⁻ eq⁻¹), and ΔG_r is the energy released during each redox reaction (kJ e⁻ eq⁻¹). ΔG_{pc} was calculated to consider either nitrate or ammonium as the nitrogen source (Rittmann & McCarty,

2020). All free-energy parameters, listed in Table 3, were found in Rittmann and McCarty

(2020).

Table 3. Bacterial Energetic Parameters for all Compounds Considered in the Model at pH = 7.

Parameter	Value (kJ e$^-$ eq^{-1})
$\Delta G_c^{0'}$: free energy of the carbon source	Acetate: 27.4 Glucose: 41.0 Molasses: 41.0
ΔG_{pc}: free energy to convert pyruvate carbon to cellular carbon, depending on the nitrogen source	Nitrate: 14.1 Ammonium: 19.5
$\Delta G_a^{0'}$: free energy required to reduce an electron acceptor	Nitrate: -41.65 Nitrite: -92.56 Sulfate: 20.85 Oxygen: -78.72
$\Delta G_d^{0'}$: free energy released to oxidize an electron donor	Acetate: 27.4 Glucose: 41.0 Molasses: 41.0

The model considers biogeochemical reactions that involve alternative electron acceptors

and the presence of alternative minerals and metals (i.e., iron, sulfate). Table 5 details the

microbial energetic values used to calculate the expected substrate utilization and

maximum specific growth rates (μ_{max}). The microbial energetics information is used to

calculate the expected substrate-utilization rates and stoichiometry, as detailed in Table 4.

Within the model, two different nitrogen sources are considered: nitrate and ammonium.

Ammonium as a nitrogen source is more thermodynamically favorable, as shown by the

G_{pc} values in Table 3. Therefore, more electron equivalents of nitrate are needed to form

biomass than ammonium. The thermodynamic favorability of ammonium over nitrate is

reflected in the fraction of electrons going to energy generation (f_e^0) and fraction of

electrons going to biomass synthesis (f_s^0) values (Table 4) and subsequent μ_{max} values,

stoichiometry, and yield calculations Table 5. Growth is described in more detail in a later

section of this chapter.

Table 4. Microbial Energetics Expected During MIDP, Considering Acetate as the Electron Donor and Natural Electron Acceptors

Electron Acceptor	Nitrogen Source	G_r (kJ e$^-$ eq^{-1})	f_e^0	f_s^0	$\hat{q}$ (mol e$^-$ donor mol^{-1} biomass d^{-1})
Nitrate	Nitrate	-69.05	0.40	0.60	8.12
Nitrite	Nitrate	-119.96	0.28	0.72	11.69
Sulfate	Nitrate	-6.55	0.88	0.12	3.74
Nitrate	Ammonium	-69.05	0.47	0.53	6.95
Nitrite	Ammonium	-119.96	0.34	0.66	9.65
Sulfate	Ammonium	-6.55	0.90	0.10	3.63

Table 5. Stoichiometry, Yield (Y), and Maximum Specific Growth Rates (μ_{max}) Expected During MIDP, Considering Acetate as the Electron Donor and Natural Electron Acceptors

Electron Acceptor	Nitrogen Source	Y (mol biomass mol^{-1} e$^-$ donor)	μ_{max} (d^{-1})	Reaction
Nitrate	Nitrate	0.82	6.68	$0.222NO_3^- + 0.125C_2H_3O_2^- + 0.146H^+ \rightarrow 0.202NO_2^- + 0.147H_2CO_3 + 0.103CH_{1.8}O_{0.5}N_{0.2} + 0.021\,H_2O$
Nitrite	Nitrate	0.99	11.6	$0.054NO_3^- + 0.202NO_2^- + 0.270C_2H_3O_2^- + 0.525H^+ \rightarrow 0.101N_2 + 0.272H_2CO_3 + 0.268CH_{1.8}O_{0.5}N_{0.2} + 0.154H_2O$
Sulfate	Nitrate	0.58	2.18	$0.015NO_3^- + 0.072SO_4^- + 0.125C_2H_3O_2^- + 0.284H^+ \rightarrow 0.072H_2S + 0.177H_2CO_3 + 0.073CH_{1.8}O_{0.5}N_{0.2} + 0.015H_2O$
Nitrate	Ammonium	1.01	6.99	$0.236NO_3^- + 0.125C_2H_3O_2^- + 0.025NH_4^+ + 0.10H^+ \rightarrow 0.236NO_2^- + 0.124H_2CO_3 + 0.126CH_{1.8}O_{0.5}N_{0.2} + 0.050\,H_2O$
Nitrite	Ammonium	1.26	12.2	$0.235NO_2^- + 0.261C_2H_3O_2^- + 0.066NH_4^+ + 0.431H^+ \rightarrow 0.118N_2 + 0.193H_2CO_3 + 0.328CH_{1.8}O_{0.5}N_{0.2} + 0.249H_2O$
Sulfate	Ammonium	0.18	0.66	$0.113SO_4^- + 0.125C_2H_3O_2^- + 0.005NH_4^+ + 0.346H^+ \rightarrow 0.113H_2S + 0.227H_2CO_3 + 0.023CH_{1.8}O_{0.5}N_{0.2} + 0.009H_2O$

K_d and K_a values in the literature vary significantly due to the wide range of native environments of the microorganisms (e.g., sediment, estuarine water, wastewater) and the high degree of diversity of microorganisms able to carry out these reactions. K_d and K_a show variability for each electron donor and acceptor pair because wide ranges have been reported, even ranging multiple orders of magnitude (i.e., 10^{-3} to 10^{-5}) (Abdul-Talib et al., 2002; Papaspyrou et al., 2014; Vavilin & Rytov, 2015). These differences have been attributed to the original environment of the microorganisms (e.g., sediment, estuarine water, wastewater), experimental conditions and methods, and the microbial utilization of each respective donor and acceptor pair. Table 6 details the constants used as representative values for each K_d and K_a (recall Eq. 13) for the relevant electron-donor and -acceptor pairs, as reported by various literature sources. The values in Table 4Table 6 are from literature in which the experiments included the respective electron donor or acceptor. If a literature source gave K_a and K_d values, then this pair was used for each environment tested. Methanogenesis was not considered in this model because the methanogens are slow growing and much less energetically favorable compared to denitrifying and sulfate reducing bacteria.

Table 6. Half-maximum-rate Concentrations, K_d and K_a, Used for Each Electron-donor and -acceptor Pair

Electron Donor	K_d (mol L^{-1})	Source	Electron Acceptor	K_a (mol L^{-1})	Source
Acetate ($C_2H_3O_2^-$)	$1.0 \cdot 10^{-5}$	(Jia et al., 2020)	Nitrate (NO_3^-)	$5.4 \cdot 10^{-5}$	(Abdul-Talib et al., 2002)
Acetate ($C_2H_3O_2^-$)	$1.0 \cdot 10^{-5}$	(Jia et al., 2020)	Nitrite (NO_2^-)	$2.4 \cdot 10^{-5}$	(Abdul-Talib et al., 2002)
Acetate ($C_2H_3O_2^-$)	$7.1 \cdot 10^{-5}$	(Ingvorsen et al., 1984)	Sulfate (SO_4^-)	$2.00 \cdot 10^{-4}$	(Ingvorsen et al., 1984)

I_i is the generic term for each inhibition mechanism, i, that is attributed to each reaction. Literature values also vary significantly, depending on bacteria, experimental conditions, etc. The form of I_i is shown in Eq. 16 and it is for non-competitive inhibition:

$$I_i = \frac{K_i}{K_i + C_i} \qquad \text{Eq. 16}$$

where K_i is the inhibition constant (mol L^{-1}), and C_i is the concentration of the inhibiting species (mol L^{-1}). The inhibition coefficients are found in Table 7, and inhibition is further detailed in a later section.

Table 7. Non-competitive Inhibition Coefficients

Inhibiting Compound	Reduction Process Inhibited	K_I (mol L^{-1})	Source
HNO$_2$	Nitrate	$2 \cdot 10^{-6}$	(Ma et al., 2010)
HNO$_2$	Nitrite	$8 \cdot 10^{-8}$	(Glass et al., 1997)
NaCl	Nitrate, nitrite	0.51[a]; 0.78[b]	[a](Panswad & Anan, 1999); [b](Mariangel et al., 2008)
H$_2$S	Nitrate, nitrite	$6 \cdot 10^{-5}$	(Pan et al., 2019)
NO$_3^-$	Sulfate	$1 \cdot 10^{-3}$	(Veshareh et al., 2021)
NO$_2^-$	Sulfate	$1 \cdot 10^{-3}$	(Veshareh et al., 2021)

[a]Unacclimated environments were DI and drinking water, [b]Acclimated environments were groundwater and sea water

Microbial growth within the model is tracked via reaction stoichiometry and is expressed in Eq. 17, which describes how the net accumulation of active biomass (X_a) for each species (i.e., denitrifying or sulfate reducing bacteria) over time during consumption of the donor substrate.

$$\frac{dX_a}{dt} = X_a Y \hat{q} - b \qquad \text{Eq. 17}$$

where Y is the yield of biomass synthesis from consumed electron donor substrate (mol biomass mol^{-1} electron donor) and b is the endogenous decay coefficient (d^{-1}). The stoichiometry between biomass synthesis and donor utilization is Y, which is proportional to f_s^0, was determined thermodynamically (Rittmann & McCarty, 2020). The Y values are shown in Table 5. For sulfate reducing bacteria, b was assumed to be 0.03 d^{-1}, whereas it was assumed to be 0.05 d^{-1} for denitrifiers (Rittmann & McCarty, 2020). As a result of decay, NH_4^+ is released. This is used as the nitrogen source, which is thermodynamically favorable over NO_3^-. The half reaction for microbial decay of all species is shown below.

$$0.24CH_{1.8}O_{0.5}N_{0.2} + 0.60H_2O \rightarrow 0.24H_2CO_3 + 0.048NH_4^+ + 0.95H^+ + e^-$$
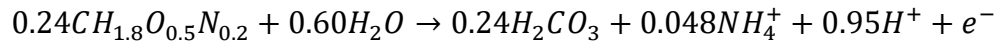
Decay involves endogenous respiration and it is assumed that 80% of decayed biomass is available as an electron donor and 20% becomes inert biomass. Further, it is assumed that the produced electron donor from decay is available as acetate, which allows for the consideration of energetically favorable reactions. The complete stoichiometric equation for decay is:

$$0.238CH_{1.8}O_{0.5}N_{0.2} + 0.012H_2CO_3 + 0.095H_2O$$
$$\rightarrow 0.125C_2H_3O_2^- + 0.048NH_4^+ + 0.077H^+$$
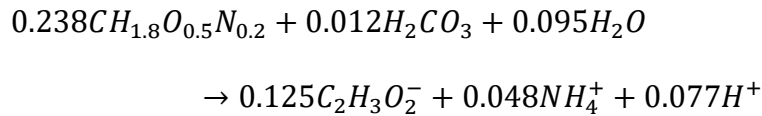
Inhibition

Denitrification inhibition can lead to very low nitrate and nitrite reduction rates and intermediate accumulation (i.e., not completing full denitrification to N_2) (Glass et al., 1997). Since the model does not include intermediate reductions steps of NO_2^- to N_2O and

N$_2$O to NO, inhibition was considered for reduction of nitrate to nitrite and nitrite to N$_2$ gas.

Several forms of inhibition could affect MIDP. The primary ones are intermediates accumulation, salinity, presence of hydrogen sulfide, and non-ideal pH levels (indicate non-ideal ranges here). Nitrite (NO$_2^-$) and nitrous acid (HNO$_2$) are well established inhibitors of denitrification (Abeling & Seyfried, 1992; Almeida et al., 1995; Estuardo et al., 2008; Glass & Silverstein, 1998; Glass et al., 1997). HNO$_2$ is by far the more significant inhibitor due to its toxicity, and inhibition from NO$_2^-$ is likely due to competition for the same electron donor (Lilja & Johnson, 2016). Significant inhibition to denitrification has been reported at 0.04 mg HNO$_2$ L^{-1} during NO$_2^-$ reduction (Abeling & Seyfried, 1992; Glass et al., 1997), and a 60% NO$_3^-$ reduction activity at 0.08 mg HNO$_2$ L^{-1} has also been reported (Ma et al., 2010). Within the model, HNO$_2$ inhibits NO$_3^-$ and NO$_2^-$ reductions using the same inhibition coefficient (Table 7). The inhibition of available HNO$_2$ is driven by pH speciation, because NO$_2^-$ is dominant at a pH of 3.4 and higher. HNO$_2$ is negligible in environments with a pH of 7.6 and higher. Since only small amounts of HNO$_2$ are required to have a significant impact on denitrification, promoting full denitrification demands that these denitrification intermediates not accumulate to inhibitory levels. pH estimation in the model is detailed in a later section of this chapter.

Competitive cross-inhibition between the nitrate and nitrite reductases has been identified, with the presence of nitrate having a larger effect on nitrite reduction than nitrite on nitrate reduction (Almeida et al., 1995; Glass & Silverstein, 1998; Lilja & Johnson, 2016; Soto et al., 2007). Glass and Silverstein (1998) showed that nitrite accumulation

69

increased in the presence of nitrate until nitrate was depleted, when nitrite reduction became the dominant process. When only nitrite remained, the rate of nitrite reduction increased. However, others have described that, so long as the electrons are adequately provided by the electron donor, competitive cross-inhibition between nitrate and nitrite reduction is not significant (Ma et al., 2010; Soto et al., 2007; van den Berg et al., 2017). Therefore, the model does not include competitive cross-inhibition.

Another well-documented inhibitor of denitrification is high salinity. Denitrification performance was found to be inhibited by up to 50% in wastewater having salinity of 15.2 g L^{-1} (Dincer & Kargi, 1999). The impacts of salinity (i.e., NaCl) on nitrate and nitrite reductions are not equal, and nitrite reduction is more sensitive to increased salinity (Mariangel et al., 2008). However, the magnitude of inhibition depends on experimental conditions and adaptation of the microorganisms (Krishna Rao & Gnanam, 1990; Zhu & Liu, 2017; Zhu, 2017). Sensitivity to saline conditions will be important for field deployment of MIDP in coastal regions and where surface water may mix with groundwater. However, the salinity effect may be mitigated if the denitrifying bacteria adapt to higher salt concentrations, as has been observed in long-running wastewater-treatment operations (Zhu & Liu, 2017). In practice, performing MIDP with injected water that has a significantly different salinity from what is in the native water of the target treatment zone should not be attempted because of significant inhibition of salinity on denitrification. Therefore, the model applies different inhibition constants for salinity (as NaCl) when the groundwater has high salinity (e.g., seawater) or low salinity (e.g., drinking water).

Hydrogen sulfide (H_2S) also can be inhibitory to denitrification (Pan et al., 2019). Nitrate, nitrite, and N_2O reduction have been reported to be particularly inhibited by H_2S, though the extent and sensitivity of reduction in the presence of H_2S is experiment-dependent (Cardoso et al., 2006; Liang et al., 2020; Pan et al., 2019; Pan et al., 2013; Senga et al., 2006; Tugtas & Pavlostathis, 2007). Within the model, one inhibition constant was used for NO_3^- and NO_2^- reduction steps.

Low pH (< 6) can significantly slow or impede complete denitrification (Glass & Silverstein, 1998) by inhibiting enzyme activity (Šimek & Cooper, 2002) and microbial growth (Estuardo et al., 2008). When the pH goes higher than 8, enzyme activity also can be impeded, leading to reduced denitrification rates or incomplete denitrification. Incidents of a high pH are temporary, as $CaCO_3$ precipitation in MIDP buffers the pH to about neutral. The benefit of including a pH inhibition function when predicting denitrification has been demonstrated, but the values of their governing parameters are environment-specific and require fitting (Estuardo et al., 2008). Within the model, I consider the indirect net effect of pH only through HNO_2 inhibition, which does not require environment-specific parameters.

Biogenic Gas Production

O'Donnell et al. (2019) considered the production of N_2 and CO_2 during denitrification but did not experimentally verify the concentrations of biogenic gas production. The relative concentrations of the produced biogenic gas can affect the distribution of gas at depth, since the gases have different solubilities as well as different stoichiometries for electron-donor consumption.

71

The next-generation MIDP model includes mass transfer kinetics for transfer of N_2, CO_2, and H_2S from the aqueous phase to the gas phase (or possibly in the opposite direction). The rate of transfer of a gaseous compound from the aqueous phase to the gas phase, $v_{i[g]}$ (mol L^{-1} d^{-1}), depends on whether it is super-saturated and the mass-transfer rate coefficient:

$$v_{i[g]} = k_l a \left(C_{i[g]} - \frac{C_{i[aq]}RT}{K_H} \right) \qquad \text{Eq. 18}$$

where k_La is the mass transfer rate constant (d^{-1}), $Ci[g]$ is the gas phase concentration of the gas species i, $Ci[aq]$ is the aqueous phase concentration of the biogenic gas species i, K_H is the Henry's Law constant (L atm mol^{-1}), R is the universal gas constant (8.21 10^{-2} L atm mol^{-1} K^{-1}), and T is the system's absolute temperature (K). It is assumed that the partial pressure was equal to the hydrostatic pressure and pore-scale gas kinetics (like bubble radius) were not considered. I assigned k_La values for N_2, CO_2, and H_2S of 5 d^{-1} (Yongsiri et al., 2004), though the exact values can vary widely and are experimentally and substrate medium dependent (e.g., if measured in a biofilm, or in a batch reactor). N_2, CO_2, and H_2S concentrations were modeled in the aqueous and gas phases. The aqueous concentration of each species impacted by pH-driven speciation is governed by the calculated pH, described later.

The biogenic gas volume needed to achieve a target level of desaturation by N_2 and CO_2 was determined by   Eq. 19:

$$[N_2]_g + [CO_2]_g = \frac{pS_g}{RT}$$

Eq. 19

where $[N_2]_g$ (mol L_{pore}^{-1}) and $[CO_2]_g$ (mol L_{pore}^{-1}) are the respective amounts of produced N_2 and CO_2 gas during MIDP, S_g (L_{gas} L_{pore}^{-1}) and p is the pressure (atm) at the treatment depth (e.g., 7.6 m in an upcoming example) and is equal to the sum of the hydraulic pressure at depth and the atmospheric pressure. H_2S is a gas that might contribute to desaturation at shallow depths or in environments with very high sulfate concentrations during denitrification, but gas-phase H_2S was not included in desaturation calculations because the solubility is much higher than N_2 and CO_2 and the expected amounts produced would not significantly add to desaturation at the deepest target depth.

Eq. 20 describes the amount of input NO_3^- required for desaturation by N_2 and CO_2 ($NO_3^-{}_d$, mol_{NO3} L_{pore}^{-1}) at the deepest target treatment depth, which is the lowest depth of the treated zone. The equation considers the amount of gas needed to overcome the solubility threshold to achieve the target level of desaturation. Eq. 20 follows work established work (C. Hall et al., 2018; Pham, 2017).

$$NO_3^-{}_d = \frac{\left(\frac{[N_2]_g}{l} + \frac{p_{N_2}}{K_{H,N_2}}\right) Y_{NO_3^-}}{Y_{N_2}} + \frac{\left(\frac{[CO_2]_g}{l} + \frac{p_{CO_2}}{K_{H,CO_2}}\right) Y_{NO_3^-}}{Y_{CO_2}}$$

Eq. 20

where l (L_{aq} L_{pore}^{-1}) considers the amount of solution in the pore space; p_{N_2} (atm) and p_{CO_2} (atm) are the partial pressures of nitrogen and carbon dioxide gasses; $K_{H,N2}$ (L_{aq} atm$_{N2}$ mol_{N2}^{-1}) is the Henry's constant for N_2 at standard temperature and was assumed to be 1600; and, $K_{H,CO2}$ (L_{aq} atm$_{CO2}$ mol_{CO2}^{-1}) is the Henry's constant for CO_2 at standard

temperature and was assumed to be 29; and Y_{NO3-} (mol_{NO3-}/mol_{donor}), Y_{N2} (mol_{N2}/mol_{donor}), and Y_{CO2} (mol_{CO2}/mol_{donor}) are the stoichiometric coefficients of N_2, NO_3^-, and CO_2 during denitrification, respectively. The lowest depth is the critical depth defining the amount of treatment that would be required to promote adequate liquefaction mitigation over the entire treatment depth, because greater depth requires a higher concentration of gas to achieve target desaturation levels, as the pressures (p values) are at their maxima. The actual amount of CO_2 that contributes to desaturation will be driven by the environment's biogeochemistry and other biogeochemical processes. For treatment substrate recipe calculations, CO_2 was estimated based on stoichiometry and pH-driven speciation assuming a neutral pH.

Eq. 21 is used to determine the biogenic gas volume over the total soil volume (V_g, $L_{gas} L_{tot}^{-1}$),

$$V_g = \frac{S_g RT\varphi}{p}$$ Eq. 21

where, φ is the soil porosity ($L_{pore} L_{total}^{-1}$).

Solids Precipitation and Dissolution

Precipitation occurs when dissolved inorganic carbon (DIC) produced from microbial substrate conversion of the electron donor exceeds the solubility of $CaCO_3$ for the concentration of Ca^{2+} present. The stoichiometry for $CaCO_3$ precipitation is:

$$Ca^{2+} + H_2CO_3 \rightarrow CaCO_3 + 2H^+$$
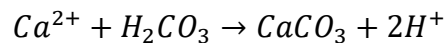
The van Turnhout Toolbox considers precipitation based on equilibrium calculations from the ORCHESTRA module (Meeussen, 2003). The van Turnhout toolbox assumed that the rates of precipitation and dissolution of minerals are much quicker than the phase transfer between the aqueous and gas phases (Salek et al., 2015); thus, it is possible to ignore precipitation and dissolution kinetics. Likewise, previous MIDP modeling efforts did not consider precipitation kinetics, but assumed instantaneous equilibrium (Pham, 2017; O'Donnell et al., 2019). Instantaneous equilibrium may be an over-simplification for environmental conditions (Singurindy et al., 2004) that affect crystal nucleation, crystal surface area, reactant absorption, and mass transfer of reactants to the contact point of crystal growth (Rittmann et al., 2002). Therefore, the next-generation model includes precipitation and dissolution kinetics.

The next-generation model considers first-order precipitation and dissolution kinetics with respect to the Ca^{2+} concentration (Rittmann et al., 2002):

$$R_p = ka \left(1 - \frac{K_{sp}}{[Ca^{2+}][CO_3^{2-}]} \right) [Ca^{2+}] \qquad \text{Eq. 22}$$

where R_p is the net rate of precipitation ($R_p > 0$) or dissolution ($R_p < 0$) of minerals (mol L^{-1} d^{-1}), ka is the combined coefficient considering a constant mineral growth rate and the average crystal surface area (L d^{-1}), K_{sp} is the constant solubility product ($1.83 \cdot 10^{-8}$ mol^2 L^{-2} as 25°C), and the use of brackets, [ ], indicates component concentration (mol L^{-1}). ka is a combined coefficient because it is difficult to separate the growth rate from the solid surface area and can vary widely, ranging multiple orders of magnitude (Rittmann et al., 2003; Rittmann et al., 2002; Spanos & Koutsoukos, 1998); ka was assumed to be

100 L d^{-1}, though this value should be evaluated in future experimentation for MIDP in soil.

Precipitation was implemented using the van Turnhout Toolbox's existing method for introducing biochemical reactions. *ka* is specified by the user as a reaction rate and K_{sp} is listed among the other governing parameters within the input spreadsheet. Precipitation kinetics is activated within the input spreadsheet and the kinetic equation is included in the code of the van Turnhout Toolbox.

Eq. 23 was used to determine the amount of substrate needed to achieve a target precipitation level, which is determined by the ratio between mass of precipitated CaCO$_3$ and mass of the soil solids (*[CaCO$_3$]*, kg CaCO$_3$ kg soil^{-1}).

$$[NO_3^-]_c = \frac{[CaCO_3]\rho_{soil}Y_{NO_3^-}}{eu_{CaCO_3}Y_{CaCO_3}}$$

Eq. 23

where Y_{CaCO3} (mol CaCO$_3$ mol$_{donor}^{-1}$) is the estimated amount of CaCO$_3$ that is precipitated from available DIC produced from MIDP; $[NO_3^-]_C$ (mol L$_{pore}^{-1}$) is the amount of NO$_3^-$ needed to achieve the target CaCO$_3$; e (L$_{pore}$ L$_{soil}^{-1}$) is the void ratio; ρ_{soil} (g soil L$_{soill}^{-1}$) is the density of the soil in the total treated area and was obtained from the unit weight of soil (kN L$_{soil}^{-1}$); and u_{CaCO3} is the molarity to molecular weight conversion coefficient for CaCO$_3$ (g CaCO$_3$ mol^{-1} CaCO$_3$). The stoichiometric coefficients consider the total amount of input NO$_3^-$ and produced H$_2$CO$_3$ for the total assumed two-step denitrification process. The DIC available for precipitation to provide Y_{CaCO3} is estimated based on pH-driven speciation at equilibrium in neutral conditions because expected groundwater and surface water pH measurements are circumneutral pH levels. Available DIC for precipitation is pH

76

dependent and is determined within the model. The amount of electron donor needed is estimated using the stoichiometric coefficients for NO_3^- and each electron donor.

pH Determination

Because pH governs the concentration of aqueous species based on acid/base speciation, the concentration of protons influences many of the geochemical reactions involved in MIDP. The pH is determined based on a fully coupled module that considers the rate-dependent biogeochemical processes, kinetic processes, and pH-driven species equilibrium. This is done using the geochemical equilibrium software ORCHESTRA, which has been incorporated into the van Turnhout Toolbox. This coupling uses a mass balance on all species already within the system and the products of rate-dependent processes as a function of time (i.e., kinetic, biogeochemical, and phase transfer processes). At each time step, the program performs a mass balance on all subsequent derived species (or the complex species) and their fate. The program's logic flow and calculation sequence are as follows (Meeussen, 2003; van Turnhout et al., 2016), using H_2CO_3, HCO_3^-, CO_3^{2-}, H^+, and OH^- to illustrate the process.

1. At $t = 0$, the program loads the input concentrations file, which includes the concentration of all total species (e.g., H_2CO_3 representing DIC, H^+) and the stoichiometry for metabolic and kinetic reactions: e.g.,

$$0.222NO_3^- + 0.125C_2H_3O_2^- + 0.146H^+$$
$$\rightarrow 0.202NO_2^- + 0.147H_2CO_3 + 0.103CH_{1.8}O_{0.5}N_{0.2} + 0.021\,H_2O$$
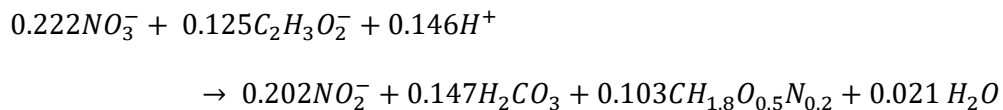
2. Ordinary differential equations are used to determine compound consumption and production based on the reaction stoichiometry and kinetic equations (i.e., precipitation and mass transfer) at each time step. The graphic below illustrates that, as $C_2H_3O_2^-$ is consumed from microbial consumption, H_2CO_3 is produced.
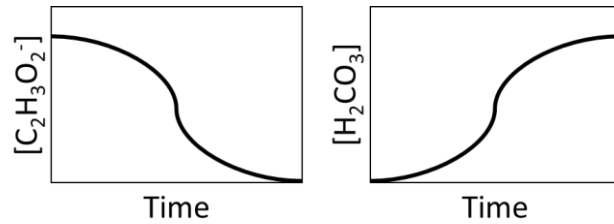
3. At each time step, the following set of linear equations are solved to determine the relative derived concentrations of H_2CO_3, HCO_3^-, CO_3^{2-}, H^+, and OH^- from H_2CO_3 produced in the previous steps. This is done in the ORCHESTRA biochemical module.

   a. Mass balance equations – the left side of the equation is the total dissolved inorganic carbon, H_2CO_3, from the stoichiometry described in steps 1 and 2. The right side are the derived concentrations of species as a result of speciation and indicated with italics.

$$H_2CO_3 = H_2CO_3 + HCO_3^- + CO_3^{2-}$$
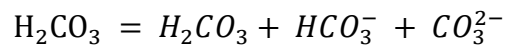
   b. Electroneutrality – all potentially produced charged species related to this balance are considered.

$$H^+ = OH^- + HCO_3^- + CO_3^{2--}$$
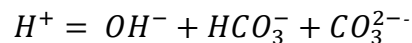
   c. Acid equilibrium for H_2CO_3

78

$$K_a = \frac{[CO_3^{2-}][2H^+]}{[H_2CO_3]}$$

    d. Acid equilibrium for HCO_3^-

$$K_a = \frac{[CO_3^{2-}][H^+]}{[HCO_3^-]}$$

    e. Water equilibrium

$$K_w = [OH^-][H^+] = 1.0 \cdot 10^{-14}$$

4. pH is calculated based on the derived H^+ concentration.

While the carbonate system is used here as an example, this stepwise process is used for all acid-base species and considers the total system set of reactions and species to achieve equilibrium. The total system electroneutrality considered in the model for all considered species is as follows:

$$\begin{aligned}
H^+ + NH_4^+ + Ca^{2+} &+ CaHCO_3^+ + CaOH^+ + CaC_2H_3O_2^+ + Fe^{3+} + Fe^{2+} + FeOH^+ \\
&+ Fe(OH)_2^+ + Na^+ \\
&= OH^- + HCO_3^- + CO_3^{2-} + NO_3^- + NO_2^- + C_2H_3O_2^- + SO_4^{2-} + HSO_4^- \\
&+ HS^- + Cl^-
\end{aligned}$$
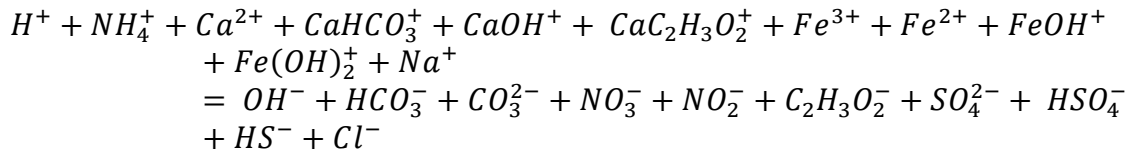
These compounds are user defined in the input spreadsheet, but are used within the model by Orchestra using the Minteq4 chemical database to determine species complexation.

Case Study: Desaturation and Precipitation Target Treatments

To illustrate MIDP behavior when targeting desaturation or calcium carbonate precipitation, I consider a coastal geochemical environment. Table 8 details the chemical characteristics used to reflect coastal conditions. Any treatment substrate is added to the baseline level of these components.

Table 8. Chemical Conditions Assumed for a Coastal Seawater Environmental Conditions When Using the MIDP Model

Compound	Coastal Seawater
Nitrate	20.3[1] μmol L^{-1}
Nitrite	0.14[1] μmol L^{-1}
Sulfate	28.2[2] mmol L^{-1}
DIC	2.13[1] mmol L^{-1}
pH	7.61[1]
Ammonium	0.25[1] μmol L^{-1}
Iron	0.60[3] nmol L^{-1}
Sodium	0.47[2] mol L^{-1}
Calcium	10.3[2] mmol L^{-1}
Chloride	0.55[2] mol L^{-1}

[1]Average of measured values (Alin et al., 2016)
[2]Reference composition of "standard seawater" from and calculated for pH = 7.61 for acid-base species (Dickson, 2010; Millero et al., 2008)
[3] (Bruland et al., 2001)

The target treatment zone's soil properties are based on a hypothetical case presented at the September 2019 National Hazard Engineering Research Infrastructure (NHERI) workshop in Portland, Oregon (NHERI, 2019). The deepest target treatment depth is 7.6 m, and the soil is uniform clean sand. The soil properties are assumed to be total unit weight of 19.5 kN m^{-3} (dry unit weight of 15.6 kN m^{-3}; bulk density of 1950 kg m^{-3}) and porosity of 0.39, based on typical values for uniform clean sand (Christopher et al., 2006).

Reported levels of desaturation required to increase the cyclic shear resistance for liquefaction mitigation range between 2 and 10%, when aiming for desaturation as the primary treatment mechanism (He & Chu, 2014; O'Donnell, Rittmann, et al., 2017). Achieving stable desaturation of 10% should be feasible, because the maximum desaturation before gas starts to migrate upward or spread laterally begins at 20% for poorly graded (i.e., uniform) fine sands (Pham, 2017), although migration variability depends on the site's geology and stratigraphy (van Paassen et al., 2017). Therefore, I

selected a desaturation level of 10% as the target at the deepest target liquefiable depth, though this might not represent the needed desaturation to mitigate liquefaction triggering in a different target environment. For example, in an environment with historically strong shaking events, more desaturation might be desirable to potentially provide a stronger defense against liquefaction mitigation.

When targeting liquefaction mitigation by $CaCO_3$ precipitation, several factors influence the relationship between soil strength and precipitation, including initial soil density, grain size, treatment additives, and degree of saturation (Cheng & Cord-Ruwisch, 2012; El Mountassir et al., 2018). Liquefaction has been shown to be significantly mitigated if the soil's cyclic shear strength is improved by precipitation of $1 - 2\%$ $CaCO_3$ (by mass) (O'Donnell, Kavazanjian, et al., 2017). Conservatively, I assumed that the needed precipitation to provide the degree of improvement necessary is 3%, though this might be excessive or insufficient depending on the liquefaction mitigation needs of a location. For example, denser soil or soil with more fines may need less $CaCO_3$ precipitation to sufficiently reduce the potential for liquefaction triggering.

MIDP Behavior in Seawater Conditions: Model Results and Discussion

MIDP Treatment Mechanism: Desaturation

In order to meet a target desaturation level of 10% for mitigating liquefaction in the example case environment, I estimated that 22.4 mmol L^{-1} of nitrate (1.84 g calcium nitrate L^{-1}) and 32.1 mmol L^{-1} of acetate (2.54 g calcium acetate L^{-1}) were needed as a baseline (using Eq. 20). However, based on background levels of nitrate and nitrite and the use of

ammonium as a nitrogen source, these levels were empirically adjusted to match these factors and these methods and the impact of matching the recipe are detailed further in Chapter 6. The input recipe used for analysis was 19.0 mmol L^{-1} of nitrate (1.56 g calcium nitrate L^{-1}) and 22.4 mmol L^{-1} of acetate (1.77 g calcium acetate L^{-1}) and this does not include the background concentrations of nitrate and nitrite.

The results of this treatment recipe on the subsurface gas volume and saturation profile are shown in Figure 12. Even with competing species for coastal seawater conditions, the target desaturation level of 10% at 7.6 m (or a degree of saturation of 90%) was achieved by N_2 in approximately 2.1 days. Therefore, the estimated amount of substrate was adequate to produce the desired levels of desaturation. The amount of CO_2 produced did not reach the saturation threshold dictated by Henry's Law and remained in the aqueous phase, and CO_2 did not contribute to desaturation at any of the modeled depths. Meeting the target treatment level lagged nitrate reduction, discussed later, because of the mass transfer kinetics from aqueous to gas phase.
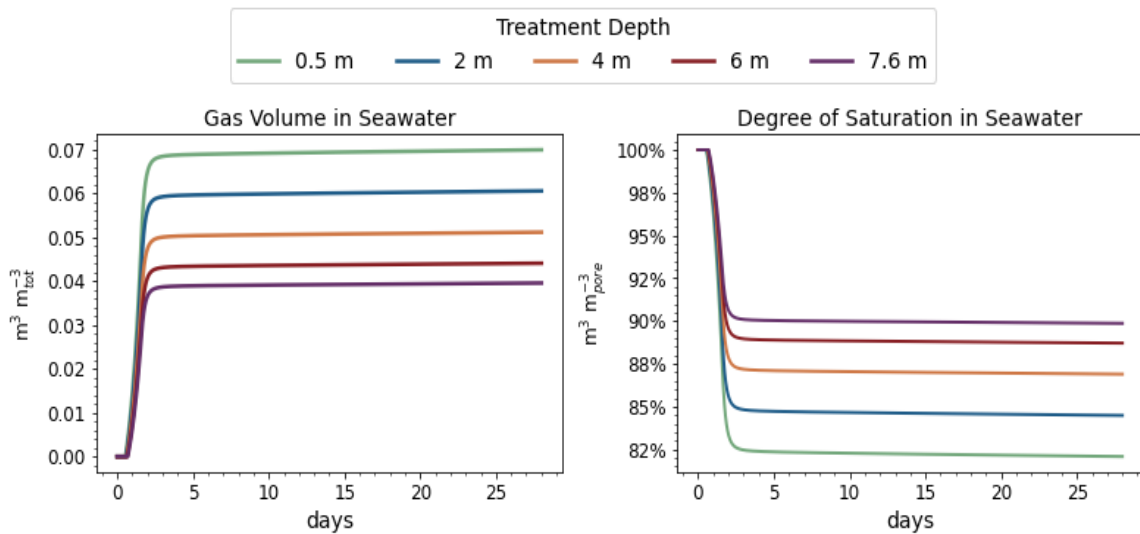
Figure 12. Gas Volume for the Total Soil Volume and Degree of Saturation from MIDP in Coastal Seawater Conditions Targeting a Desaturation Level of 10%.

The impact of the MIDP treatment over 28 days is shown in Figure 13, and the initial 3 days are highlighted in Figure 14. By 1.6 days, almost all nitrate and MIDP intermediates (nitrate and nitrous acid) were consumed, N_2 was produced in aqueous and gas phases, and only $1 \cdot 10^{-4}$ mol L-1 of acetate remained. This indicates that N-intermediate accumulation was transient, with complete denitrification achieved with this treatment recipe in coastal seawater conditions. Denitrification was the dominating process until all nitrate and nitrite species were reduced. After 1.6 days, sulfate reduction began and continued to occur using the products from microbial decay (i.e., electron donor, carbon source) the rate of which gradually increasing over time, resulting in a production of more DIC and gas-phase CO_2 over time.

Figure 13. Results over 28 Days for the Biogeochemical Batch Model for MIDP in Coastal Seawater Conditions Targeting a Desaturation Level of 10%.

Figure 14. Results over the First 3 Days for the Biogeochemical Batch Model for MIDP in Coastal Seawater Conditions Targeting a Desaturation Level of 10%.

Nitrite reduction produces most of the base, which is demonstrated by the spike in pH at between 1.3 and 1.6 days (Figure 14), when the rate of nitrite reduction is at its maximum. After 1.6 days, the pH returns to about circumneutral to precipitation of calcium carbonate, which consumes base. This trend is reinforced by rapid calcium consumption (Figure 14) and production of $CaCO_3$ in the first ~ 2 days, shown in Figure 15. Microbial decay coupled to sulfate reduction also produced DIC, promoting additional $CaCO_3$ precipitation after the completion of denitrification (after day 2 in Figure 15). However, less than 0.1% $CaCO_3$ was produced, which means that cementation did not contribute significantly to strength needed for liquefaction mitigation (O'Donnell, Kavazanjian, et al., 2017).
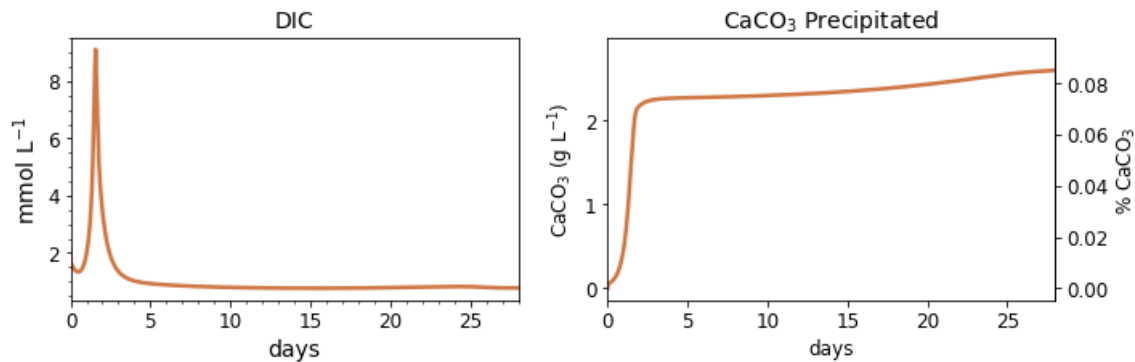
Figure 15. Concentration of $CaCO_3$ Precipitated and the Ratio of g of Precipitated $CaCO_3$ to g of Soil, Represented in %, During Targeted Desaturation.

MIDP Treatment Mechanism: Precipitation

In order to meet a conservative target $CaCO_3$ precipitation level of 3% to mitigate liquefaction via mineral precipitation in the case environment, I estimated that 803 mmol L^{-1} of nitrate (65.9 g calcium nitrate L^{-1}) and 1150 mmol L^{-1} of acetate (90.8 g calcium acetate L^{-1}) were needed (Eq. 23). However, these concentrations of substrate have been demonstrated to be inhibitory to denitrifying microorganisms (Pham, 2017), and would

have to be added in flushes or stages in real experimental circumstances, assuming that the permeability reduction by MIDP did not compromise the ability to deliver additional flushes directly targeted at carbonate precipitation. As mentioned earlier when exploring desaturation, the baseline substrate estimation did not account for alternative nitrogenous sources for growth, the background levels of nitrate and nitrite, and the amount of DIC that speciated to CO_2 than was available for precipitation due to the lower pH and is explored further in Chapter 6. The input recipe considers these factors and was empirically determined to be 803 mmol L^{-1} of nitrate (65.9 g calcium nitrate L^{-1}) and 1253 mmol L^{-1} of acetate (99.0 g calcium acetate L^{-1}), such that a 3% $CaCO_3$ precipitation and complete denitrification were achieved without excess acetate. This is 42 times the amount of nitrate and 56 times the amount of acetate needed for liquefaction mitigation via desaturation.

For coastal seawater conditions, the target precipitation of 3% was achieved after about 3 days, as shown in Figure 16. Therefore, the estimated amount of substrate led to adequate precipitation levels. Precipitation lagged denitrification because of relatively slower precipitation kinetics; this trend also occurred when targeting desaturation (Figure 15). The rate of precipitation in Figure 16 is higher compared to what was reported to achieve adequate precipitation via MIDP: on the order of weeks in sand column experimentation (O'Donnell, Kavazanjian, et al., 2017). Conversely, others have demonstrated more rapid precipitation rates during column experimentation, though the modeled results shown in this study still are about 4 times higher than what was experimentally observed (Pham, 2017). The predicted fast kinetics likely are related to the model assumption that the reactants are well-mixed and readily available to precipitate to

87

CaCO₃, whereas sorption may occur in lab experimentation. Further, the *ka* value assumed in the model may lead to over-estimations of the actual rate of mineral growth via MIDP. When the *ka* value is lowered, the pH increases well beyond what has been measured in the laboratory tests, though the precipitation rates are closer to what has been seen during experimentation. Potential model fitting should be explored further to find a balance between experimentally observed pH and precipitation trends, though this may be challenging because there is no strong consensus of precipitation rates (O'Donnell, Kavazanjian, et al., 2017; Pham, 2017).
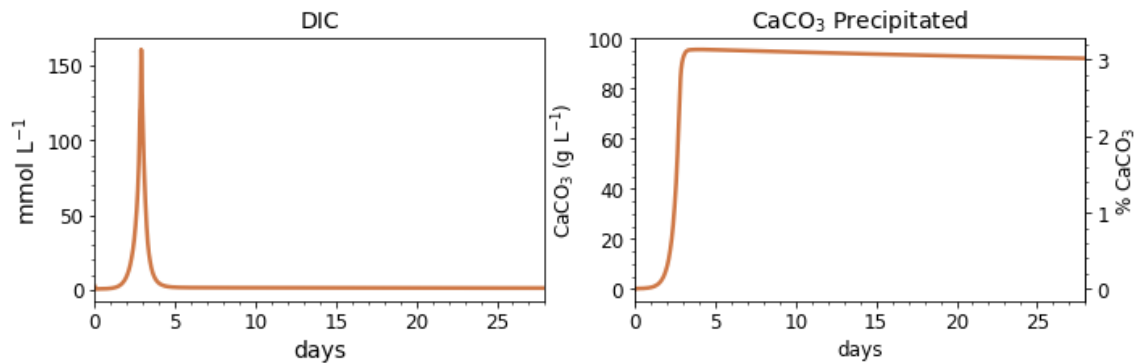
Figure 16. Concentration of CaCO₃ Precipitated and the Ratio of g of Precipitated CaCO₃ to g of Soil, Represented in %, During Targeted Precipitation.

The impact of the MIDP treatment over 28 days is shown in Figure 17, and the initial 10 days are highlighted in Figure 18. By nearly 3 days, the system underwent complete denitrification, which was the dominating biochemical process. Even with the higher substrate concentrations in the precipitation recipe, N-intermediate accumulation was temporary, and denitrification was complete for the coastal seawater conditions.
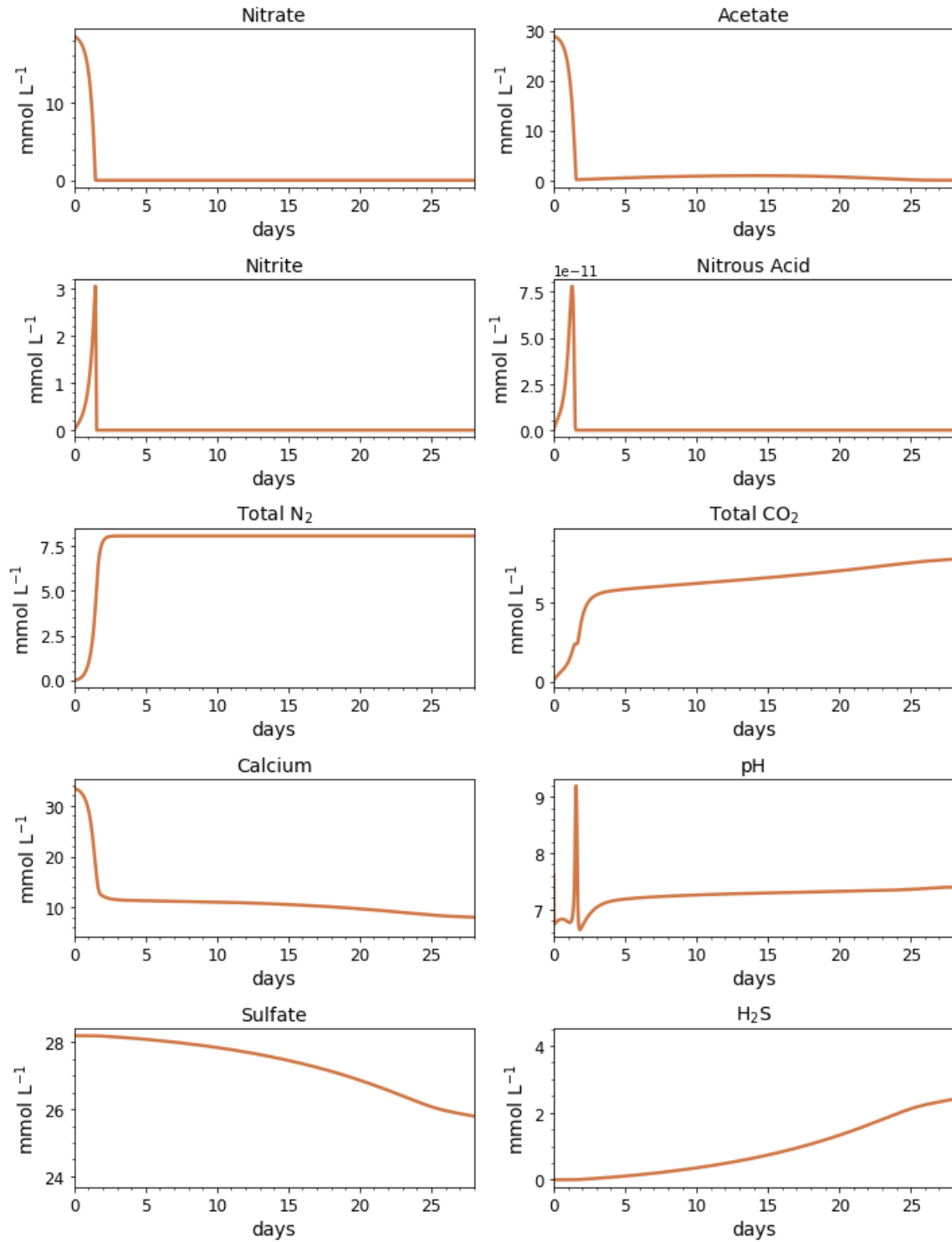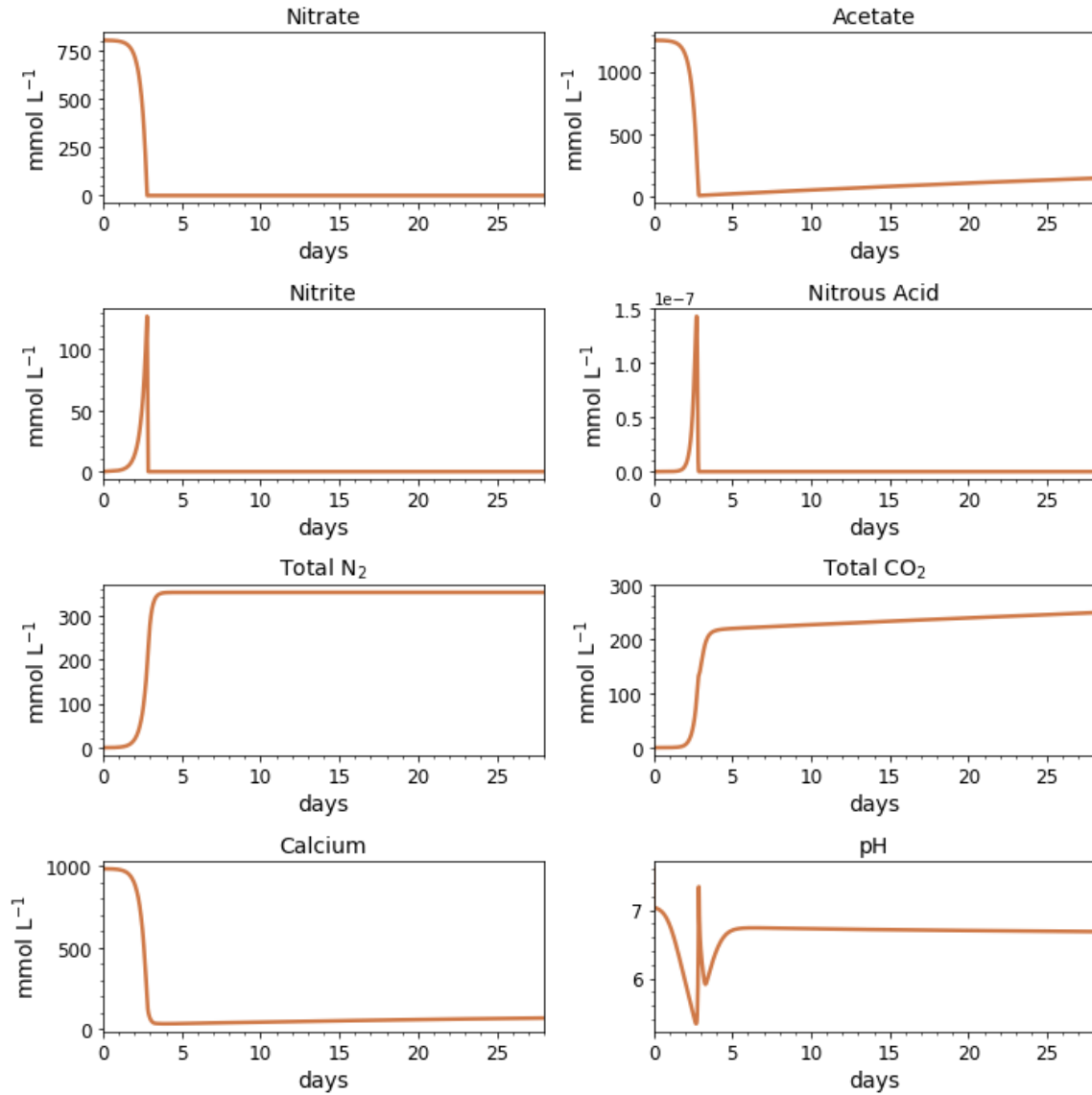
Figure 17. Results over 28 Days for the Biogeochemical Batch Model for MIDP in Coastal Seawater Conditions Targeting a CaCO₃ Precipitation Level of 3%.
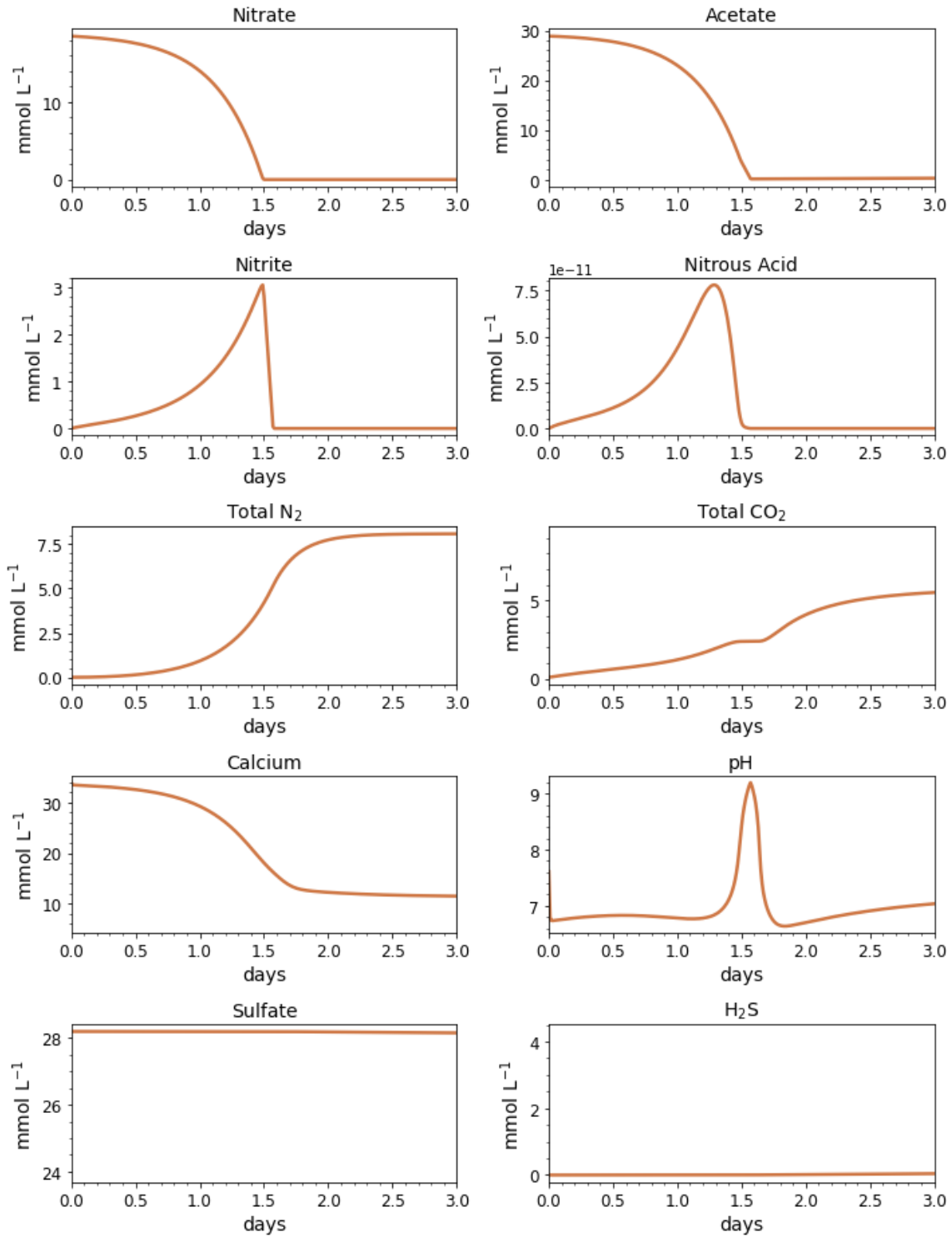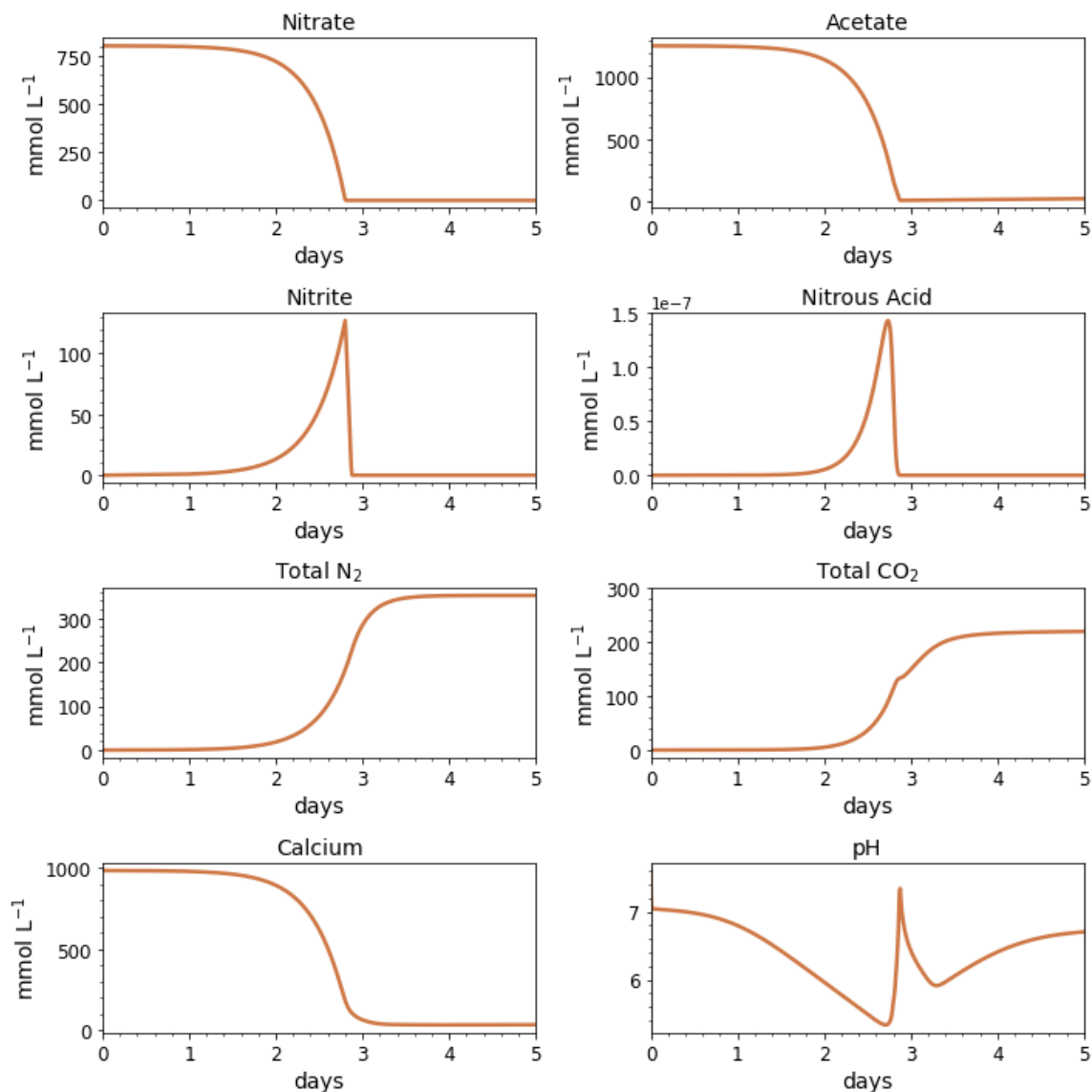
Figure 18. Results Over the First 10 Days for the Biogeochemical Batch Model for MIDP in Coastal Seawater Conditions Targeting a $CaCO_3$ Precipitation Level of 3%.

The sharp drop of pH during the initial stages of nitrate reduction coincided with a sharp increase of accumulated nitrite (Figure 17). The pH spiked up at the time of maximum nitrite reduction due to the production of base (~ day 3), which also facilitated a pH that favored $CaCO_3$ precipitation. Then, the pH returned to circumneutral once all nitrite had been reduced and the rate of $CaCO_3$ precipitation was at its highest and able to

buffer the pH. When the dominating biochemical process switches from denitrification to sulfate reduction, as facilitated by endogenous respiration, the pH again rises due to the production of base during sulfate reduction.

After 3 days, sulfate reduction continued to occur steadily because the consumption of nitrate and nitrite no longer posed as an inhibition to sulfate reduction, as shown in Figure 19. All the sulfate was reduced at about 52 days due to endogenous respiration. H_2S, DIC, and CO_2 continued to be produced during this period of sulfate reduction. In contrast to the scenario targeting desaturation, much more biomass is produced, and the electrons gained from decay lead to a high degree of sulfate reduction over time.
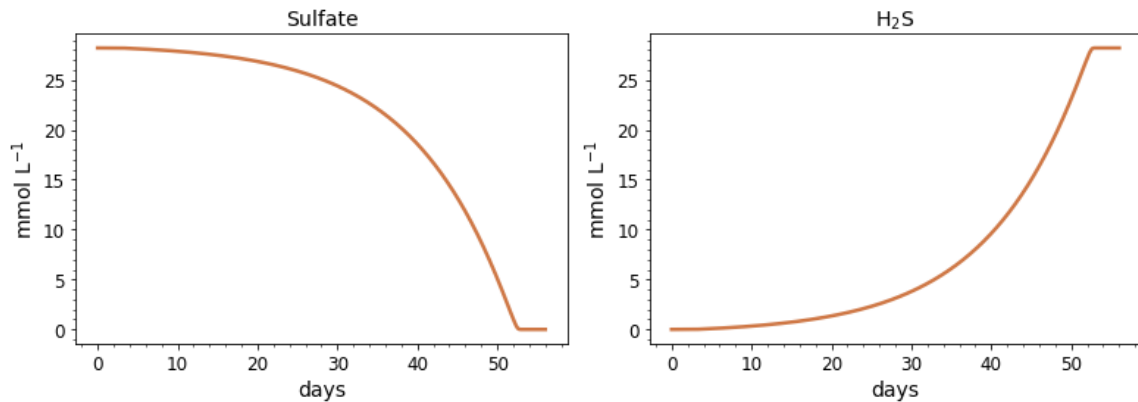
Figure 19. Batch Results over 56 Days for Sulfur Species for Biogeochemical Modeling of MIDP in Seawater Targeting a Precipitation Level of 3%.

The amount of biogenic gas produced when reaching sufficient mineral precipitation is inconsistent with physical system restraints. The amounts of N_2 and CO_2 gas produced during precipitation of 3% $CaCO_3$ exceeded the maximum amount of gas that can be produced in the subsurface without needing to vent it. N_2 and CO_2 contribute to the volume of biogenic gas and the corresponding degree of saturation, shown in Figure 20. The maximum amount of allowable gas is the volume of pore space in the soil, in

which at 1 m^3 gas m^{-3} pore the pore space is completely full of biogenic gas. At the deepest target treatment depth (7.6 m in the presented case), where gas saturation will be lowest due to the overburden pressure, the amount of gas produced was nearly 8 times the available pore space. At shallowest illustrated depth, 0.5 m, the amount of gas produced was nearly 14 times that of the available pore volume by the amount of substrate required to precipitate 3% CaCO$_3$.
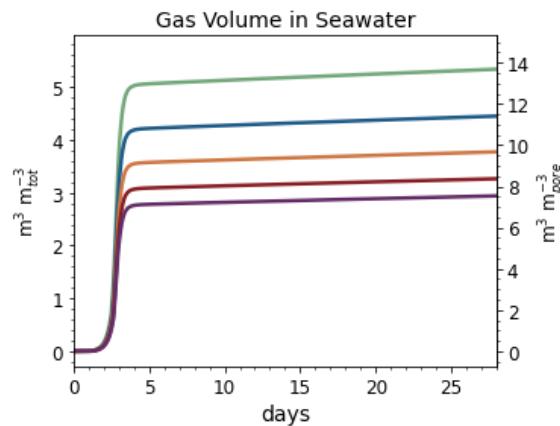
Figure 20. Gas Volume for the Total Soil Volume and for the Total Pore Volume from MIDP in Seawater Conditions Targeting a CaCO$_3$ Precipitation of 3%.

Here, I assumed one high-concentration treatment to achieve the theoretical needed precipitation levels, but the amount of produced gas greatly exceeds the amount of available pore space of the soil and is not reasonable considering realistic conditions, like gas venting and gas migration. One possible strategy to mitigate the problem of excessive gas formation is using multiple additions (flushes) of nitrate and donor. However, the same amount of gas would be produced ultimately, thereby still exceeding the available pore space of the soil. A venting mechanism still would be required. An additional complication is that, as gas is produced during each flush, the hydraulic conductivity of the soil would decrease due to accumulation of biogenic gas, calcium carbonate, and biomass.

While it may be possible to vent the excess gas, the other clogging mechanisms are not readily relieved. Therefore, this modeling results suggests that the precipitation part of MIDP may be impractical, although the desaturation part appears to be viable.

Conclusions

I expanded previous biogeochemical models for MIDP by considering metabolic, mass transfer, and kinetic reactions, microbial competition, by-product inhibition, and compound speciation and thermodynamic equilibrium. My next-generation model now can predict changes to the subsurface environment by MIDP products and by-products and indicate how these changes affect the success of MIDP. For example, the model can predict the required amount of substrate needed when targeting either desaturation or precipitation as the primary mechanism for liquefaction mitigation. Based upon a hypothetical example, the model's outputs suggest that desaturation is a viable mitigation goal because biogenic gas generation far exceeds the available pore space of the soil, but precipitation may not be feasible due to the impact of gas and biomass generation on hydraulic conductivity.

The model also allows me to look at how MIDP progresses. For example, aiming for precipitation requires a much greater amount of substrate than what is needed for desaturation. The resulting biomass growth and, later, biomass decay promote unwanted sulfate reduction that leads to the undesired accumulation of H_2S and continued pH increase. These aspects must be considered to ensure future successful applications of MIDP in large-scale field conditions. The following two chapters utilize the model developed herein to investigate MIDP considering different environmental conditions and

treatment recipes. Chapter 6 compares MIDP behavior and the process environmental impacts using groundwater and coastal seawater as the source-water for substrate dilution. Chapter 7 investigates the MIDP products and by-products if different electron donors (i.e., acetate, glucose, and molasses) are used as the treatment recipe.

CHAPTER 6

EFFECTS OF DIFFERENT SOURCE-WATER CONDITIONS ON MIDP

When considering the feasibility of deploying MIDP for the range of potential environmental conditions, the impact of local conditions on MIDP, and vice versa, must be investigated. In particular, MIDP can be sensitive to source-water conditions. Conditions that lead to accumulation of nitrous acid, such as low pH values (Almeida et al., 1995; Glass & Silverstein, 1998), may lead to incomplete denitrification. Furthermore, while denitrification is expected to be the dominant respiration process in the subsurface, other electron acceptors (e.g., SO_4^{2-}) may compete for the added electron donor and lead to unwanted by-product formation (e.g., H_2S) (Yamamoto-Ikemoto et al., 1996). I used the next-generation biogeochemical model and methods described in Chapter 5 to predict the impact of source-water conditions on MIDP and how MIDP can affect local water quality. These evaluations lead to recommendations for successful field deployment.

Comparing Source-water Conditions

To investigate the impact of source-water conditions on MIDP, I considered two distinct source-waters that are representative of potential conditions at sites where MIDP is likely to be deployed: groundwater and seawater. I chose these source waters because they are relevant for saturated environments at risk for liquefaction and thus of locations where MIDP may be employed (DeJong et al., 2010; O'Donnell, Rittmann, et al., 2017; Silva et al., 2018). I anticipate that, in the field, groundwater would be pumped out and used to as the source-water to dilute the substrates for MIDP treatment. The MIDP substrate-native water solution would then be pumped back into the target treatment zone. The source-

water compositions are detailed in Table 9. These values are intended to be representative values and are mostly the averages of reported values for groundwater and seawater in geospatially different locations.

The source-water composition for each water source is found in Table 9. Dissolved inorganic carbon (DIC) is the sum of H_2CO_3, HCO_3^-, and CO_3^{2-}. These baseline values do not reflect any added treatment substrate.

Table 9. Source-water Compositions Used for the MIDP Model.

Compound	Groundwater[4]	Coastal Seawater
Nitrate	0.34 mmol L^{-1}	20.3[1] µmol L^{-1}
Nitrite	0.85 µmol L^{-1}	0.14[1] µmol L^{-1}
Sulfate	0.61 mmol L^{-1}	28.2[2] mmol L^{-1}
DIC	3.25 mmol L^{-1}	2.13[1] mmol L^{-1}
pH	7.02	7.61[1]
Ammonium	7.19 µmol L^{-1}	0.25[1] µmol L^{-1}
Iron	0.01 µmol L^{-1}	0.60[3] nmol L^{-1}
Sodium	2.20 mmol L^{-1}	0.47[2] mol L^{-1}
Calcium	1.21 mmol L^{-1}	10.3[2] mmol L^{-1}
Chloride	1.52 mmol L^{-1}	0.55[2] mol L^{-1}

[1]Average of measured values (Alin et al., 2016)
[2]Reference composition of "standard seawater" from and calculated for pH = 7.61 for acid-base species (Dickson, 2010; Millero et al., 2008)
[3] (Bruland et al., 2001)
[4] pH and DIC (as carbonate and bicarbonate) considered field measurements only, all else considered all measurement methods (Arnold et al., 2020)

Using source water with characteristics most compatible with the natural environment is necessary to minimize environmental impacts and to promote successful application of MIDP. For example, adding highly saline waters into a non-saline environment may lead to microbial inhibition, thereby slowing or preventing MIDP, because the indigenous denitrifiers are not acclimated to highly saline water (Zhu & Liu, 2017). Furthermore, using source-water with a high concentration of electron acceptors

may lead to unwanted by-products and potential inhibition of denitrifiers (Pan et al., 2019). Groundwater and soil contamination (e.g., hydrocarbon) was not considered in this model because of the wide-ranging potential impacts on MIDP, including acting as an inhibitor or as an alternative electron donor. The model can be augmented to include contaminating compounds found during site exploration.

To design the MIDP treatment plan for the two source water conditions, I adapted the liquefiable-soil case study presented at the September 2019 National Hazard Engineering Research Infrastructure (NHERI) workshop in Portland, Oregon and detailed in Chapter 5 (NHERI, 2019). I assumed that the geology and physical characteristics (i.e., porosity, treatment volume) were the same for each condition, but source-water quality changed for each considered environment. The subsurface in each environment was assumed to be at 100% saturation initially.

Following the methods described in Chapter 5, I established the baseline substrate requirements to achieve a desaturation level of 10% (i.e., saturation of 90%) at a 7.6-m depth to be 22.4 mmol L^{-1} nitrate (via 1.84 g calcium nitrate L^{-1}) and 32.1 mmol L^{-1} acetate (via 2.54 g calcium acetate L^{-1}). The baseline substrate estimations are determined using a simplified equation for all sources of water and assumes that only nitrate is used for growth and denitrification. As a result, the needed amount of nitrate is overestimated because ammonium is also used for growth and the source-water may already include background concentrations of nitrate. A few amendments to the estimated baseline recipes for the Seawater (hereafter, "Matched Seawater") and Groundwater (hereafter, "Matched Groundwater") treatments are needed to match the background source-water

97

characteristics and reach target treatment levels without adding an excess of substrate. These amendments and why they are needed are described here:

1. NH_4^+ is produced during decay and is used for synthesis instead of nitrate because it is more energetically favorable. This results in less nitrate use for synthesis, which leads to a small excess of nitrate and acetate over what is needed when nitrate is the sole nitrogen source when the baseline estimates are considered. The excess nitrate ultimately brings about desaturation beyond the target desaturation and transient accumulation of nitrite. I used the model to empirically determine the fractional amount (f_N) of the baseline nitrate estimation ($NO_3^-{}_d$, mol L^{-1}) and the fractional amount (f_A) of the baseline acetate estimation ($Ace^-{}_d$, mol L^{-1}) needed to avoid having excess nitrate so that the 10% target desaturation level is achieved. Because f_N and f_A may vary depending on the environmental characteristics (e.g., an environment with a high concentration of organic mass acting as an electron donor) the f_N and f_A value should be considered on a case-by-case basis using the model.

2. A high initial background concentrations of nitrate and/or nitrite (N_i, mol L^{-1}) also should be removed from the baseline nitrate estimation, to give the final amount of nitrate to be added ($NO_3^-{}_f$, mol L^{-1}). The added acetate concentration should be related to $NO_3^-{}_f$. Eq. 24 and Eq. 25 take both amendments into account.

$$NO_{3~f}^{-} = f_N NO_{3~d}^{-} - N_i \qquad \text{Eq. 24}$$

$$Ace_f^- = f_A NO_{3~d}^- \qquad \text{Eq. 25}$$

Adding acetate greater than $NO_{3~f}^-$ risks stimulating biogeochemical processes that generate

harmful by-products, particularly sulfate reduction to H_2S. Furthermore, adding excess

acetate or nitrate leads to unnecessary additional cost.

To illustrate the necessity of matching the nitrate and acetate additions for MIDP

treatment, I compared the behavior of MIDP in seawater using the Matched Seawater,

baseline treatment without amendments (hereafter, "Unmatched Seawater"), and with an

15% excess of acetate beyond the baseline estimation (hereafter "Excess Acetate

Seawater") scenarios. The substrate recipes and the f_N and f_A coefficients are found in

Table 10 for the three Seawater scenarios, as well as a Matched Groundwater scenario.

Table 10. MIDP Treatment Recipe for Each of the Investigated Scenarios to Achieve 10%
Desaturation at 7.6 m of Depth.

	Matched Groundwater	Unmatched Groundwater	Matched Seawater	Excess-Acetate Seawater
Acetate (mmol L^{-1})	29.2	32.5	29.2	32.2
Nitrate (mmol L^{-1})	18.7	20.5	18.9	20.5
f_N	0.85	1.00	0.85	1.00
f_A	0.91	1.00	0.91	1.15

For assessing when metabolic reactions ceased (i.e., when all of an electron

acceptor was reduced), I assumed that full substrate consumption occurred when its

concentration went below 0.01 mmol L^{-1}. If a substrate had a residual concentration greater

than 0.01 mmol L^{-1}, I then assumed that the reaction had stopped when the slope for the reaction's substrate was less than -0.02 mol L^{-1} d^{-1} over a half-day period. The median time for when a reaction was completed is calculated from the relevant criterion of considering a reaction to be stopped.

Comparing MIDP Behavior for the Different Source-Water Conditions

Desaturation Using Matched Treatment Recipes

The rate of MIDP treatment varied depending on source-water, but no excess acetate, nitrate, or nitrite remained when the substrate treatment recipe was matched, which is demonstrated in the initial days of treatment in Figure 21. With Matched Groundwater, nitrate, nitrite, and acetate were removed by 0.8 days, but the reactions took longer in Matched Seawater, for which all substrate and MIDP intermediates were removed by 1.3 days. The lower rates of MIDP in Matched Seawater were due primarily to inhibition from its high salinity, which was exacerbated by inhibition from transiently accumulating nitrous acid.
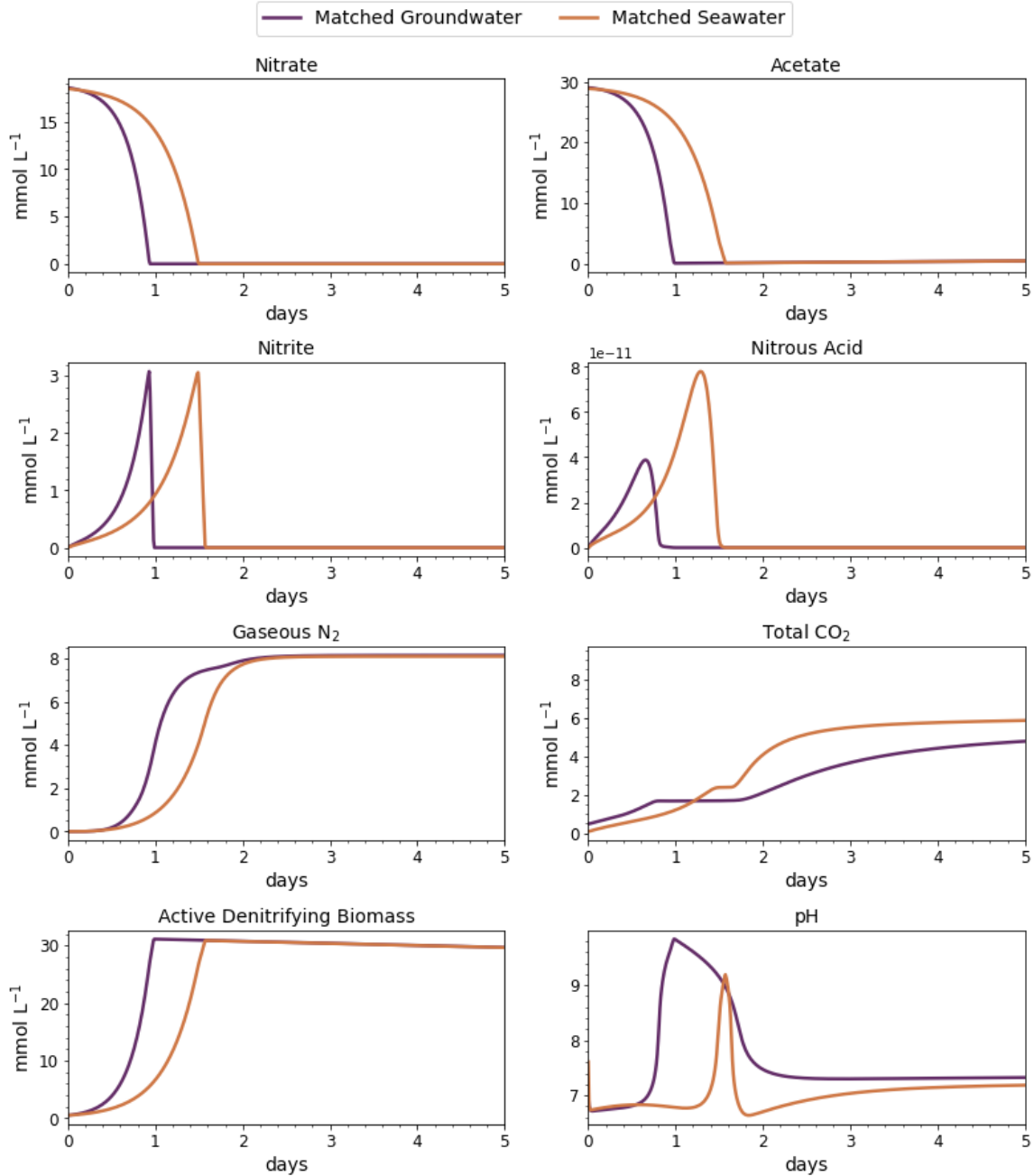
Figure 21. Batch Results Using the Biogeochemical Model for MIDP in Matched Groundwater and Matched Seawater and Targeting a Desaturation Level of 10%.

The pH behavior during MIDP differed in the initial two days of treatment. In Matched Groundwater, a sharp increase in pH to 9.8 between 0.5 and 1 day was due to the production of base from rapid nitrite reduction. Subsequently, $CaCO_3$ precipitation (shown

by loss of calcium in Figure 22) brought the pH down to circumneutral. Since MIDP in Matched Seawater was delayed, the pH rose to 9.2 from rapid nitrite reduction, but the effect was attenuated by the prior loss of alkalinity due to on-going coincident $CaCO_3$ precipitation. The phenomena affecting pH are further illustrated by the changes in DIC and precipitated $CaCO_3$ in Figure 22: The sharp rise in DIC (from acetate oxidation) around day 2 preceded the onset of rapid precipitation of $CaCO_3$. The extent of DIC production mirrored the oxidation of acetate, with the slower oxidation rate with seawater leading to a smaller DIC peak, since $CaCO_3$ precipitation had already begun. Slightly more $CaCO_3$ was precipitated in seawater (thereby removing slightly more DIC) because of its higher initial concentration of calcium ion. Neither scenario precipitated enough $CaCO_3$ to mitigate liquefaction by cementation when aiming for 90% saturation (O'Donnell, Rittmann, et al., 2017).
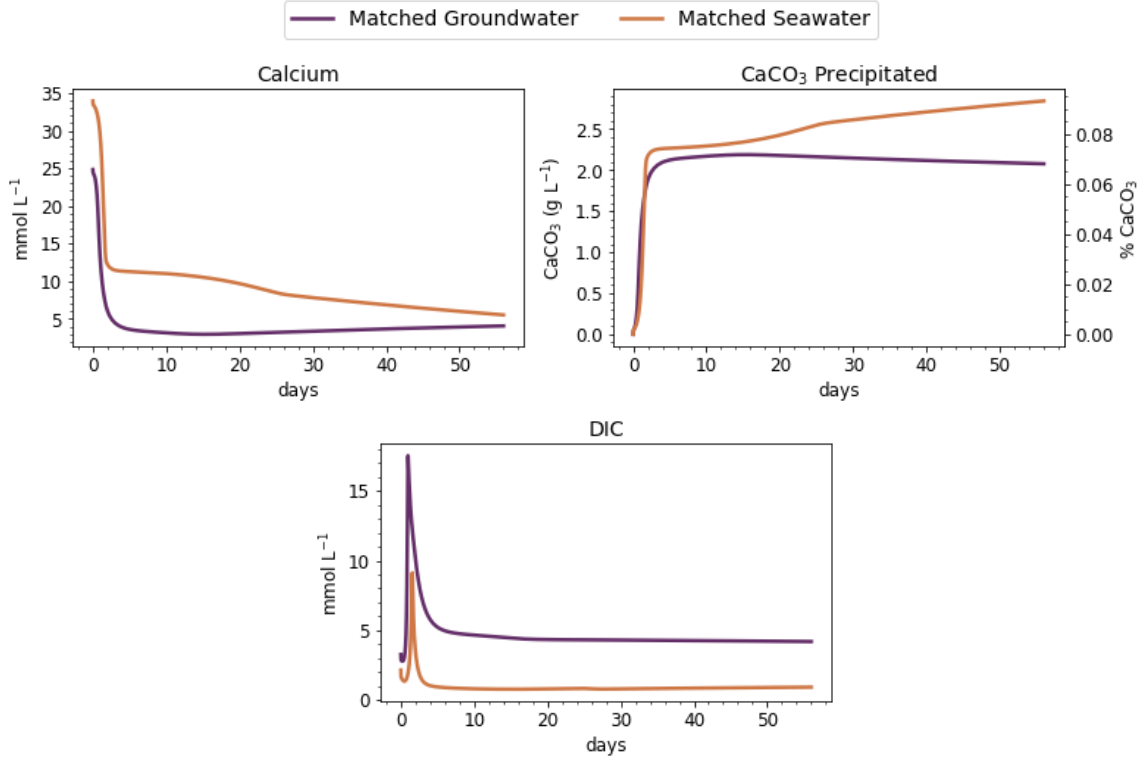
Figure 22. Concentration of Calcium, CaCO₃, and DIC Precipitated and the Ratio of g of Precipitated CaCO₃ to g of Soil, Represented in %, During Targeted Desaturation in Matched Groundwater and Matched Seawater.

The treatment time to reach the desaturation criterion (90% saturation at 7.6-m depth) was achieved in Matched Groundwater by 1.7 days and in Matched Seawater by 1.9 days, as shown in Figure 23. The difference in treatment time reflects slower denitrification kinetics in the seawater. Gas-phase N_2 production for desaturation lagged the overall output of N_2 because Henry's Law equilibrium was not achieved immediately due to gas-transfer kinetics. CO_2 and H_2S did not contribute significantly to desaturation at any of the modeled depths in either scenario, because neither exceeded the saturation threshold to transfer to the gas phase. While this model aims to achieve 10% desaturation based on laboratory experimentation that demonstrated that a 5-10% desaturation mitigated liquefaction triggering (O'Donnell, Kavazanjian, et al., 2017), this target may be ultra-

conservative in denser soil and may not be conservative enough in locales expected to experience strong earthquake shaking.
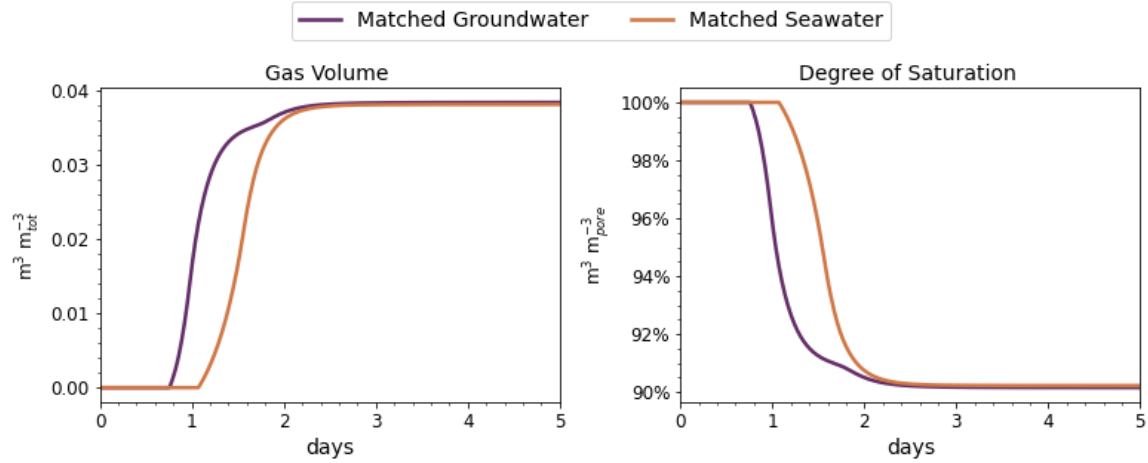
Figure 23. Gas Volume for the Total Soil Volume and Degree of Saturation from MIDP in Matched Groundwater and Matched Seawater Targeting a Desaturation Level of 10% at 7.6-m Depth.

The model was used to simulate a total time of 56 days to illustrate the long-term effects of MIDP on sulfate reduction, as shown in Figure 24. The presence of a of a high concentration of sulfate in the Matched Seawater led to continued sulfate reduction and H_2S accumulation due to long-term biomass endogenous respiration of accumulated biomass. At 56 days, 4.2 mmol L^{-1} of soluble H_2S was produced with the Matched Seawater. In Matched Groundwater, all available sulfate was reduced by 12 days, leading to the production of 0.51 mmol L^{-1} of soluble H_2S (about 8 times less than in Matched Seawater at the end of 56 days). In both scenarios, the amount of produced H_2S did not exceed the saturation threshold described by Henry's Law, and all H_2S remained in solution. Even when the model was run to over 400 days and approached the limit of the maximum possible amount of sulfate reduction if the entire amount of available biomass for electron donor were consumed, the maximum amount of H_2S produced was around 10

mmol L^{-1}. This concentration does not exceed the solubility threshold, and, thus, the H$_2$S remained in solution. Thus, the primary risk of H$_2$S formation would come mainly upon water withdrawal from the subsurface, at which time H$_2$S would be expected to come out of solution and transfer to the gas phase in the open air. While acute exposure is unlikely in an open-air environment, exposure could be an important for workers involved in activities that disturb the ground (e.g., drilling and excavating). Serious health impacts, like vomiting and loss of consciousness, have been documented after acute exposure to concentrations that exceed 100 ppm, approximately $4.1 \cdot 10^{-6}$ mol L^{-1} of H$_2$S, and thus elevated H$_2$S concentrations should be avoided (United States National Research Council, 2009). These risks are more elevated when doing MIDP with seawater or a high-sulfate water source.
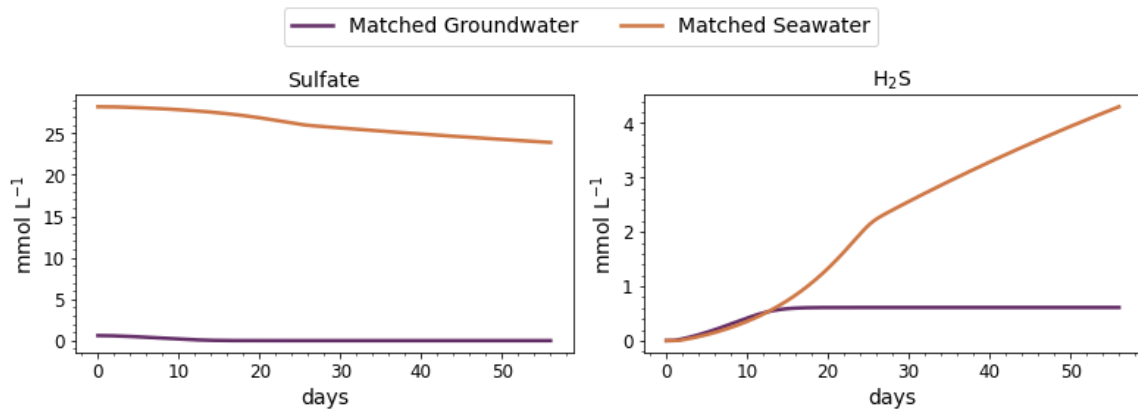
Figure 24. Batch Results Over 56 days for Sulfur Species for Biogeochemical Modeling of MIDP for the Matched Groundwater and Matched Seawater Targeting a Desaturation Level of 10%.

Desaturation with Unmatched Source Water

Not matching the substrate addition for background source-water constituents and for ammonium release from endogenous decay can lead to unwanted by-products and

incomplete denitrification. Figure 25 illustrates the consequences of the Unmatched Seawater and the Excess Acetate Seawater scenarios. In the Unmatched Seawater scenario, the source water has too much nitrate, and denitrification did not go to completion before all acetate was consumed in the baseline treatment concentrations. Therefore, full nitrate reduction to N_2 required ~19 days and was driven by endogenous respiration of biomass, a slow process. As a result, nitrite and nitrous acid accumulated. In the Excess Acetate Seawater scenario, nitrate and nitrite were completely reduced after 1.6 days, but 3.93 mmol L^{-1} of acetate remained. The residual acetate has a profound impact on increasing sulfate reduction to H_2S, as is shown in Figure 27. After 56 days, the produced H_2S in the Excess Acetate Seawater scenario was 6.8 mmol L^{-1}, or about double that in the Matched Seawater scenario. At this concentration, H_2S is likely to stay in solution unless agitated due to groundwater removal.
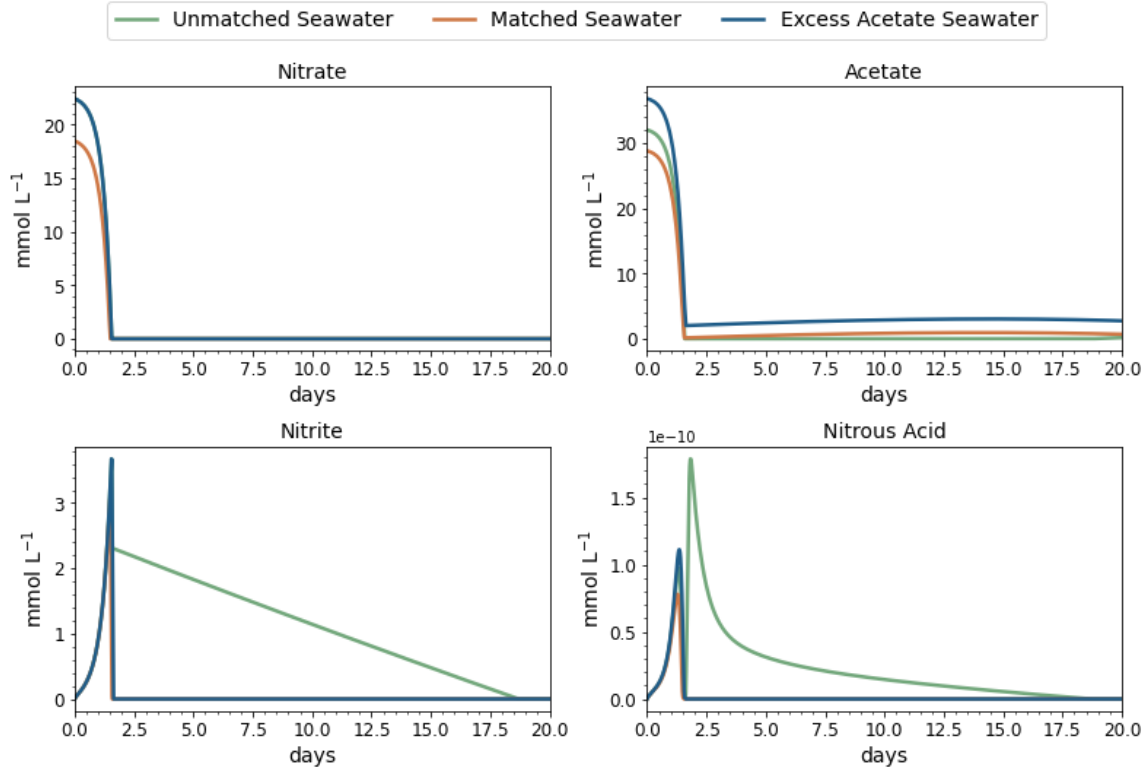
Figure 25. Trends for Nitrate, Acetate, and N-intermediates with MIDP for the Unmatched Seawater, Matched Seawater, and Excess Acetate Seawater Scenarios.

Due to the excess of nitrate present in the Unmatched Seawater and Excess Acetate Seawater scenarios, saturation was driven to below the target of 90%, shown in Figure 26. Saturation declined to 87.8% (or 12.2% desaturation), and it was completely due to evolution of N_2 gas, since CO_2 and H_2S remained completely dissolved at 7.6 m of depth. Since desaturation exceeded the target level, the Unmatched Seawater and Excess Acetate Seawater scenarios led to added costs associated with extra additions of nitrate or acetate over the Matched Seawater treatment.
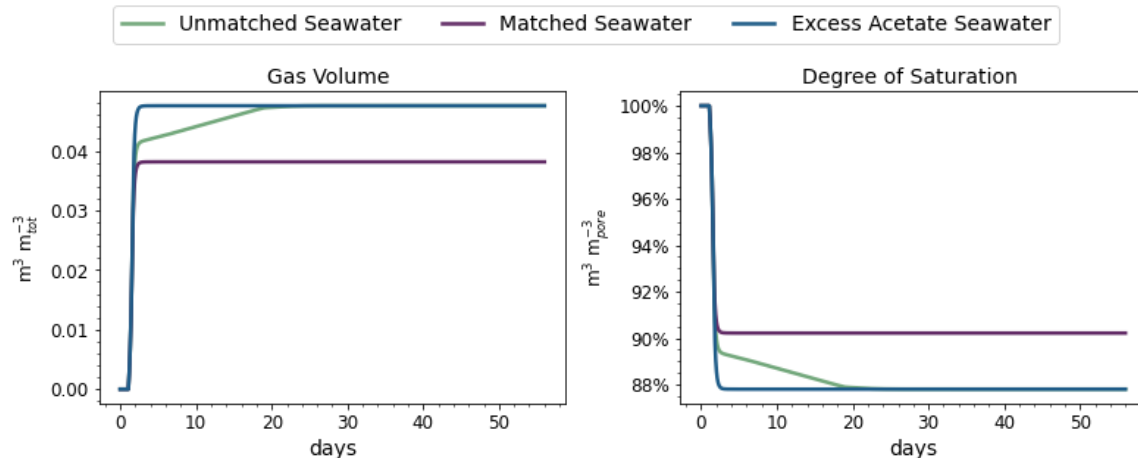
Figure 26. Trends in Gas Production and Saturation for MIDP for the Unmatched Seawater, Matched Seawater, and Excess Acetate Seawater Scenarios.

The modeled time period was extended to 56 days to illustrate the potential long-term production of unwanted MIDP by-products through increased sulfate reduction. As illustrated in in Figure 27, more H_2S was produced during the 56-day modeled period in Unmatched Seawater and Excess Acetate Seawater, compared to Matched Seawater. The difference was greater for Excess Acetate Seawater. The increased sulfate reduction was driven by a combination of acetate oxidation and endogenous respiration of biomass. Excess Acetate Seawater led to the largest amount of sulfate reduction to H_2S because of its higher input of initial acetate and electron donor from exogenous decay (acetate). For Unmatched Seawater, nitrate and nitrite reduction were dominant until nearly halfway through the modeled time period due to the excess nitrate in the source water and in the initial treatment recipe (because it was not adjusted to account for growth using NH_4^+). Sulfate reduction became important after about 14 days, when nitrate was depleted (Figure 25). Denitrification consumed only a small fraction of the endogenous electron donor consumed via respiration. Thus, most endogenous respiration was through sulfate

108

reduction in the long term because the remaining available electron acceptor is sulfate in all scenarios.

The Excess Acetate scenario generated significant H_2S, compared to Matched Groundwater. If H_2S were to escape from the subsurface as a gas in any scenario, it would pose a risk of a nuisance from its rotten-egg smell at concentrations in air as low as 0.3 ppb (or approximately, $3.6 \cdot 10^{-13}$ mol L^{-1}) (Council, 2009; "Hydrogen Sulfide," 2009). A more insidious risk of nerve paralysis, nausea, memory, and motor dysfunction comes from concentrations in air above 100 ppm (or approximately $1.8 \cdot 10^{-7}$ mol L^{-1}) (United States National Research Council, 2009). Concentrations above 100 ppm in air are deemed to be immediately dangerous to life and health (Administration). If a majority of the accumulated H_2S by-product were to escape to the atmosphere in a short time, the amount of produced H_2S would well exceed the nerve-paralysis threshold and risk more significant respiratory, cardiovascular, and nervous system damage (United States National Research Council, 2009). Therefore, the potential for a rapid release of H_2S must be minimized. Residual dissolved H_2S in the water would severely impair the usability of the groundwater due to the taste and odor threshold of $1.5 \cdot 10^{-5}$ mol L^{-1} in water (Fawell et al., 1996) though drinking water standards are likely to be less of a concern for seawater that has higher sulfate levels. H_2S in water is not explicitly regulated, though sulfate has a secondary drinking water standard of $7.3 \cdot 10^{-3}$ mol L^{-1} (Extension, 2007). Thus, matching the substrate additions minimizes cost and minimized unwanted H_2S, with the latter being especially important when seawater is the source water.
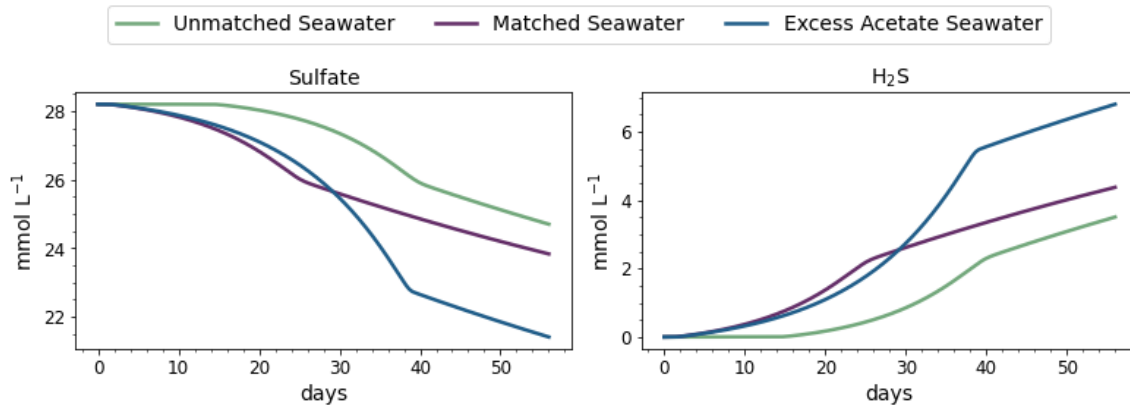
Figure 27. Concentrations of Sulfur Species During MIDP for the Unmatched Seawater, Matched Seawater, and Excess Acetate Seawater Scenarios.

Conclusions

I compared the effect of source-water composition on MIDP behavior and the subsequent impacts on the environmental characteristics when the treatment recipe was matched to consider the background chemical species and alternative nitrogen sources for denitrification. Complete denitrification and reaching desired desaturation levels took longer in Matched Seawater than in Matched Groundwater primarily due to inhibition caused by high salinity. Secondarily, an accumulation of nitrous acid led to further inhibition in Matched Seawater. Lower concentrations of potential inhibitors resulted in relatively rapid denitrification in Matched Groundwater, leading to a high pH that prevented prolonged accumulation of HNO_2.

Altering the treatment recipe to account for high concentrations of background nitrogenous species and growth on NH_4^+ from endogenous decay was critical to promote complete denitrification and limit unwanted by-products. Unmatched Seawater employed the baseline estimations of needed acetate and nitrate, but this led to an excess of nitrate when the acetate was completely consumed because alternative nitrogen sources were used

for growth. As a result, prolonged accumulation of potentially toxic intermediates occurred compared to Matched Seawater. Increasing the amount of input acetate to compensate for the high levels of nitrate in the Excess Acetate Seawater scenario exacerbated unwanted sulfate reduction and H_2S production. H_2S is a nuisance at low concentrations in the water and air and can be potentially harmful at higher concentrations in the air. A water quality analysis should be conducted to understand the potential impact of all native water quality constituents that may lead to unwanted by-products due to MIDP inhibition to inform treatment design.

CHAPTER 7

EXPLORING THE EFFECTS OF DIFFERENT ELECTRON DONORS ON MIDP

To facilitate the transition of MIDP from the lab to the field, the substrate recipe must be investigated in terms of its efficacy for desaturation and precipitation. In MIDP, nitrate is used as the electron acceptor and nitrogen source for denitrification and microbial growth, while acetate (added as calcium acetate) typically has been the primary electron donor (O'Donnell, Rittmann, et al., 2017; Pham, 2017). Because the cost of the substrate is a factor in the feasibility of a field application, using an electron donor that is less expensive than acetate is of interest. Substrate costs have some variability, but the estimated cost based on communication and quotes from Concentrates, Inc. (Milwaukie, OR) for calcium acetate is \$2.50 kg^{-1} and calcium nitrate is \$1.50 kg^{-1}. Industry practitioners also have suggested using less-expensive alternative electron donors to make MIDP more cost competitive. Glucose (as dextrose) and molasses are two candidates at \$1.50 kg^{-1} and \$1.25 kg^{-1}, respectively, according to estimates by Webstaurant Store (Lancaster, PA).

A potential counter factor to the use of these less expensive electron donors is that introducing a less-expensive substrate may stimulate unwanted microbial process, like sulfate reduction. Competition for electron donor, which may influence the rate and completeness of denitrification, has been investigated in wastewater treatment (e.g., (Wilderer et al., 1987)) and agricultural soils (e.g., (Paul et al., 1989)), but not for MIDP. To systematically evaluate the pros and cons using less-expensive electron donors, I used

the model presented in Chapter 5 to compare acetate, glucose, and molasses as the electron donor in a seawater environment (i.e., with seawater as the source-water).

Establishing the Model Inputs to Compare Different Electron Donors

To understand the impact on MIDP behavior from different treatment recipes with seawater as the source-water (seawater composition is detailed in Chapter 5), I used the biogeochemical model developed in Chapter 5 to consider biogeochemical reactions that involve naturally occurring compounds and competing electron acceptors. The details of relevant bacterial energetics and stoichiometry for the alternative electron donors are provided in Table 11, which includes all relevant combinations of possible electron donors, electron acceptors, and nitrogen sources for biomass growth.

Two different nitrogen sources were considered: nitrate and ammonium. Nitrate was considered as a primary nitrogen source for growth because of it already being introduced through the MIDP treatment for denitrification. Ammonium is released during endogenous decay and is used preferentially for growth. Ammonium is used preferentially because it is more energetically favorable, since fewer electron equivalents are required to incorporate ammonium into biomass than a more oxidized N source, like nitrate.

I chose acetate ($C_2H_4O_2^-$) because acetate showed success in MIDP experiments in the laboratory (O'Donnell, Kavazanjian, et al., 2017; O'Donnell, Rittmann, et al., 2017; Pham, Nakano, et al., 2018), is readily available, and is relatively easy to deliver. Most important is that acetate is not fermentable, which means that it can only drive respiration reactions, such as denitrification. I selected glucose ($C_6H_{12}O_6$) for comparison because it

113

has the same number of electron equivalents per mole of C as acetate but is more energetically favorable compared to acetate. Glucose also is readily available and easy to deliver, and its cost per electron equivalent is about 60% the cost of acetate. I also consider molasses as an alternative lower-cost electron donor. Its cost per available electron equivalent is about 50% that of acetate. Molasses is a complex electron donor, comprised of sugars, lipids, proteins, and ash (Olbrich, 1963). Molasses's composition can vary among batches, feedstock (i.e., made from sugar cane vs sugar beets), and manufacturer; I next discuss how I incorporated these characteristics of molasses in the model.

Table 11. Stoichiometry Expected During MIDP, Considering the Range of Introduced Electron Donors and Natural Electron Acceptors

Electron Donor	Electron Acceptor	Nitrogen Source	$\widehat{q}$ (mol electron donor mol^{-1} biomass d^{-1})	f_e^0	Y (mol biomass mol^{-1} donor)	Reaction
Acetate	Nitrate	Nitrate	7.6	0.40	0.82	$0.222NO_3^- + 0.125C_2H_3O_2^- + 0.146H^+$ $\rightarrow 0.202NO_2^- + 0.147H_2CO_3$ $+ 0.103CH_{1.8}O_{0.5}N_{0.2} + 0.021H_2O$
Acetate	Nitrite	Nitrate	11.0	0.28	0.99	$0.054NO_3^- + 0.202NO_2^- + 0.270C_2H_3O_2^- + 0.525H^+$ $\rightarrow 0.101N_2 + 0.272H_2CO_3$ $+ 0.268CH_{1.8}O_{0.5}N_{0.2} + 0.154H_2O$
Acetate	Sulfate	Nitrate	3.5	0.88	0.95	$0.015NO_3^- + 0.072SO_4^- + 0.125C_2H_3O_2^- + 0.284H^+$ $\rightarrow 0.072H_2S + 0.177H_2CO_3$ $+ 0.073CH_{1.8}O_{0.5}N_{0.2} + 0.015H_2O$
Acetate	Nitrate	Ammonium	6.5	0.47	1.0	$0.236NO_3^- + 0.125C_2H_3O_2^- + 0.025NH_4^+ + 0.100H^+$ $\rightarrow 0.236NO_2^- + 0.124H_2CO_3$ $+ 0.126CH_{1.8}O_{0.5}N_{0.2} + 0.050\ H_2O$
Acetate	Nitrite	Ammonium	9.1	0.34	1.3	$0.236NO_2^- + 0.261C_2H_3O_2^- + 0.066NH_4^+ + 0.431H^+$ $\rightarrow 0.118N_2 + 0.193H_2CO_3$ $+ 0.328CH_{1.8}O_{0.5}N_{0.2} + 0.249H_2O$
Acetate	Sulfate	Ammonium	3.4	0.90	0.18	$0.113SO_4^- + 0.125C_2H_3O_2^- + 0.005NH_4^+ + 0.346H^+$ $\rightarrow 0.113H_2S + 0.227H_2CO_3$ $+ 0.023CH_{1.8}O_{0.5}N_{0.2} + 0.009H_2O$
Glucose	Nitrate	Nitrate	4.1	0.25	3.1	$0.152NO_3^- + 0.042C_6H_{12}O_6 + 0.026H^+$ $\rightarrow 0.126NO_2^- + 0.121H_2CO_3$ $+ 0.129CH_{1.8}O_{0.5}N_{0.2} + 0.026\ H_2O$

Glucose	Nitrite	Nitrate	5.9	0.17	3.4	$0.062NO_3^- + 0.126NO_2^- + 0.091C_6H_{12}O_6 + 0.189H^+$ $\rightarrow 0.063N_2 + 0.235H_2CO_3$ $+ 0.312CH_{1.8}O_{0.5}N_{0.2} + 0.126H_2O$
Glucose	Sulfate	Nitrate	1.8	0.58	0.81	$0.007NO_3^- + 0.101SO_4^- + 0.042C_6H_{12}O_6 + 0.208H^+$ $\rightarrow 0.101H_2S + 0.216H_2CO_3$ $+ 0.034CH_{1.8}O_{0.5}N_{0.2} + 0.007H_2O$
Glucose	Nitrate	Ammonium	3.0	0.34	3.8	$0.170NO_3^- + 0.042C_6H_{12}O_6 + 0.031NH_4^+$ $\rightarrow 0.170NO_2^- + 0.093H_2CO_3$ $+ 0.157CH_{1.8}O_{0.5}N_{0.2} + 0.031H^+$ $+ 0.045\ H_2O$
Glucose	Nitrite	Ammonium	4.2	0.24	4.3	$0.170NO_2^- + 0.088C_6H_{12}O_6 + 0.076NH_4^+ + 0.094H^+$ $\rightarrow 0.085N_2 + 0.147H_2CO_3$ $+ 0.380CH_{1.8}O_{0.5}N_{0.2} + 0.237H_2O$
Glucose	Sulfate	Ammonium	1.5	0.68	0.73	$0.085SO_4^- + 0.042C_6H_{12}O_6 + 0.005NH_4^+ + 0.346H^+$ $\rightarrow 0.085H_2S + 0.227H_2CO_3$ $+ 0.023CH_{1.8}O_{0.5}N_{0.2} + 0.009H_2O$
Molasses	Nitrate	Nitrate	2.0	0.25	3.1	$0.152NO_3^- + 0.042C_6H_{12}O_{6\ molasses} + 0.026H^+$ $\rightarrow 0.126NO_2^- + 0.121H_2CO_3$ $+ 0.129CH_{1.8}O_{0.5}N_{0.2} + 0.026\ H_2O$
Molasses	Nitrite	Nitrate	3.0	0.17	3.4	$0.062NO_3^- + 0.126NO_2^- + 0.091C_6H_{12}O_{6\ molasses}$ $+ 0.189H^+$ $\rightarrow 0.063N_2 + 0.235H_2CO_3$ $+ 0.312CH_{1.8}O_{0.5}N_{0.2} + 0.126H_2O$
Molasses	Sulfate	Nitrate	0.9	0.58	0.81	$0.007NO_3^- + 0.101SO_4^- + 0.042C_6H_{12}O_{6\ molasses}$ $+ 0.208H^+$ $\rightarrow 0.101H_2S + 0.216H_2CO_3$ $+ 0.034CH_{1.8}O_{0.5}N_{0.2} + 0.007H_2O$

Molasses	Nitrate	Ammonium	1.5	0.34	3.8	$0.170NO_3^- + 0.042C_6H_{12}O_{6_{molasses}} + 0.031NH_4^+$ $\rightarrow 0.170NO_2^- + 0.093H_2CO_3$ $+ 0.157CH_{1.8}O_{0.5}N_{0.2} + 0.031H^+$ $+ 0.045\ H_2O$
Molasses	Nitrite	Ammonium	2.1	0.24	4.3	$0.170NO_2^- + 0.088C_6H_{12}O_{6_{molasses}} + 0.076NH_4^+$ $+ 0.094H^+$ $\rightarrow 0.085N_2 + 0.147H_2CO_3$ $+ 0.380CH_{1.8}O_{0.5}N_{0.2} + 0.237H_2O$
Molasses	Sulfate	Ammonium	0.8	0.68	0.73	$0.085SO_4^- + 0.042C_6H_{12}O_{6_{molasses}} + 0.005NH_4^+$ $+ 0.346H^+$ $\rightarrow 0.085H_2S + 0.227H_2CO_3$ $+ 0.023CH_{1.8}O_{0.5}N_{0.2} + 0.009H_2O$

The electron donor in molasses is made up of complex sugars (i.e., polysaccharides) and simple sugars (i.e., sucrose, glucose, and fructose). While a wide range of the percent sugar composition has been reported (Clarke, 2003; Heidari et al., 2011; Nikodinovic-Runic et al., 2013), I assumed that 60% of bulk molasses is comprised of glucose (as $C_6H_{12}O_{6molasses}$), with the remaining 40% being non-utilizable material. These non-utilizable components include, but are not limited to protein, potassium oxide, sulfur trioxide, and other non-sugar carbohydrates; amounts of each typically are small (<5%) and vary significantly depending on molasses batch (Clarke, 2003).

Due to its complex nature, molasses must first be hydrolyzed to biodegradable glucose (Najafpour & Shan, 2003), and this can be a rate-limiting step. For example, the rate of nitrate reduction using unhydrolyzed molasses was less than one-half that of hydrolyzed molasses (Quan et al., 2005). However, the rate of nitrate reduction when comparing molasses to different electron donors can vary greatly between experimentation (Hamlin et al., 2008). In this model, I assumed that the molasses used as an electron-donor source not hydrolyzed. I represented the effect of rate-limiting hydrolysis by lowering the maximum utilization rate of glucose by 50% to consider observations in literature that molasses must be hydrolyzed to be readily accessible for biotransformation (Quan et al., 2005).

The growth equations used in the model are the same as in Chapter 5. Table 12 details the values used for the half-maximum-rate concentrations for the electron donors (K_d) and the electron acceptors (K_a) for the relevant pairs, as reported by the noted literature sources.

118

Table 12. Half-maximum-rate Concentrations for Each MIDP Electron-donor and -acceptor Pair, K_d and K_a.

Electron Donor	K_d (mol L^{-1})	Source	Electron Acceptor	K_a (mol L^{-1})	Source
Acetate ($C_2H_3O_2^-$)	$1.0 \cdot 10^{-5}$	(Jia et al., 2020)	Nitrate (NO_3^-)	$5.4 \cdot 10^{-5}$	(Abdul-Talib et al., 2002)
Acetate ($C_2H_3O_2^-$)	$1.0 \cdot 10^{-5}$	(Jia et al., 2020)	Nitrite (NO_2^-)	$2.4 \cdot 10^{-5}$	(Abdul-Talib et al., 2002)
Glucose ($C_6H_{12}O_6$) from Molasses	$8.2 \cdot 10^{-5}$	(Calderer et al., 2010; Lin, 2008)	Nitrate (NO_3^-)	$1.1 \cdot 10^{-5}$	(Calderer et al., 2010; Lin, 2008)
Glucose ($C_6H_{12}O_6$) from Molasses	$8.2 \cdot 10^{-5}$	(Calderer et al., 2010; Lin, 2008)	Nitrite (NO_2^-)	$1.1 \cdot 10^{-5}$	(Lin, 2008)
Acetate ($C_2H_3O_2^-$)	$7.1 \cdot 10^{-5}$	(Ingvorsen et al., 1984)	Sulfate (SO_4^-)	$2.00 \cdot 10^{-4}$	(Ingvorsen et al., 1984)
Glucose ($C_6H_{12}O_6$)	$8.2 \cdot 10^{-5}$	(Calderer et al., 2010; Lin, 2008)	Sulfate (SO_4^-)	$2.00 \cdot 10^{-4}$	Ingvorsen et al., 1984

The estimated baseline substrate recipe was established following methods described in Chapter 5. As discussed in Chapter 6, the input substrate recipe should be adjusted to account for the background concentrations of nitrogenous species and ammonium gained from decay for growth. I used the method of Chapter 6 to match the donor and acceptor concentrations so that neither the donor nor the acceptor was added in excess. Table 13 details the matched substrate recipes. The adjustment factors for the input electron donor (f_D) and nitrate (f_N) were empirically determined used to achieve target desaturation levels without inducing substrate limitations or leaving an excess of electron donor. Calcium nitrate ($Ca(NO_3)_2$) and calcium acetate ($Ca(C_2H_3O_2)_2$) provide nitrate and acetate, and the corresponding calcium levels also are given (Table 13).

Overall, fewer moles of glucose and glucose from molasses are needed than acetate, because they have three-fold more electrons available per mole available for respiration.

The key difference in each case is that the matched recipe had 10% to 15% less added electron donor, due to the differences in the fraction of donor electrons sent to the acceptor for energy generation (f_e^0) and biomass yield (Y) (Table 11). The differences in f_e^0 values when using acetate versus glucose range from -10% to -15%, depending on if reducing nitrate or nitrite and the nitrogen source. These decreases in f_e^0 resulted in smaller Y values and less need for electron donor for synthesis when glucose is the donor, compared to acetate.

Table 13. Matched MIDP Treatment Recipe for Each of the Investigated Scenarios with Varying Electron Donor to Achieve 10% Desaturation at 7.6 m of Depth. Value in Parentheses is the Added Electron Donor Amount Normalized to 1 mmol L^{-1} of Added Nitrate.

	Matched Acetate	Matched Glucose	Matched Molasses
Electron Donor (mmol L^{-1})	28.9 (1.56)	14.5 (0.71)	14.5 (0.71)
Nitrate (mmol L^{-1})	18.5	20.4	20.4
Calcium (mmol L^{-1})	23.8	10.2	10.2
f_N	0.83	0.74	0.74
f_D	0.90	0.84	0.84

Results and Discussion

The behavior and rate of MIDP treatment varied among the different treatment recipes, as illustrated in Figure 28
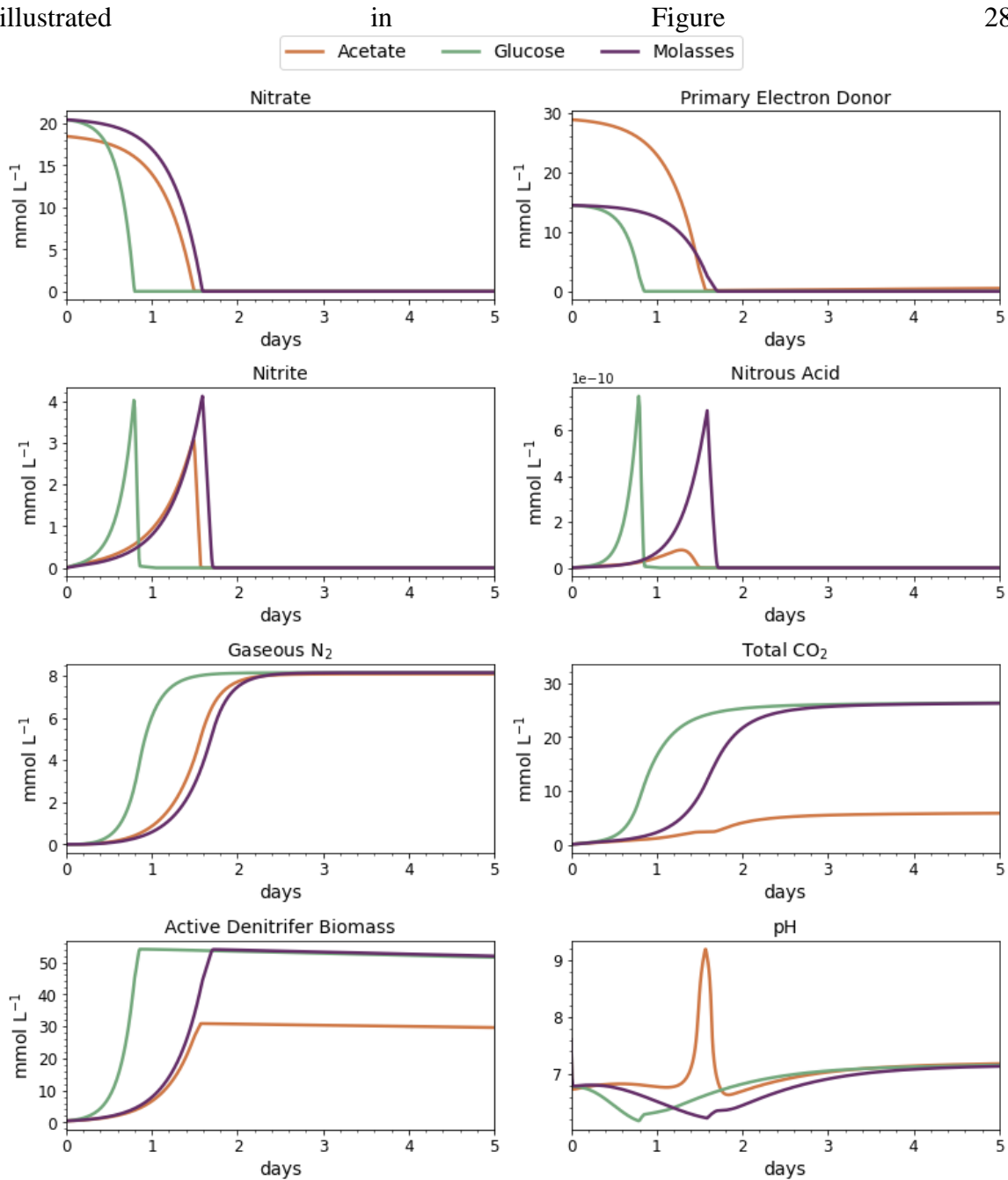
. Complete denitrification was achieved fastest using glucose as the electron donor (0.9 days), then acetate (1.6 days), and then molasses (1.7 days). Even though the maximum specific rate of substrate utilization ($\hat{q}$) was larger when using acetate, glucose led to the fastest denitrification rates because of glucose's higher yield (Table 11Table 4), which led

to a to faster biomass growth rates and accumulation of active biomass able to perform denitrification. Use of glucose from molasses resulted to the slowest treatment rate because it needed to be hydrolyzed before treatment and, thus, had a 50% slower rate of denitrification and growth.
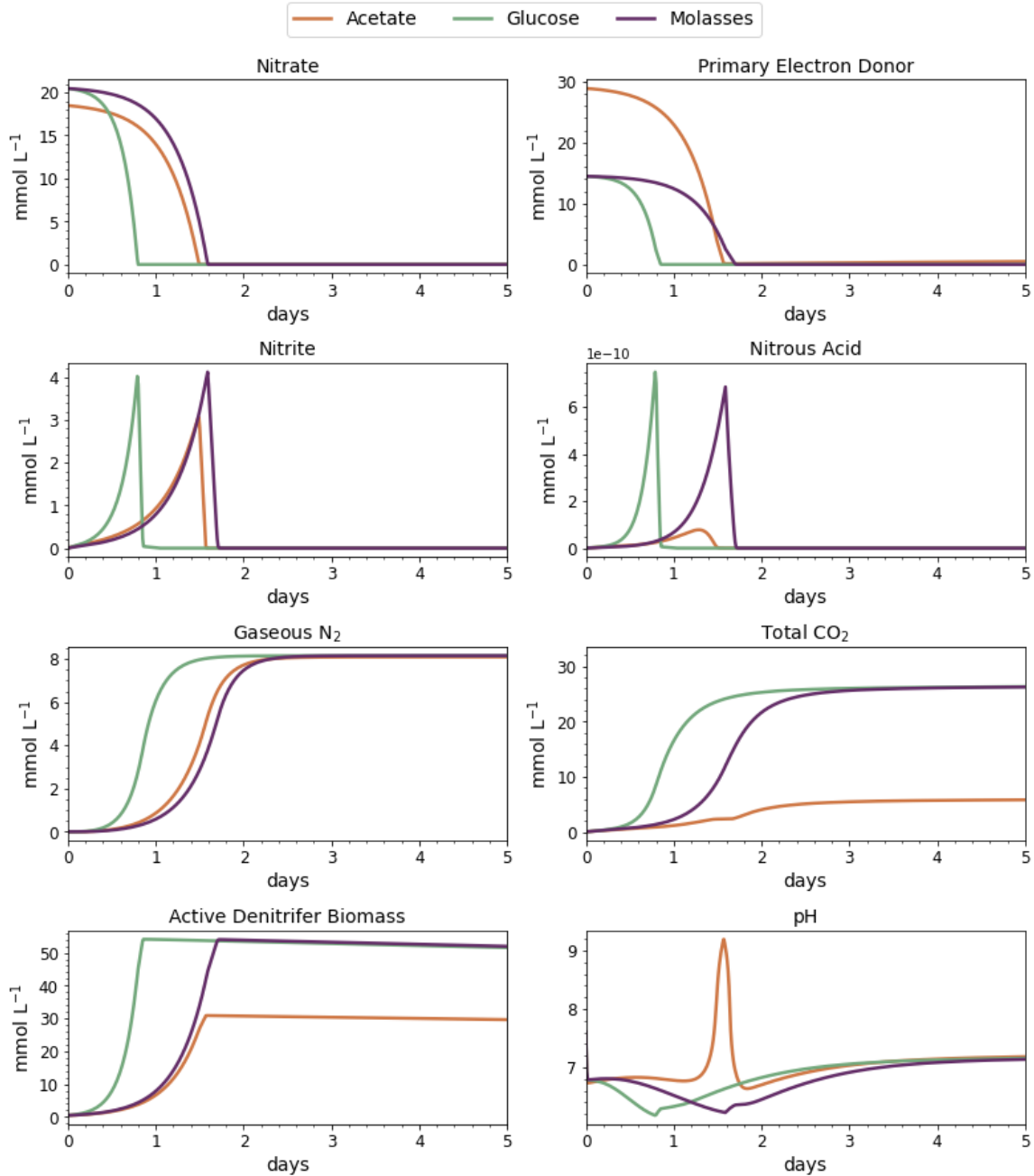
Figure 28. Batch Results Using the Biogeochemical Model for MIDP with Acetate, Glucose, or Molasses as the Electron Donor Source and Targeting a Desaturation Level of 10%.

Since glucose and molasses produced less base during respiration when reducing nitrate and nitrite (see the relative consumptions of H^+ in Table 11), the pH was consistently lower compared to when acetate was the electron donor. The more-acidic environments

led to higher concentrations of accumulated HNO_2, a compound inhibitory to denitrifying microorganisms (Almeida et al., 1995; Glass & Silverstein, 1998). However, intermediate accumulation was only temporary in all scenarios.

The times to reach target desaturation levels in all scenarios followed the trends to achieve complete denitrification (Figure 28): As shown in Figure 29, glucose reached a degree of saturation of 90% first (~1.5 d), with acetate and molasses being about the same (~ 2.4 d). O'Donnell et al. (2019) also predicted that glucose resulted in a higher production of biogenic gas (from CO_2) than acetate. Even though a greater amount of CO_2 was produced in the glucose and molasses scenarios than acetate (mainly due to the lower pH), CO_2 did not contribute to desaturation because of its high solubility in water at the target treatment depth of 7.6 m precluded its release as a gas; the same was true at the surface level.
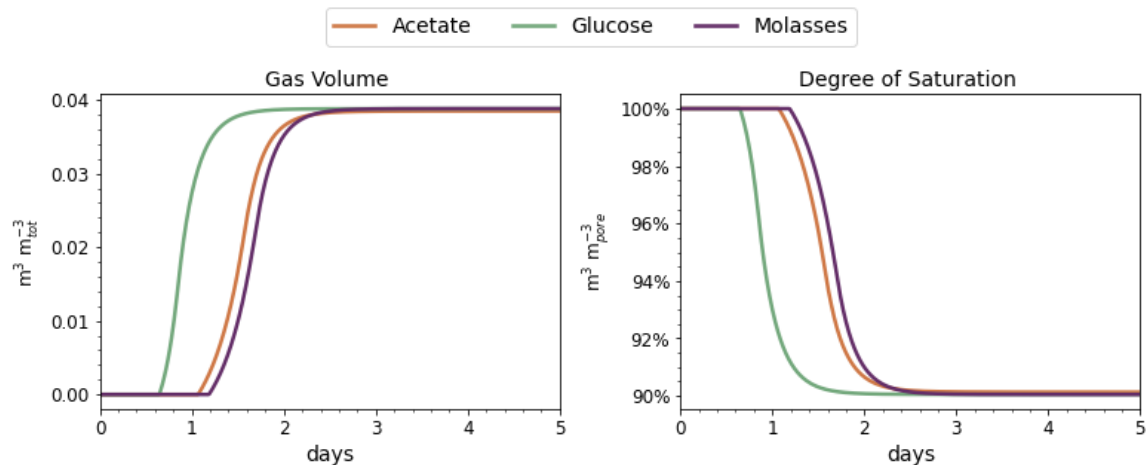
Figure 29. Trends in Gas Production and Saturation for MIDP with Acetate, Glucose, or Molasses as the Electron Donor Source.

Figure 30 shows that MIDP using acetate precipitated more than 3 times as much $CaCO_3$ than in either the glucose or the molasses scenario, even with adequate amounts of

available calcium in all cases. A larger fraction of available DIC in glucose and molasses speciated to CO_2, as illustrated in Figure 28, which resulted in less CO_3^{2-} available for $CaCO_3$ precipitation. Therefore, the greater amount of base produced during MIDP with acetate led to more favorable conditions for mineral precipitation. Since $CaCO_3$ precipitation consumes base, the precipitation reaction was an auto-compensation mechanism that reduced the potential for over-alkalinization.
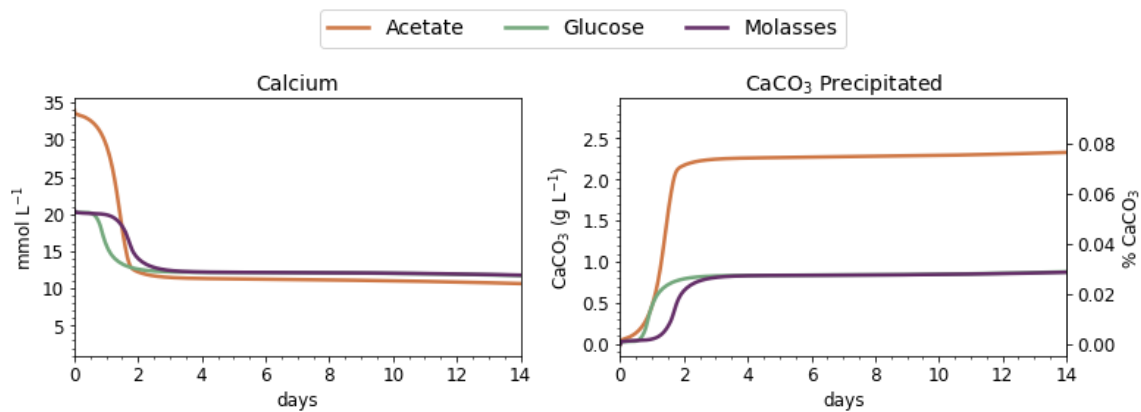
Figure 30. Concentrations of Calcium and $CaCO_3$ Precipitated and the Ratio of g of Precipitated $CaCO_3$ to g of Soil, Represented in %, During Targeted Desaturation in MIDP with Acetate, Glucose, or Molasses as the Electron Donor.

Figure 31 shows that the MIDP scenarios using glucose and molasses resulted in almost twice as much H_2S and ammonium generation than using acetate over the long term. The biomass yield (Table 11Table 4) for denitrifiers using glucose and molasses is higher than with acetate, and the extra biomass provided a greater source of electron donor for endogenous respiration of sulfate. Since the overall biomass production was greater with glucose and molasses than acetate, more ammonium also was produced from endogenous decay. Therefore, another negative effect of using the less-expensive electron donors is formation of more undesired H_2S and total ammonium nitrogen over the long-term.
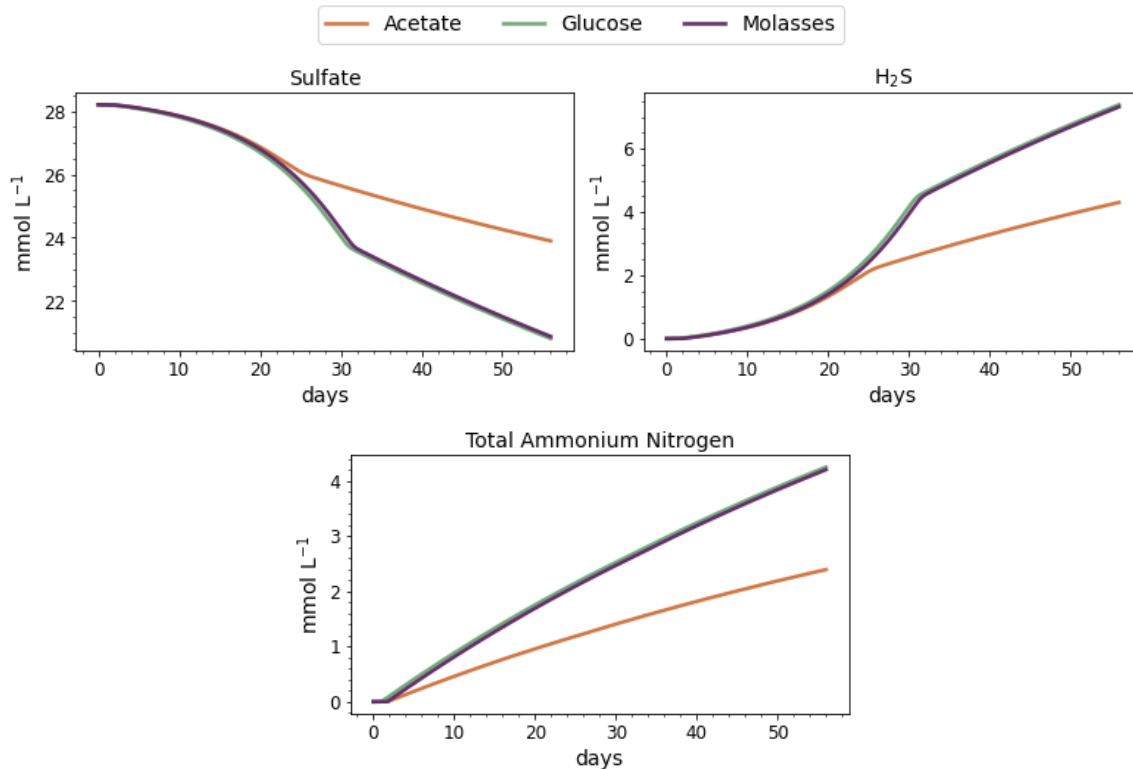
Figure 31. Concentrations of Sulfur and Total Ammonium Nitrogen Species During MIDP with Acetate, Glucose, or Molasses as the Electron Donor Source.

As discussed in Chapter 6, the production of unwanted H_2S is a potential health concern in drinking water or in air if it off-gasses. For health reasons, the United States Occupational Safety and Health Administration (OSHA) limits airborne exposure to H_2S to 10 ppm over an 8-hour period. When a person is acutely exposed to airborne concentrations that exceed 100 ppm, approximately $4.1 \cdot 10^{-6}$ mol L^{-1}, the impact to human health can be very serious, including loss of memory or consciousness, vomiting, and convulsions in extreme cases (United States National Research Council, 2009). Even very small concentrations of H_2S in air (0.3 ppb, approximately $1.2 \cdot 10^{-11}$ mol L^{-1}) are a nuisance because of the associated smell, ranging from smelling "musty" or "swampy" to intense "rotten eggs" (United States National Research Council, 2009). To avoid these

adverse outcomes, the MIDP substrate treatment recipes should be selected to minimize potential production of H_2S, and this is a factor working against using glucose and molasses, versus acetate.

Ammonium nitrogen is the sum of the ionized form (NH_4^+) and the unionized form (NH_3). Currently, by the U.S. Environmental Protection Agency (EPA) has no Maximum Contaminant Level for ammonium, nor is it considered as secondary drinking water contaminant. However, ammonium nitrogen has a taste threshold in water at 1.76 mmol L^{-1} (*2018 Edition of the Drinking Water Standards and Health Advisories Tables*, 2018), and when airborne has a detectable odor limit of $2.1 \cdot 10^{-4}$ mmol L^{-1} (Padappayil & Borger, 2021). In surface water, ammonium nitrogen is well-known to be toxic to aquatic life, and the maximum acute concentration level (at a pH of 7 and 20°C) is 1.0 mmol L^{-1} (*Aquatic Life Ambient Qater Quality Criteria For Ammonia - Freshwater*, 2013). Ammonium also exerts a large oxygen demand, up to 4.57 g O_2 per g N. All scenarios exceeded these thresholds, and the ammonium-N concentration with glucose and molasses at 56 days was nearly double that of acetate. Care should be taken to minimize ammonium-N escape to the atmosphere, surface water, and drinking water sources.

Conclusion

To explore the impact of different recipes on MIDP behavior and the surrounding environment, I compared three different electron donors in a seawater environment: acetate, glucose, and molasses. While acetate has been the primary electron donor used in laboratory experimentation, glucose and molasses have relatively lower cost. Complete denitrification in MIDP was successful in all scenarios, with glucose being the fastest, then

acetate, then molasses. All times to achieve the desaturation target (10% desaturation at 7.6 m depth) were shorter than two days, and the difference between glucose and molasses was less than one day, which means that the kinetics of denitrification and N_2 release was not a drawback for using any donor source.

The modeling comparisons yielded other results that illustrate two phenomena that may cause problems using glucose and molasses to drive MIDP. First, using glucose and molasses led a lower pH caused by their relative lack of base production during denitrification, compared to using acetate. The lower pH caused more DIC to speciate to CO_2, and this slowed and lowered $CaCO_3$ precipitation. The lower pH also led to more accumulation of HNO_2, which inhibits denitrification, although the effect was transient for the source water evaluated.

Second, glucose and molasses had higher biomass yields than acetate, and the higher yields resulted in significantly more biomass accumulation. A long-term effect (i.e., after about 24 days) of more biomass accumulation was that endogenous respiration by sulfate reduction and ammonium production by decay were substantially greater using glucose and molasses. As a result, much more unwanted H_2S and ammonium was produced in the scenarios using glucose and molasses.

TECHNO-ECONOMIC ASSESSMENT OF LIQUEFACTION MITIGATION BY

MICROBIALLY INDUCED DESATURATION

Submitted (currently in review) in part as Hall, C.A., van Paassen, L.A., Kamalzare, S., Parmantier, D., and Kavazanjian, E. Techno-Economic Assessment of Liquefaction Mitigation by Microbially Induced Desaturation. ASCE Lifelines Conference 2022.

INTRODUCTION

Microbially induced desaturation (MID) has been suggested as a cost-effective means of mitigating the potential for triggering of earthquake-induced soil liquefaction under and around lifelines and other civil facilities (Chu et al., 2015; O'Donnell, Rittmann, et al., 2017). Earthquake-induced liquefaction of saturated, cohesionless soil poses a significant threat to civil infrastructure globally (Silva et al., 2018). At the present time, mitigating liquefaction risk under or around existing facilities is an especially large challenge due to the high costs and disruptive nature of existing mitigation technologies (Orense, 2015).

The most common techniques used in practice for mitigation of liquefaction and its consequences rely upon either densification of the liquefiable soil, soil mixing, or injecting the liquefiable soil with cement-based or chemical grouts. These techniques can be either too disruptive or too costly to be used beneath and around existing facilities. Densification can induce settlement, heave, or lateral displacements that can be damaging to structures, lifelines, and utilities in the densification zone. Soil mixing in grid patterns while considered effective against liquefaction is not generally feasible in low headroom

situations or locations where battered columns are required; inversely while jet grouting is technically possible it is generally cost prohibitive. While permeation grouting technologies can be effective, application of the technology can be challenging to design and implement and is costly (*Grouting Technology*, 2017). Grouting can be particularly challenging in finer-grained liquefiable soils due to the particulate nature of cement-based grout suspensions and the high viscosity of chemical grouting solutions.

Abiotic desaturation of liquefiable sand has been investigated for over a decade as a technique to reduce liquefaction triggering potential (Okamura et al., 2011; Yegian et al., 2007). Desaturation can be achieved abiotically either by injecting air or some other gas from an external source into the soil directly (Okamura et al., 2011), by inducing a chemical reaction in the soil or through hydrolysis induced by an electrical current (Yegian et al., 2007). Laboratory testing shows that a degree of saturation as low as 75% can be achieved in soils before a continuous gas phase is formed and the gas starts to migrate upward and that a degree of saturation of 95% is sufficient to significantly reduce pore-pressure build up during cyclic loading (He & Chu, 2014; O'Donnell, Rittmann, et al., 2017; Pham, van Paassen, et al., 2018; Rebata-Landa & Santamarina, 2012; van Paassen et al., 2017; Wang et al., 2020; Yegian et al., 2007).

Important issues affecting the ability of abiotic desaturation to mitigate liquefaction non-disruptively and cost-effectively include the solubility of the gas introduced to the soil, the manner and rate at which the gas is introduced into the soil, the spacing of the gas introduction points, and the persistence of the induced desaturation. Gases of higher solubility become less effective for liquefaction mitigation because greater volumes of

production are needed to achieve adequate desaturation. Further, soluble gas may dissolve again into flowing groundwater, thus requiring additional desaturation treatments. For gas injection, the rate of gas introduction must be high enough to enter the soil pores at a significant distance from the injection point but low enough in order not to disturb the soil through fracking as a result of high injection pressures (Shi et al., 2019). Soil stratification and groundwater flow greatly influence the distribution and persistence of desaturation (Okamura et al., 2011; Shi et al., 2019). However, abiotic desaturation with air has been shown to persist in the presence of slowly moving groundwater in the laboratory (Yegian et al., 2007) and for up to 20 years in the field (Okamura et al., 2011), substantiating the promise of desaturation as a liquefaction mitigation measure.

Microbially induced desaturation (MID), a bio-mediated ground improvement technique, has also been proposed as a cost-effective non-disruptive means of mitigating liquefaction (Chu et al., 2015; O'Donnell, Rittmann, et al., 2017). To evaluate the economic viability of MID, I conducted a preliminary techno-economic analysis (TEA) to compare MID for liquefaction mitigation to permeation grouting of a uniform deposit of clean sand. Permeation grouting of a clean sand is one of the few cases where current technology may be cost effective for liquefaction mitigation under or around existing facilities without soil displacement or fracturing (Rasouli et al., 2016). If MID is shown to be cost competitive or superior to penetration grouting for this case, it should be cost-competitive for mitigation of liquefaction triggering in a much broader range of liquefiable subsurface conditions where there are no economically feasible mitigation technologies at the current time. For

instance, recent field trials in the Portland, Oregon area have shown that MID can desaturate even fine-grained liquefiable soils (Moug et al., 2020).

Microbially Induced Desaturation (MID) via Denitrification for Liquefaction Mitigation

Laboratory testing showed microbially induced desaturation (MID) via denitrification can successfully reduce the potential for triggering of liquefaction (O'Donnell, Rittmann, et al., 2017). In MID, nutrients are injected into the porewater to stimulate biogenic production of inert and relatively insoluble nitrogen gas (N_2) through dissimilatory reduction of nitrate, or denitrification (O'Donnell, Rittmann, et al., 2017; Pham, van Paassen, et al., 2018). Denitrification is a multi-step microbial process that transforms nitrate to nitrite to nitrous oxide to nitric oxide to nitrogen gas. This process also produces carbon dioxide (CO_2). However, as the solubility of CO_2 in water is relatively high, much more CO_2 than N_2 needs to be produced to significantly contribute to desaturation of the soil, particularly at greater depths. Denitrification can also induce calcium carbonate precipitation in the soil when the treatment substrates (e.g., nitrate or acetate) are provided as calcium salts in a process that has been referred to as microbially induced desaturation and precipitation, or MIDP (O'Donnell, Kavazanjian, et al., 2017). In MIDP, dissolved inorganic carbon (CO_2, H_2CO_3, HCO_3^-, CO_3^{2-}) introduced into solution from microbial processes combines with the calcium cations resulting in calcium carbonate precipitation. The calcium carbonate precipitation in MIDP can induce inter-particle cementation and enhance soil dilatancy along with desaturation, providing additional liquefaction mitigation mechanisms.

In MIDP, desaturation occurs at a much faster rate than carbonate precipitation. Hence, desaturation (i.e., MID) has been described as the first stage of the two-stage MIDP process (O'Donnell, Kavazanjian, et al., 2017; O'Donnell, Rittmann, et al., 2017). However, the volume of treatment substrates required to effectively cement the soil is much greater than what is required to desaturate the soil. So, if the persistence of the gas phase can be demonstrated to be of sufficient duration, MID will be economically favorable over MIDP, at least in terms of mitigating liquefaction triggering (cementation may have additional benefits with respect to mitigation of the consequences of earthquake loading). A variety of factors influence the technical and economic viability of MID for mitigation liquefaction triggering, including the substrate (nutrient) recipe, groundwater composition, persistence of biogenic gas, impact of soil conditions on treatment, capital and operating costs, and settlement of desaturated soil subject to seismic shaking.

Goal and Scope

This paper presents a techno-economic analysis (TEA) of microbially induced desaturation (MID) via microbial denitrification as a liquefaction triggering mitigation technique. The results of this analysis can be used to inform future laboratory and field studies and can be expanded into a complete life cycle sustainability assessment for MID. Within this TEA I aimed to:

1. Determine the required amount of materials and equipment to achieve the needed level of desaturation for liquefaction triggering mitigation by MID using acetate as the electron donor and carbon source in the treatment recipe.

2. Compare the costs to deploy MID treatment recipes to permeation grouting for mitigation of liquefaction triggering in a uniform clean sand deposit.

3. Identify uncertainties in the analysis and future steps needed to establish the feasibility of MID as a practical method for mitigation of liquefaction triggering beneath and around existing lifeline structures and other civil facilities.

TEA Framework

For the purposes of this TEA, I selected a hypothetical case study developed for a National Hazard Engineering Research Infrastructure (NHERI) workshop in Portland, Oregon in September 2019 with the assistance of a local ground improvement contractor (NHERI, 2019). Portland was chosen as the location for the hypothetical site because it is situated at the confluence of the Columbia and Willamette rivers and critical lifeline facilities, including the Portland International airport and oil and gas storage facilities in the Port of Portland containing 90% of the state's energy reserves, are founded on potentially liquefiable soils along the banks of these rivers. The TEA case history assumed a power substation with a 12.2 m x 24 m square footprint founded on top of a soil profile that included 7 m of liquefiable clean sand that required remediation. A plan and profile of the substation site is presented in Figure 32.

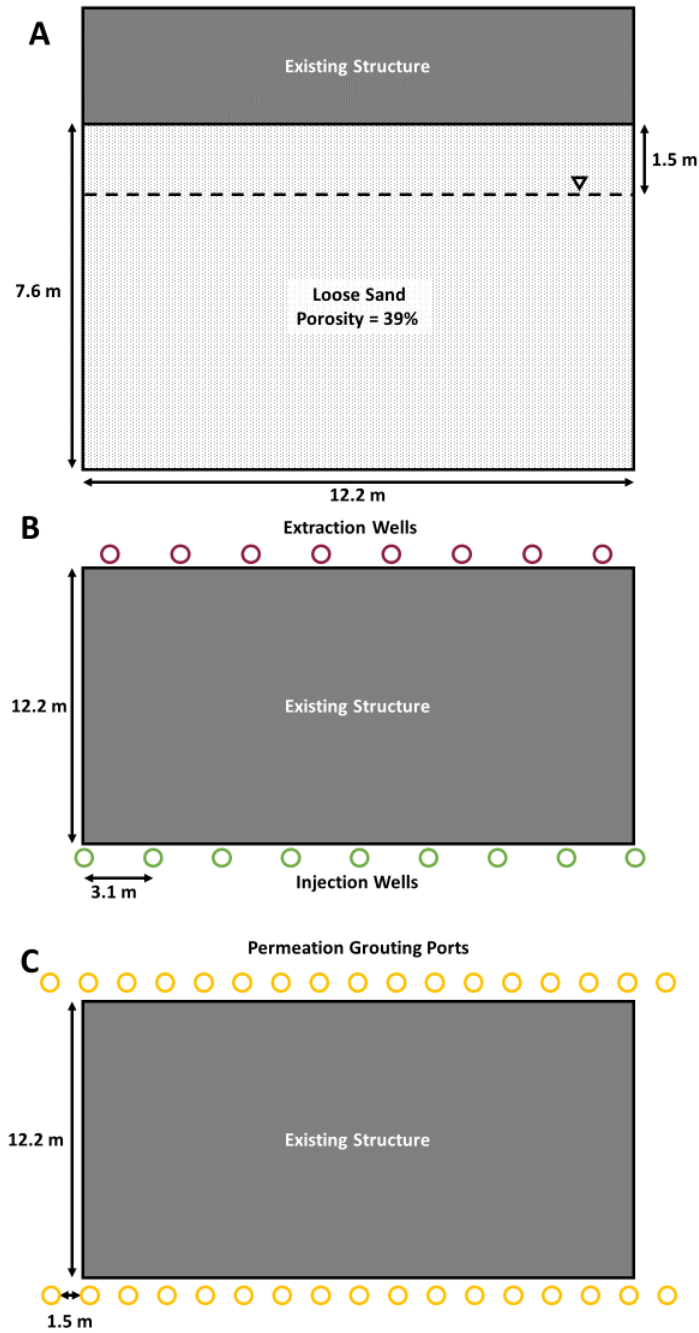Figure 32. [A] Section View, [B] Plan View Schematic of the Test Case for Evaluating Liquefaction Mitigation via MID Beneath an Existing Structure, and [C] Plan View Schematic of the Proposed Permeation Grouting Port Placement

The volume of soil requiring treatment, referred to herein as the functional unit, is 6.1 m (depth) x 24.4 m (width) x 12.2 m (length), giving a total of 1812 m³ of liquefiable soil.

The soil in the functional unit was assumed to be a uniform sand clean sand with a total unit weight 19.5 KN/m^3 (dry unit weight of 15.6 KN/m^3) and a porosity of 0.39 (void ratio 0.67) based upon typical soil properties (Christopher et al., 2006). It was assumed that the saturated hydraulic conductivity was 5x10^{-4} m/s, representative of a uniform clean sand.

Technical Assessment

Acetate has been identified as the preferred carbon source and electron donor for MIDP due to its biodegradability and its pH buffering capacity during carbonate precipitation (O'Donnell, Kavazanjian, et al., 2017). When only targeting desaturation, i.e., in MID, less expensive electron donors that also lead to N_2 and CO_2 production when oxidized, like glucose, can be considered (O'Donnell et al., 2019). However, for this analysis only acetate was considered due to the uncertainties associated with using these alternatives, including potential acidification and accumulation of intermediates.

Considering that 95% degree of saturation has been shown to be sufficient to significantly decrease liquefaction triggering potential (He et al., 2013; O'Donnell et al., 2019), I assumed (conservatively) that the target level of gas saturation at the deepest level of the treated zone to be 10% (note that, as the solubility increases the volume decreases with increasing pressure, gas saturation is expected to decrease with depth below the water table), as discussed in Chapter 3. This target desaturation level was used to estimate the required amount of substrate in the treatment recipe. Due to the high solubility of CO_2, only N_2 production was considered as contributing to desaturation. The stoichiometric equation assumed to estimate the needed materials to achieve the desired level of desaturation with MID is shown as follows.

$$0.30NO_3^- + 0.386C_2H_3O_2^- + 0.686H^+ + 0.148\,H_2O$$
$$\rightarrow 0.117N_2 + 0.441H_2CO_3 + 0.331CH_{1.8}O_{0.5}N_{0.2}$$
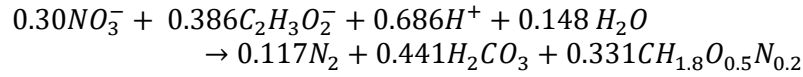
In developing the treatment recipe, I assumed that groundwater was used to constitute the substrate solutions and that any additional trace elements needed to stimulate microbial substrate conversion were in the groundwater. Our quantity estimates based upon these recipes assumed complete conversion of substrate by the denitrifying microorganisms and that no excess substrate was applied.

Eq. 26 was used to estimate the amount of nitrate (NO_3^-) required for the level of desaturation ($NO_3^-{}_d$, mol_{NO3}/m_{tot}^3) required to provide liquefaction mitigation over the entire treatment depth.

$$NO_3^-{}_d = \frac{Y_{NO_3^-}\left(\dfrac{[N_2]_g}{\ell} + \dfrac{p_{N_2}}{K_{H,N_2}}\right)\varphi}{Y_{N_2}} \qquad \text{Eq. 26}$$

where, Y_{NO3^-} (mol_{NO3^-}/mol_{donor}) and Y_{N2} (mol_{N2}/mol_{donor}) are the stoichiometric coefficients of N_2 and NO_3^- during denitrification, respectively, $[N_2]_g$ (mol/m_{pore}^3) describes the required amount of N_2 to achieve a target level of gas saturation (m_{gas}^3/m_{pore}^3), ℓ (m_{aq}^3/m_{pore}^3) considers the amount of solution in the pore space, p_{N_2} is the partial pressure of nitrogen gas (N_2) and is assumed to be equal to the sum of the hydraulic pressure at depth and the atmospheric pressure, $K_{H,N2}$ ($m_{aq}^3\,atm_{N2}/mol_{N2}$) is the Henry's constant for N_2 at standard temperature, and, φ (m_{pore}^3/m_{tot}^3) is soil porosity. I assumed that the MID treatment takes place in the subsurface and does not occur prior to the substrate reaching the end of the target treatment zone.

For the MID treatment system, I assumed that two parallel rows of injection and extraction wells were used to promote flow to desired treated areas beneath the structure for MID, as illustrated in Figure 32. These wells would have been placed using a hollow-stem auger. Each well was a 10.8 m-long PVC pipe extending 1.6 m above the ground surface and extending 1.5 m beyond the target treatment depth of 7.6 m. The pipe was slotted over the 6.1 m treatment zone and placed in a borehole and backfilled with gravel from the bottom up to 1.6 m from the ground surface. The top 1.5 m of pipe below the ground surface was then backfilled with a bentonite grout mixture to seal the well and to prevent flow of injected substrate to the surface. The number of wells (9 injection, 8 extraction) was determined based upon the estimated hydraulic conductivity of the liquefiable sand and the treatment substrate's viscosity and density to promote complete treatment over the target treatment area without inducing soil fracturing (Fradel et al., 2017). The time required to install and decommission each well was estimated based on personal communication with Condon Johnson Associates. The treatment was applied through an automated injection system to allow low flow without an attendant beyond a typical 8-hour workday.

A cumulative pumping time for all injection wells was estimated to be 260 hours based on the hydraulic conductivity of the soil (or 32.5 hours per well), an assumed flow length of 13.5 m, an assumed driving head of 4.5 m, and injection/extraction equipment (e.g., pipe diameter), such that the flow rate would not lead to fracking based on the theoretical test case soil conditions (Condon Johnson Associates, personal communication). Since it was assumed that only one treatment flush was needed to achieve

the needed desaturation, the relationship between reactant transport and reaction time did not need to be considered. I also assumed that the flow rate of the treatment solution was fast enough that the total travel time was not impacted by reduced hydraulic conductivity in the soil due to gas formation. While wells can be left in place for possible future re-injection, I assumed all would be decommissioned for cost estimation purposes.

Permeation grouting works to prevent liquefaction triggering by filling voids in the soil with microfine cement through injection (Rasouli et al., 2016). I assumed a treatment recipe water to cement ratio of 3:1 to promote flow and adequate cementation across the target area (Condon Johnson Associates, personal communication). Each of the 16-treatment point is spaced 1.5 m from the adjacent point. Each point has one vertical sleeve port pipe (12.2 m in length) and two battered pipes (one length being 6.1 m and the other 4.6 m). Each pipe is wet set in the ground using a cement-bentonite mud rotary drilling technique. It was assumed that treatment time would be 420 hours based on the Contractor's experience with typical pumping rates for the assumed soil type and injection equipment (Condon Johnson Associates, personal communication). Treatment is not applied autonomously and always requires an attendant.

Economic Assessment

A schematic showing the boundaries of what was included in the TEA is shown in Figure 33. To provide a realistic economic assessment, transportation of materials from the suppliers to the site has been included in the TEA. For MID treatment, use of industrial grade calcium acetate ($Ca(NO_3)_2$) and calcium nitrate ($Ca(C_2H_3O_2)_2$) was assumed. Cost

estimates were based on communication and quotes from an industrial supplier of chemicals in Milwaukie, OR for both calcium acetate ($2.50/kg) and calcium nitrate ($1.50/kg). Estimated costs for labor, well installation, decommissioning, and equipment mobilization and demobilization were provided by Condon-Johnson and Associates, Inc. (Portland, OR), who developed this case history for the NHERI workshop. These costs are detailed in

Table 14. Equipment mobilization and demobilization was assumed to be 10% of the well installation and treatment cost. When overhead and markup was considered, it was assumed to be 25% of the affiliated project aspect for both treatments. The best method to directly compare the liquefaction mitigation potential for both methods and conduct quality assurance and control is tomography (i.e., use of s-waves for grouting and p-waves for desaturation). The exact cost can vary widely, but is expected to be similar for both treatments and thereby wasn't considered in this comparison.
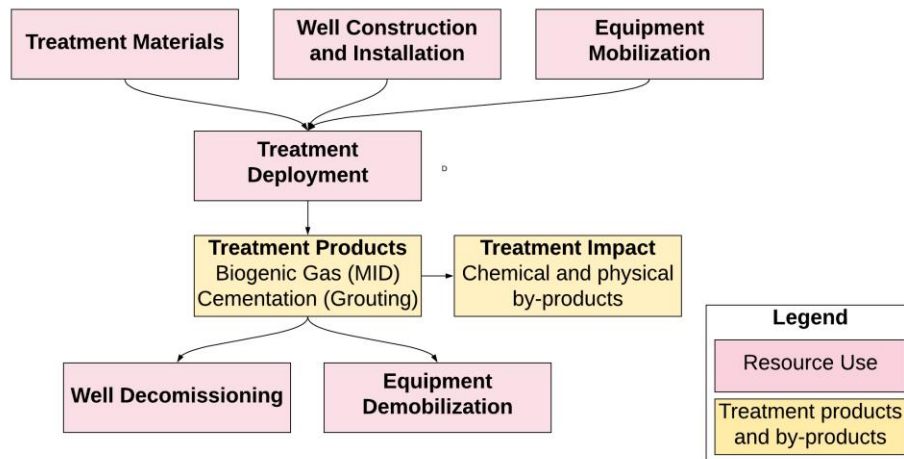
Figure 33. Aspects Considered for MID and Grouting Treatment in the TEA

Results and Discussion

The expected quantity of treatment substrate needed for MID using acetate as the electron donor is 0.61 kg/m_{tot}^3 of calcium nitrate ($0.91/$m_{tot}^3$) and 0.69 kg/$m_{tot}^3$ of calcium acetate ($1.73/$m_{tot}^3$), assuming a seawater environment as explored in Chapter 5 and Chapter 6. These estimates assumed simplified stoichiometry and did not consider potential inhibitions from the environment or accumulation microbial intermediates and by-products from MID. These costs were estimated using industrial grade chemicals purchased in bulk and price will vary depending on quantity purchased and supplier. The cost to rent equipment to install wells, perform treatments, and decommission wells and pay operators was estimated as a lumped cost based on the experience of the ground improvement contractor who prepared the estimate.

Table 14. Materials, Labor, and Permitting Costs for MID and Permeation Grouting

Well Installation	per well	Sleeve Port Pipe Installation	per sleeve port pipe
Installation equipment and labor	$1,500	Installation equipment and labor	$1,036
Construction Materials		Construction Materials	
Pump	$150	*Sleeve Port Pipe*	*$468*
Locking Cap	$150	*Drill Tooling*	*$117*
Lock and Cap	$25	*Fittings*	*$35*
End Cap	$5	*Cement*	*$66*
Well Screen	$75	*Bentonite*	*$20*
Blank	$13		
Sand	$384		
Bentonite	$54		
Permitting		Permitting	
Well Start Permit	$250	*Report and Start Permit*	$145
Report	$35		
Overhead and Markup	$660	*Overhead and Markup*	$472
Well Installation Total	$56,111	***Well Installation Total***	$80,225
Treatment Materials	kg/m³ MID solution	**Treatment Materials**	kg/m³ grout injection
Calcium Nitrate	$2.34	Microfine Cement	$290
Calcium Acetate	$4.43		
Overhead and Markup	$1.69	*Overhead and Markup*	$73
Treatment Materials Total	$6,043	***Treatment Materials Total***	$258,625
Injection	per hour	**Injection**	per hour
Equipment and labor	$259	Equipment and labor	$413
Overhead and Markup	$65	*Overhead and Markup*	$103
Injection Total	$84,723	***Injection Total***	$215,923
Well Decommissioning	per well		
Equipment and labor	$500		
Cement	$15		
Decommissioning Report	$50		
Overhead and Markup	$141		
Well Decommissioning Total	$12,006		
Mobilization and Demobilization	Project total	**Mobilization and Demobilization**	Project total
Installation	$5,611	Installation	$8,023
Treatment	$9,077	Treatment	$47,455
Decommissioning	$2,500		
Mobilization and Demobilization Total	$17,188	***Mobilization and Demobilization Total***	$55,477
Project Total	$176,070	**Project Total**	$610,250

For the hypothetical case described above, MID is the clearly a more cost-effective technology to mitigate liquefaction beneath the power substation compared to permeation grouting. However, it must be noted that, while both cases were designed to effectively mitigate liquefaction triggering, the treatment mechanisms cannot be directly compared due to significant differences, e.g., the consideration that grouting also provides mitigation of seismic settlement, which has not been demonstrated for MID. The total installation and injection labor time for MID and permeation grouting is estimated to be 360 and 650 hours, respectively. Permeation grouting is expected to disturb the physical environment, e.g. groundwater flow conditions, more than MID because of the technique's production of a very low permeability barrier (Rasouli et al., 2016). The environmental pH must be greater than 9 for permeation grouting to result in adequate hardening (Fan et al., 2018), which is greater than typical subsurface pH levels. This may result in long-term alkaline conditions and may be toxic to the surrounding environment (Fan et al., 2018). Whereas, MID is expected to impact the treatment zone's biochemical characteristics, but mostly remain within reasonable levels over the treatment duration as demonstrated in Chapter 6. Experimental research has also shown that the self-buffering capacity of the treatment does not lead to extreme change under lab conditions by the treatment's end (O'Donnell et al., 2019; O'Donnell, Rittmann, et al., 2017; Pham, van Paassen, et al., 2018). As such, MID has been identified as the lesser invasive and disruptive technique considering short-term factors and consequences.

Research is now progressing on several fronts to understand the long-term efficacy of desaturation as a ground improvement technique, critical for the health of lifelines. If

the site has rapid groundwater flow, gas may solubilize back into solution over time (Okamura et al., 2011; Shi et al., 2019). Injected air, primarily N_2 and O_2, has been shown to be resilient for up to 20 years (Okamura et al., 2011). This is promising for MID because N_2 is less soluble than O_2, and thereby less likely to resolubilize back into solution. Process monitoring during and after MID application is critical to understand the impact of the treatment and if reapplication is needed. However, considering the substantial cost savings from MID when compared to permeation grouting, reapplication of MID would still be more cost effective.

The results of this TEA are based on an idealized case. There are several additional factors that need to be considered when assessing the technical feasibility of MID for liquefaction mitigation. Subsurface heterogeneity and groundwater constituents and characteristics will influence MID. Soil heterogeneity at various scales (e.g. variations in pore size, hydraulic conductivity, stratification) will affect the delivery of substrate solution and the distribution, migration and entrapment of the produced gas phase (van Paassen et al. 2017). In the natural environment, the presence of other microbial species may lead to electron donor competition (Wilderer et al., 1987; Yamamoto-Ikemoto et al., 1996) and may lead to the production of microbial inhibitory compounds (e.g., H_2S) (Pan et al., 2019). pH will alter the species available for MID and may lead to the inhibition of denitrification, thereby adversely impacting MID (Almeida et al., 1995; Glass & Silverstein, 1998). Salinity has also been shown to impact denitrifying microorganisms, which may lead to process or output changes from MID (Mariangel et al., 2008) and should be considered depending on the intended treatment location (e.g., if coastal or riverine). Additionally, the

use of alternative electron donors that may be less expensive than acetate has should be explored, to further optimize the process. The natural conditions that are likely to surround a lifeline can be accommodated by adequately planning for MID treatment and bench scale and field testing prior to field deployment to better understand the processes behavior. These location-specific environmental and geotechnical conditions will impact the technical and economic feasibility of all ground improvement techniques, including permeation grouting, and must be taken into consideration during treatment design.

Conclusion

This TEA shows MID holds promise as a cost-effective liquefaction triggering mitigation technique to enhance the resiliency of lifelines constructed on liquefiable soil. In the TEA, permeation grouting and MID were compared using a generalized case study for liquefaction mitigation beneath a power substation under idealized geoenvironmental conditions. Both treatments were designed such that each technique achieved the estimated required liquefaction triggering potential reduction. MID was found to more than 3.5 times less expensive and require almost half of the labor. However, as the treatment mechanisms are different, a direct comparison for a simplified case, may not be fully appropriate and there are still significant factors, which may affect the technical and economical feasibility of the MID process, such as the use of alternative electron donors, the impact of local soil properties (i.e., heterogeneity and saturated hydraulic conductivity), and the groundwater environmental conditions process, and require further investigation.

CHAPTER 9

OVERVIEW, CONCLUSIONS, AND RECOMMENDATIONS FOR FUTURE
WORK

Overview

This work presented in this dissertation explored the issues associated with taking Microbially Induced Desaturation and Precipitation (MIDP) via denitrification from the laboratory to the field for mitigating earthquake-induced liquefaction. These issues included designing substrate recipes that account for background water constituents in the source-water, inhibition, microbial competition, and the cost of MIDP compared to alternative mitigation technologies. Chapter 2 reviewed recent work relevant to modeling MIDP. Chapter 3 focused on use of a simplified model for microbial denitrification to predict MIDP behavior in the 1-m geotechnical modeling centrifuge at the University of California, Davis. The simplified model developed in Chapter 3 generated basic predictions for how biogenic gas from MIDP behaves under simulated field stresses to design the treatment regimen used in the centrifuge experiment. In Chapter 4, the centrifuge testing program for MIDP and the associated monitoring and analyses are described. I used the simple model to design a treatment to achieve a target degree of saturation for mitigation of liquefaction triggering and then compared the observed behavior in the model to these predictions (to good effect).

Chapter 5 details a next-generation biogeochemical model for MIDP. It expands previous MIDP biogeochemical modelling efforts (O'Donnell et al., 2019; Pham, 2017) by including competitive biochemical processes, phase transfer and precipitation kinetics,

chemical speciation, and inhibition. Within the model's framework, I developed a baseline recipe for field application and then computed the impact of MIDP treatment on liquefaction mitigation (i.e., degree of saturation and percent carbonate precipitation).

In Chapter 6, I applied the model detailed in Chapter 5 to explore the impact of different source-water conditions on MIDP and the surrounding environment. Additionally, I identified the required adjustment to the substrate treatment recipe to account for background characteristics of the typical groundwater and coastal seawater source waters. Especially important in considering these source-water conditions was the roles and impacts of different nitrogen sources and electron acceptors other than nitrate and nitrite. In Chapter 7, I applied the model developed in Chapter 5 to investigate the impacts of alternative electron donor sources on MIDP behavior. Chapter 8 applied the information gathered during modeling to conduct a preliminary techno-economic analysis comparing liquefaction mitigation by desaturation using acetate as the electron donor to liquefaction mitigation by permeation grouting.

Conclusions

The goal of this dissertation was to explore and predict MIDP behavior in the field. By conducting centrifuge experimentation, I demonstrated how biogenic gas from MIDP may behave over a prototype soil profile under field stresses. As the soil desaturated over time due to biogenic gas production, the cyclic resistance increased. Based on simulated earthquake shaking for a magnitude 7.5 earthquake (i.e., 15 cycles of uniform cyclic loading), liquefaction was never induced in the desaturated soil for peak ground accelerations (PGAs) up to 0.45 g in a soil. The main cause of liquefaction mitigation was

desaturation, although a secondary factor was soil densification during later stages of the experiment. These tests confirmed that desaturating the soil to a degree of saturation of 90-95% can mitigate liquefaction triggering, reinforcing the promise of MIDP as a practical liquefaction mitigation technique

Experimental results from centrifuge testing are not a complete analogue to what may be experienced in the field, even if identical soil conditions could be achieved (achieving identical soil condition in centrifuge testing is inherently difficult). First, since the soil container had to be spun up and down to conduct necessary measurements, gas likely traveled between the layers. Second, since the pore fluid was not scaled for centrifuge conditions, the pore pressure dissipation rate likely was higher than what would be observed in the field and thus the soil in the centrifuge may not have behaved in a truly undrained manner (as expected in the field). Third, de-aired and de-ionized water containing no alternative electron acceptors and thereby did not evaluate any alternative biogeochemical reactions to denitrification, as expected in the field. Larger-scale experimentation (via additional centrifuge or pilot scale testing) can be done to overcome these challenges and fill current many of these knowledge gaps. Treatment monitoring can be done by tracking the consumption of substrate and by measuring changes in the soil, via p-wave benders, pore pressure sensors, and/or soil moisture content sensors, as demonstrated successfully here.

I advanced MIDP modeling from previous work I was associated with to a next-generation biogeochemical model to better understand the effect of the expected biochemical reactions in a mixed natural environment, substrate consumption, and product

formation, and the influence of the factors on MIDP. Through this, I identified some of the most important environmental aspects and biochemical reactions in representative natural environments that need to be considered to develop field treatment regimens. As I developed the model, I had to consider the background source-water composition and identify potential inhibition mechanisms. For example, denitrifiers are sensitive to saline conditions, which results in a slower rate of denitrification in seawater compared to groundwater. The background characteristics must also be measured to predict potential by-products and account for their effects. In particular, I included alternative electron acceptors and incorporated their biochemical processes in the model. For instance, seawater has a much higher concentration of sulfate compared to groundwater, and this creates the risk that more H_2S will be produced. Not only is H_2S potentially harmful to humans if present at high concentrations, it inhibits denitrification when it remains in solution. So, consideration of sulfate reduction and its by-products is essential to proper modeling of MIDP in a field setting.

One important outcome of the modeling I conducted is that I quantified the trade-off associated with MIDP treatment using three alternative electron-donor substrates, glucose, glucose via molasses, and acetate. While denitrification using glucose as the electron donor is faster than with acetate, H_2S production is a greater risk with glucose, due to the greater endogenous decay linked to sulfate reduction. Another difference stemming from the donor source is its impact on pH. A decreased pH can slow denitrification from HNO_2. Denitrification using added acetate (e.g., as calcium acetate) produces more base than adding glucose. This mitigates the pH decline from rapid CO_2 generation, and this

promotes coincident $CaCO_3$ precipitation, which also acts as a sink to prevent alkalinization and helps keep the pH circumneutral. In contrast, glucose produces more protons during it oxidation reaction, and this leads to slight acidification, temporary accumulation of HNO_2, and less $CaCO_3$ precipitation. As cost savings for using glucose (or molasses) are not large as the electron donor in MIDP, the pre-eminent factor for the substrate recipe should be maximizing treatment efficacy and minimizing unwanted by-products. On this basis, calcium acetate appears to be the preferred electron donor for MIDP.

Recommendations for Further Study

The work presented here is a necessary step in deploying MIDP in practice as a cost-effective and environmentally sound technique for mitigation of earthquake induced soil liquefaction. Additional testing is necessary to evaluate experimentally if inhibition and microbial competition is under- or over-estimated by the next generation biogeochemical model. Using such testing, parameters determined mechanistically or pulled from literature can be verified by comparison to and analysis of the experimental and numerical modeling results. Since a batch model was used to develop the biogeochemical model presented herein, the model can most directly be experimentally evaluated through microcosm experiments. In these experiments, dissolved organic carbon, dissolved inorganic carbon, and pH should be measured to estimate the dissolved inorganic carbon species, and biogenic gas species (i.e. N_2, CO_2, H_2S, NO, N_2O), and aqueous ionic species should be measured to promote robust model and MIDP process evaluation. One potential limitation of using microcosms is sorption of substrates and microbial products on to the soil matrix

used in the microcosm, and this should be considered during analysis for mass balance. Another limitation of using microcosms is that these do not represent substrate transport, as would be experienced in the field. Combining numerical and physical experiments will point out the most critical phenomena controlling MIDP and inform future field efforts.

The generic biogeochemical modeling toolbox by van Turnhout et al. (2016) should be applied to evaluate or calibrate the model to microcosm experimental and numerical results considering multiple microbial metabolisms that consume different electron acceptors and donors. Currently, many of the parameters have been assumed from literature sources, but these values can vary widely between experiments. Within the toolbox, Bayesian statistical inference can used as a statistical method to calibrate the model to experiments using the probability of a parameter's value within a user-defined reasonable range that adheres to mechanistic principles (Laloy and Vrught, 2012; Vrugt et al., 2003; van Turnhout et al., 2016). The probability is updated with each optimization iteration as more information becomes available about the previous probability distribution of a parameter during fitting optimization and the likelihood of the parameters given the measured data improves, thereby limiting uncertainty. This numerical technique may be useful when trying to represent the experimental scenario through modeling, like investigating the change in inhibition constants and phase transfer coefficients for a specific environment. Care should be taken to not fit an excess of parameters, thereby risking uncertainty in the model leading to computational errors (i.e., numerical divergence) and numerical modeling errors that are difficult to measure (e.g., overfitting). These parameter values can be applied to more complex transport models for MIDP, though since parameters vary wildly between

experiments and environments, these should only be used to predict treatment trends rather than exact values.

From this work, multi-dimensional modeling to predict MIDP in field considering groundwater flow should be established to maximize future applicability. While I demonstrated that diffusion is unlikely to be a significant driving force in the transport of MIDP products and by-products, advection from treatment flow (e.g., through injection and extraction) and groundwater flow surely will have a significant impact on MIDP for field conditions. While the van Turnhout Toolbox had been adapted to consider 1-D diffusive (vertical or horizontal) transport to analyze the distribution of MIDP products and gas distribution over depth, it will be important to explore alternative modeling software capable of modeling reactant fate and transport in the subsurface. This will be particularly important when exploring the changes in the environment during MIDP substrate injection, which inherently creates subsurface flow. The advanced transport model must be able to retain the biogeochemical complexity established from the work done in this dissertation (e.g., H_2S production from coincident sulfate reduction and HNO_2 accumulation due to low pH). It also must be able to represent changes in biogenic gas composition, mineral products, and by-products over the soil profile. This more advanced model will lead to better understanding to the anticipated biogeochemical complexities that are likely to affect field-scale MIDP deployment.

Finally, a framework for MIDP field-scale treatment, monitoring, and analysis should be designed and evaluated by field-scale testing. The framework will make it possible to understand the impacts of the substrate recipe, source-water and other

environmental characteristics, and geologic conditions in the field. The output from this dissertation and future work can then be used to establish field treatment plasn, including the initial substrate concentrations, experiment duration, and sampling frequency. Groundwater and soil quality analyses should also be conducted during and post-treatment, such that potential process inhibitions, microbial competition, and by-products and side effects can be accounted for. Process monitoring during and after MIDP application is critical to observe treatment and understand the impact of the treatment. Establishing a repeatable framework will allow comparison of trends of MIDP behavior and changes in the surrounding environment; observed differences and their causes can be learned from and applied to future efforts: e.g., better informed MIDP implementation (including injection and extraction well location and substrate recipe), such that the desired liquefaction mitigation is achieved while achieving cost-effectiveness, environmental protection, and sustainability goals.

REFERENCES

2018 Edition of the Drinking Water Standards and Health Advisories Tables. (2018). https://www.epa.gov/sites/production/files/2018-03/documents/dwtable2018.pdf

Abdul-Talib, S., Hvitved-Jacobsen, T., Vollertsen, J., & Ujang, Z. (2002). Half saturation constants for nitrate and nitrite by in-sewer anoxic transformations of wastewater organic matter. *Water Science and Technology*, *46*(9), 185-192.

Abeling, U., & Seyfried, C. F. (1992). ANAEROBIC-AEROBIC TREATMENT OF HIGH-STRENGTH AMMONIUM WASTE-WATER - NITROGEN REMOVAL VIA NITRITE. *Water Science and Technology*, *26*(5-6), 1007-1015.

Achal, V., Pan, X. L., & Zhang, D. Y. (2012). Bioremediation of strontium (Sr) contaminated aquifer quartz sand based on carbonate precipitation induced by Sr resistant Halomonas sp. *Chemosphere*, *89*(6), 764-768. https://doi.org/10.1016/j.chemosphere.2012.06.064

Achtnich, C., Bak, F., & Conrad, R. (1995). COMPETITION FOR ELECTRON-DONORS AMONG NITRATE REDUCERS, FERRIC IRON REDUCERS, SULFATE REDUCERS, AND METHANOGENS IN ANOXIC PADDY SOIL. *Biology and Fertility of Soils*, *19*(1), 65-72. https://doi.org/10.1007/bf00336349

Adamidis, O., & Madabhushi, G. S. P. (2015). Use of viscous pore fluids in dynamic centrifuge modelling. *International Journal of Physical Modelling in Geotechnics*, *15*(3), 141-149. https://doi.org/10.1680/ijpmg.14.00022

Adamidis, O., & Madabhushi, S. P. G. (2018). Experimental investigation of drainage during earthquake-induced liquefaction. *Geotechnique*, *68*(8), 655-665. https://doi.org/10.1680/jgeot.16.P.090

Administration, O. S. a. H. *Hydrogen Sulfide*. United States Department of Labor. https://www.osha.gov/hydrogen-sulfide/standards

Al Qabany, A., Soga, K., & Santamarina, C. (2012). Factors Affecting Efficiency of Microbially Induced Calcite Precipitation. *Journal of Geotechnical and Geoenvironmental Engineering*, *138*(8), 992-1001. https://doi.org/10.1061/(asce)gt.1943-5606.0000666

Alin, S., Greeley, D., Feely, R., & Herndon, J. (2016). *2016 West Coast Ocean Acidification Cruise* National Oceanic and Atmospheric Administration.

Almeida, J. S., Julio, S. M., Reis, M. A. M., & Carrondo, M. J. T. (1995). NITRITE INHIBITION OF DENITRIFICATION BY PSEUDOMONAS-FLUORESCENS.

Biotechnology and Bioengineering, *46*(3), 194-201. https://doi.org/10.1002/bit.260460303

Anbu, P., Kang, C. H., Shin, Y. J., & So, J. S. (2016). Formations of calcium carbonate minerals by bacteria and its multiple applications. *Springerplus*, *5*, Article 250. https://doi.org/10.1186/s40064-016-1869-2

Aquatic Life Ambient Qater Quality Criteria For Ammonia - Freshwater. (2013). https://www.epa.gov/sites/production/files/2015-08/documents/aquatic-life-ambient-water-quality-criteria-for-ammonia-freshwater-2013.pdf

Arnold, T. L., Sharpe, J. B., Bexfield, L. M., Musgrove, M., Erickson, M.L., Kingsbury, J. A., Degnan, J. R., Tesoriero, A. J., Kulongoski, J. T., & Belitz, K. (2020). Datasets from Groundwater-Quality and Select Quality-Control Data from the National Water-Quality Assessment Project, January through December 2016, and Previously Unpublished Data from 2013 to 2015. In U. S. G. Survey (Ed.). https://doi.org/https://doi.org/10.5066/P9W4RR74

Bae, W., & Rittmann, B. E. (1996). A structured model of dual-limitation kinetics. *Biotechnology and Bioengineering*, *49*(6), 683-689. https://doi.org/https://doi.org/10.1002/(SICI)1097-0290(19960320)49:6<683::AID-BIT10>3.0.CO;2-7

Baird, A. J., & Waldron, S. (2003). Shallow horizontal groundwater flow in peatlands is reduced by bacteriogenic gas production. *Geophysical Research Letters*, *30*(20), Article 2043. https://doi.org/10.1029/2003gl018233

Bongoua-Devisme, A. J., Mustin, C., & Berthelin, J. (2012). Responses of Iron-Reducing Bacteria to Salinity and Organic Matter Amendment in Paddy Soils of Thailand. *Pedosphere*, *22*(3), 375-393. https://doi.org/10.1016/s1002-0160(12)60024-1

Bruland, K. W., Rue, E. L., & Smith, G. J. (2001). Iron and macronutrients in California coastal upwelling regimes: Implications for diatom blooms [https://doi.org/10.4319/lo.2001.46.7.1661]. *Limnology and Oceanography*, *46*(7), 1661-1674. https://doi.org/https://doi.org/10.4319/lo.2001.46.7.1661

Burbank, M. B., Weaver, T. J., Green, T. L., Williams, B. C., & Crawford, R. L. (2011). Precipitation of Calcite by Indigenous Microorganisms to Strengthen Liquefiable Soils. *Geomicrobiology Journal*, *28*(4), 301-312, Article Pii 938115271. https://doi.org/10.1080/01490451.2010.499929

Cadogan, S. P., Mistry, B., Wong, Y., Maitland, G. C., & Trusler, J. P. M. (2016). Diffusion Coefficients of Carbon Dioxide in Eight Hydrocarbon Liquids at Temperatures between (298.15 and 423.15) K at Pressures up to 69 MPa. *Journal of Chemical and Engineering Data*, *61*(11), 3922-3932. https://doi.org/10.1021/acs.jced.6b00691

Caicedo, B., & Thorel, L. (2014). Centrifuge modelling of unsaturated soils. *Journal of Geo-Engineering Sciences*, *2*(1-2), 83-103. https://doi.org/10.3233/JGS-130013

Calderer, M., Jubany, I., Pérez, R., Martí, V., & de Pablo, J. (2010). Modelling enhanced groundwater denitrification in batch micrococosm tests. *Chemical Engineering Journal*, *165*(1), 2-9. https://doi.org/https://doi.org/10.1016/j.cej.2010.08.042

Cardoso, R. B., Sierra-Alvarez, R., Rowlette, P., Flores, E. R., Gómez, J., & Field, J. A. (2006). Sulfide oxidation under chemolithoautotrophic denitrifying conditions. *Biotechnol Bioeng*, *95*(6), 1148-1157. https://doi.org/10.1002/bit.21084

Castanier, Métayer-Levrel, & Perthuisot. (2000). Bacterial Roles in the Precipitation of Carbonate Minerals. In A. S. M. Riding R.E. (Ed.), *Microbial Sediments*. Springer.

Cheng, L., & Cord-Ruwisch, R. (2012). In situ soil cementation with ureolytic bacteria by surface percolation. *Ecological Engineering*, *42*, 64-72. https://doi.org/10.1016/j.ecoleng.2012.01.013

Chong, T. H., & Sheikholeslami, R. (2001). Thermodynamics and kinetics for mixed calcium carbonate and calcium sulfate precipitation. *Chemical Engineering Science*, *56*(18), 5391-5400. https://doi.org/10.1016/s0009-2509(01)00237-8

Christopher, B., Schwartz, C., & Boudreau, R. (2006). Chapter 5.0 Geotechnical Inputs For Pavement Design. In *Geotechnical Aspects of Pavements Reference Manual*. U.S. Department of Transportation Federal Highway Administration.

Chu, J., Ivanov, V., He, J., & Naeimi, M. (2015). Use of biogeotechnologies for disaster mitigation. In S. Iai (Ed.), *Geotechnics for Catastrophic Flooding Events* (1st ed.).

Clarke, M. A. (2003). SYRUPS. In B. Caballero (Ed.), *Encyclopedia of Food Sciences and Nutrition (Second Edition)* (pp. 5711-5717). Academic Press. https://doi.org/https://doi.org/10.1016/B0-12-227055-X/01175-5

Council, U. S. N. R. (2009). Hydrogen Sulfide. In *Emergency and Continuous Exposure Guidance Levels for Selected Submarine Contaminants: Volume 3*. National Academies Press.

Craft, C., Clough, J., Ehman, J., Joye, S., Park, R., Pennings, S., Guo, H. Y., & Machmuller, M. (2009). Forecasting the effects of accelerated sea-level rise on tidal marsh ecosystem services. *Frontiers in Ecology and the Environment*, *7*(2), 73-78. https://doi.org/10.1890/070219

Darby, K. M., Boulanger, R. W., & DeJong, J. T. (2017). *Effect of multiple shaking events on cone penetration resistances in saturated sand* Performance-based Design in Earthquake Geotechnical Engineering (PBD-III), Vancouver.

Darby, K. M., Hernandez, G. L., DeJong, J. T., Boulanger, R. W., Gomez, M. G., & Wilson, D. W. (2019). Centrifuge Model Testing of Liquefaction Mitigation via Microbially Induced Calcite Precipitation. *Journal of Geotechnical and Geoenvironmental Engineering*, *145*(10), Article 04019084. https://doi.org/10.1061/(asce)gt.1943-5606.0002122

DeJong, J. T., Mortensen, B. M., Martinez, B. C., & Nelson, D. C. (2010). Bio-mediated soil improvement. *Ecological Engineering*, *36*(2), 197-210. https://doi.org/10.1016/j.ecoleng.2008.12.029

Dickson, A. (2010). The carbon dioxide system in seawater: equilibrium chemistry and measurement. In *Guide to best practices for ocean acidifi cation research and data reporting* (pp. 17 - 52). Publications Office of the European Union.

Dincer, A. R., & Kargi, F. (1999). Salt inhibition of nitrification and denitrification in saline wastewater. *Environmental Technology*, *20*(11), 1147-1153. https://doi.org/10.1080/09593332008616912

El Mountassir, G., Minto, J. M., van Paassen, L. A., Salifu, E., & Lunn, R. J. (2018). Applications of Microbial Processes in Geotechnical Engineering. In G. M. Gadd & S. Sariaslani (Eds.), *Advances in Applied Microbiology, Vol 104* (Vol. 104, pp. 39-91). https://doi.org/10.1016/bs.aambs.2018.05.001

Estuardo, C., Marti, M. C., Huilinir, C., Lillo, E. A., & von Bennewitz, M. R. (2008). Improvement of nitrate and nitrite reduction rates prediction. *Electronic Journal of Biotechnology*, *11*(3), Article 6. https://doi.org/10.2225/vol11-issue3-fulltext-6

Extension, U. (2007). *Healthy Drinking Waters for Massachusetts*. https://ag.umass.edu/sites/ag.umass.edu/files/fact-sheets/pdf/hydrogensulfide.pdf

Fan, J., Wang, D., & Qian, D. (2018). Soil-cement mixture properties and design considerations for reinforced excavation. *Journal of Rock Mechanics and Geotechnical Engineering*, *10*(4), 791-797. https://doi.org/https://doi.org/10.1016/j.jrmge.2018.03.004

Fawell, J. K., Lund, U., Mintz, B., Galal-Gorchev, H., Helmer, R., Bonnefoy, X., & Espinoza, O. (1996). *Hydrogen Sulfide in Drinking-water*. https://www.who.int/water_sanitation_health/dwq/hydrogensulfide.pdf

Folger, H. S. (2011). *Essentials of Chemical Reaction Engineering* International Series in the Physical and Chemical Engineering Sciences,

Fradel, J., Van de Zilver, M., Grabiak, T., & Morrow, D. (2017). *In Situ Remediation: Design Considerations and Performance Monitoring Technical Guidance Document*. https://www.nj.gov/dep/srp/guidance/srra/in_situ_remediation.pdf?version_1_0

Garnier, J., Gaudin, C., Springman, S. M., Culligan, P. J., Goodings, D., Konig, D., Kutter, B., Phillips, R., Randolph, M. F., & Thorel, L. (2007). Catalogue of scaling laws and similitude questions in geotechnical centrifuge modelling. *International Journal of Physical Modelling in Geotechnics*, *7*(3), 01-23. https://doi.org/10.1680/ijpmg.2007.070301

Glass, C., & Silverstein, J. (1998). Denitrification kinetics of high nitrate concentration water: pH effect on inhibition and nitrite accumulation. *Water Research*, *32*(3), 831-839. https://doi.org/10.1016/s0043-1354(97)00260-1

Glass, C., Silverstein, J., & Oh, J. (1997). Inhibition of denitrification in activated sludge by nitrite. *Water Environment Research*, *69*(6), 1086-1093. https://doi.org/10.2175/106143097x125803

Gomez, M. G., Graddy, C. M. R., DeJong, J. T., Nelson, D. C., & Tsesarsky, M. (2018). Stimulation of Native Microorganisms for Biocementation in Samples Recovered from Field-Scale Treatment Depths. *Journal of Geotechnical and Geoenvironmental Engineering*, *144*(1), Article 04017098. https://doi.org/10.1061/(asce)gt.1943-5606.0001804

Grigoryan, A. A., Cornish, S. L., Buziak, B., Lin, S., Cavallaro, A., Arensdorf, J. J., & Voordouw, G. (2008). Competitive oxidation of volatile fatty acids by sulfate- and nitrate-reducing bacteria from an oil field in Argentina. *Applied and Environmental Microbiology*, *74*(14), 4324-4335. https://doi.org/10.1128/aem.00419-08

Grouting Technology. (2017). https://www.publications.usace.army.mil/Portals/76/Publications/EngineerManuals/EM_1110-2-3506.pdf

Hall, C., van Paassen, L., Rittmann, B., Kavazanjian, E., DeJong, J., & Wilson, D. (2018). *Predicting desaturation by biogenic gas formation via denitrification during centrifugal loading 7th International Conference on Unsaturated Soils*, Hong Kong, China.

Hall, C. A., Hernandez, G., Darby, K. M., van Paassen, L., Kavazanjian Jr., E., DeJong, J., & Wilson, D. (2018). Centrifuge Model Testing of Liquefaction Mitigation via Denitrification-Induced Desaturation. In *Geotechnical Earthquake Engineering and Soil Dynamics V* (pp. 117-126). https://doi.org/doi:10.1061/9780784481455.011

Hamlin, H. J., Michaels, J. T., Beaulaton, C. M., Graham, W. F., Dutt, W., Steinbach, P., Losordo, T. M., Schrader, K. K., & Main, K. L. (2008). Comparing denitrification rates and carbon sources in commercial scale upflow denitrification biological filters in aquaculture. *Aquacultural Engineering*, *38*(2), 79-92. https://doi.org/https://doi.org/10.1016/j.aquaeng.2007.11.003

He, J., & Chu, J. (2014). Undrained Responses of Microbially Desaturated Sand under Monotonic Loading. *Journal of Geotechnical and Geoenvironmental Engineering*, *140*(5), 04014003. https://doi.org/doi:10.1061/(ASCE)GT.1943-5606.0001082

He, J., Chu, J., & Ivanov, V. (2013). Mitigation of liquefaction of saturated sand using biogas. *Geotechnique*, *63*(4), 267-275. https://doi.org/10.1680/geot.SIP13.P.004

Heidari, P., Kordestany, A., & Ghazanfari, M. H. (2011). *An Experimental Investigation of Parameters Affecting Oil Recovery Efficiency Alteration during a Microbially Aided Water Flooding Process* (Petroleum Science and Technology, Issue.

Henze, M., Gujer, W., Mino, T., Matsuo, T., Wentzel, M. C., Marais, G. V. R., & Van Loosdrecht, M. C. M. (1999). Activated Sludge Model No.2d, ASM2d. *Water Science and Technology*, *39*(1), 165-182. https://doi.org/10.1016/s0273-1223(98)00829-4

Hydrogen Sulfide. (2009). In U. S. N. R. Council (Ed.), *Emergency and Continuous Exposure Guidance Levels for Selected Submarine Contaminants: Volume 3*. National Academies Press.

Ingvorsen, K., Zehnder, A. J. B., & Jørgensen, B. B. (1984). Kinetics of Sulfate and Acetate Uptake by Desulfobacter postgatei. *Applied and Environmental Microbiology*, *47*(2), 403.

Jia, M., Winkler, M. K. H., & Volcke, E. I. P. (2020). Elucidating the Competition between Heterotrophic Denitrification and DNRA Using the Resource-Ratio Theory. *Environmental Science & Technology*, *54*(21), 13953-13962. https://doi.org/10.1021/acs.est.0c01776

Karatas, I., Kavazanjian, E., & Rittmann, B. (2008). *Microbially Induced Precipitation of Calcite Using Pseudomonas Denitrificans First International Conference on Biogeotechnical Engineering*, Delft, Netherlands.

Kavazanjian, E., O'Donnell, S. T., & Hamdan, N. (2015). Biogeotechnical Mitigation of Earthquake-Induced Soil Liquefaction by Denitrification: A Two-Stage Process. 6th International Conference on Earthquake Geotechnical Engineering, Christchurch, NZ.

Khodadadi, T.H., Kavazanjian, E., van Paassen, L. A., & DeJong, J. T. (2017). *Bio-Ground Materials: A Review* Hawaii, US.

Krishna Rao, R., & Gnanam, A. (1990). Inhibition of nitrate and nitrite reductase activities by salinity stress in Sorghum vulgare. *Phytochemistry*, *29*(4), 1047-1049. https://doi.org/https://doi.org/10.1016/0031-9422(90)85400-A

Kutter, B. L. (2013). Effects of capillary number, Bond number, and gas solubility on water saturation of sand specimens. *Canadian Geotechnical Journal*, *50*(2), 133-144. https://doi.org/10.1139/cgj-2011-0250

Liang, Z., Sun, J., Zhan, C., Wu, S., Zhang, L., & Jiang, F. (2020). Effects of sulfide on mixotrophic denitrification by Thauera-dominated denitrifying sludge [10.1039/C9EW01014A]. *Environmental Science: Water Research & Technology*, *6*(4), 1186-1195. https://doi.org/10.1039/C9EW01014A

Lilja, E. E., & Johnson, D. R. (2016). Segregating metabolic processes into different microbial cells accelerates the consumption of inhibitory substrates. *The ISME journal*, *10*(7), 1568-1578. https://doi.org/10.1038/ismej.2015.243

Lin, H., Suleiman, M. T., Brown, D. G., & Kavazanjian, E. (2016). Mechanical Behavior of Sands Treated by Microbially Induced Carbonate Precipitation. *Journal of Geotechnical and Geoenvironmental Engineering*, *142*(2), Article 04015066. https://doi.org/10.1061/(asce)gt.1943-5606.0001383

Lin, Y.-H. (2008). Kinetics of nitrogen and carbon removal in a moving-fixed bed biofilm reactor. *Applied Mathematical Modelling*, *32*(11), 2360-2377. https://doi.org/https://doi.org/10.1016/j.apm.2007.09.009

Ma, J., Yang, Q., Wang, S. Y., Wang, L., Takigawa, A., & Peng, Y. Z. (2010). Effect of free nitrous acid as inhibitors on nitrate reduction by a biological nutrient removal sludge. *Journal of Hazardous Materials*, *175*(1-3), 518-523. https://doi.org/10.1016/j.jhazmat.2009.10.036

Mahabadi, N., Dai, S., Seol, Y., Yun, T. S., & Jang, J. (2016). The water retention curve and relative permeability for gas production from hydrate-bearing sediments: pore-network model simulation. *Geochemistry Geophysics Geosystems*, *17*(8), 3099-3110. https://doi.org/10.1002/2016gc006372

Mahabadi, N., & Jang, J. (2014). Relative water and gas permeability for gas production from hydrate-bearing sediments. *Geochemistry Geophysics Geosystems*, *15*(6), 2346-2353. https://doi.org/10.1002/2014gc005331

Mariangel, L., Aspe, E., Marti, M. C., & Roeckel, M. (2008). The effect of sodium chloride on the denitrification of saline fishery wastewaters. *Environmental Technology*, *29*(8), 871-879. https://doi.org/10.1080/09593330802015318

Martin, D., Dodds, K., Butler, I. B., & Ngwenya, B. T. (2013). Carbonate Precipitation under Pressure for Bioengineering in the Anaerobic Subsurface via Denitrification. *Environmental Science & Technology*, *47*(15), 8692-8699. https://doi.org/10.1021/es401270q

Marton, J. M., Herbert, E. R., & Craft, C. B. (2012). Effects of Salinity on Denitrification and Greenhouse Gas Production from Laboratory-incubated Tidal Forest Soils. *Wetlands*, *32*(2), 347-357. https://doi.org/10.1007/s13157-012-0270-3

McCarty, G. W., & Bremner, J. M. (1991). PRODUCTION OF UREASE BY MICROBIAL ACTIVITY IN SOILS UNDER AEROBIC AND ANAEROBIC CONDITIONS. *Biology and Fertility of Soils*, *11*(3), 228-230. https://doi.org/10.1007/bf00335772

Meeussen, J. C. L. (2003). ORCHESTRA: An object-oriented framework for implementing chemical equilibrium models. *Environmental Science & Technology*, *37*(6), 1175-1182. https://doi.org/10.1021/es025597s

Millero, F. J., Feistel, R., Wright, D. G., & McDougall, T. J. (2008). The composition of Standard Seawater and the definition of the Reference-Composition Salinity Scale. *Deep Sea Research Part I: Oceanographic Research Papers*, *55*(1), 50-72. https://doi.org/https://doi.org/10.1016/j.dsr.2007.10.001

Mitchell, J. K., & Santamarina, J. C. (2005). Biological considerations in geotechnical engineering. *Journal of Geotechnical and Geoenvironmental Engineering*, *131*(10), 1222-1233. https://doi.org/10.1061/(asce)1090-0241(2005)131:10(1222)

Montoya, B. M., & DeJong, J. T. (2015). Stress-Strain Behavior of Sands Cemented by Microbially Induced Calcite Precipitation. *Journal of Geotechnical and Geoenvironmental Engineering*, *141*(6), Article 04015019. https://doi.org/10.1061/(asce)gt.1943-5606.0001302

Montoya, B. M., Dejong, J. T., & Boulanger, R. W. (2013). Dynamic response of liquefiable sand improved by microbial-induced calcite precipitation. *Geotechnique*, *63*(4), 302-312. https://doi.org/10.1680/geot.SIP13.P.019

Mortensen, B. M., Haber, M. J., DeJong, J. T., Caslake, L. F., & Nelson, D. C. (2011). Effects of environmental factors on microbial induced calcium carbonate precipitation. *Journal of Applied Microbiology*, *111*(2), 338-349. https://doi.org/10.1111/j.1365-2672.2011.05065.x

Moug, D., Khosravifar, A., Preciado, M., Sorenson, K., Stokoe, K., Menq, F., Zhang, B., van Paassen, L., Kavazanjian, E., Stallings Young, E., & Wang, Y. (2020). Field evaluation of microbially induced desaturation for liquefaction mitigation of silty soils. 17th World Conference on Earthquake Eng ineering (17WCEE), Sendai, Japan.

Najafpour, G. D., & Shan, C. P. (2003). Enzymatic hydrolysis of molasses. *Bioresour Technol*, *86*(1), 91-94. https://doi.org/10.1016/s0960-8524(02)00103-7

NHERI. (2019). *Stiffness-based Ground Improvement Monitoring Workshop September 11-12, 2019*. https://www.designsafe-ci.org/learning-center/workshop-190911/

Nikodinovic-Runic, J., Guzik, M., Kenny, S. T., Babu, R., Werker, A., & O Connor, K. E. (2013). Chapter Four - Carbon-Rich Wastes as Feedstocks for Biodegradable Polymer (Polyhydroxyalkanoate) Production Using Bacteria. In S. Sariaslani & G. M. Gadd (Eds.), *Advances in Applied Microbiology* (Vol. 84, pp. 139-200). Academic Press. https://doi.org/https://doi.org/10.1016/B978-0-12-407673-0.00004-7

O'Donnell, S. (2016). *Mitigation of Earthquake-Induced Soil Liquefaction via Microbial Denitrification: A Two-Stage Process* Arizona State University]. Tempe, AZ.

O'Donnell, S. T., Hall, C. A., Kavazanjian, E., & Rittmann, B. E. (2019). Biogeochemical Model for Soil Improvement by Denitrification. *Journal of Geotechnical and Geoenvironmental Engineering*, *145*(11), Article 04019091. https://doi.org/10.1061/(asce)gt.1943-5606.0002126

O'Donnell, S. T., Kavazanjian, E., & Rittmann, B. E. (2017). MIDP: Liquefaction Mitigation via Microbial Denitrification as a Two-Stage Process. II: MICP. *Journal of Geotechnical and Geoenvironmental Engineering*, *143*(12), Article 04017095. https://doi.org/10.1061/(asce)gt.1943-5606.0001806

O'Donnell, S. T., Rittmann, B. E., & Kavazanjian, E. (2017). MIDP: Liquefaction Mitigation via Microbial Denitrification as a Two-Stage Process. I: Desaturation. *Journal of Geotechnical and Geoenvironmental Engineering*, *143*(12), Article 04017094. https://doi.org/10.1061/(asce)gt.1943-5606.0001818

O'Donnelli, S. T., Hall, C. A., Kavazanjian, E., & Rittmann, B. E. (2019). Biogeochemical Model for Soil Improvement by Denitrification. *Journal of Geotechnical and Geoenvironmental Engineering*, *145*(11), Article 04019091. https://doi.org/10.1061/(asce)gt.1943-5606.0002126

Okamura, M., & Soga, Y. (2006). Effects of pore fluid compressibility on liquefaction resistance of partially saturated sand. *Soils and Foundations*, *46*(5), 695-700. https://doi.org/10.3208/sandf.46.695

Okamura, M., Takebayashi, M., Nishida, K., Fujii, N., Jinguji, M., Imasato, T., Yasuhara, H., & Nakagawa, E. (2011). In-Situ Desaturation Test by Air Injection and Its Evaluation through Field Monitoring and Multiphase Flow Simulation. *Journal of Geotechnical and Geoenvironmental Engineering*, *137*(7), 643-652. https://doi.org/10.1061/(ASCE)GT.1943-5606.0000483

Olbrich, H. (1963). *The Molasses*.

Orense, R. P. (2015). *Recent Trends in Ground Improvement Methods as Countermeasure against Liquefaction* (6th International Conference on Earthquake Geotechnical Engineering, Issue.

Padappayil, R. P., & Borger, J. (2021). *Ammonia Toxicity*. https://www.ncbi.nlm.nih.gov/books/NBK546677/

Pan, Y., Liu, Y., Wang, D., & Ni, B.-J. (2019). Modeling effects of H2S on electron competition among nitrogen oxide reduction and N2O accumulation during denitrification [10.1039/C8EW00873F]. *Environmental Science: Water Research & Technology*, *5*(3), 533-542. https://doi.org/10.1039/C8EW00873F

Pan, Y., Ye, L., & Yuan, Z. (2013). Effect of H2S on N2O reduction and accumulation during denitrification by methanol utilizing denitrifiers. *Environ Sci Technol*, *47*(15), 8408-8415. https://doi.org/10.1021/es401632r

Panswad, T., & Anan, C. (1999). Specific oxygen, ammonia, and nitrate uptake rates of a biological nutrient removal process treating elevated salinity wastewater. *Bioresource Technology*, *70*(3), 237-243. https://doi.org/https://doi.org/10.1016/S0960-8524(99)00041-3

Papaspyrou, S., Smith, C. J., Dong, L. F., Whitby, C., Dumbrell, A. J., & Nedwell, D. B. (2014). Nitrate Reduction Functional Genes and Nitrate Reduction Potentials Persist in Deeper Estuarine Sediments. Why? *PLOS ONE*, *9*(4), e94111. https://doi.org/10.1371/journal.pone.0094111

Paul, J. W., Beauchamp, E. G., & Trevors, J. T. (1989). ACETATE, PROPIONATE, BUTYRATE, GLUCOSE, AND SUCROSE AS CARBON-SOURCES FOR DENITRIFYING BACTERIA IN SOIL. *Canadian Journal of Microbiology*, *35*(8), 754-759. https://doi.org/10.1139/m89-126

Pham, V. (2017). *Bio-based Ground Improvement through Microbial Induced Desaturation and Precipitation (MIDP)*. Delft University of Technology.

Pham, V. P., Nakano, A., van der Star, W. R. L., Heimovaara, T. J., & van Paassen, L. A. (2018). Applying MICP by denitrification in soils: a process analysis. *Environmental Geotechnics*, *5*(2), 79-93, Article 1500078. https://doi.org/10.1680/jenge.15.00078

Pham, V. P., van Paassen, L. A., van der Star, W. R. L., & Heimovaara, T. J. (2018). Evaluating Strategies to Improve Process Efficiency of Denitrification-Based MICP. *Journal of Geotechnical and Geoenvironmental Engineering*, *144*(8), Article 04018049. https://doi.org/10.1061/(asce)gt.1943-5606.0001909

Phillips, A. J., Gerlach, R., Lauchnor, E., Mitchell, A. C., Cunningham, A. B., & Spangler, L. (2013). Engineered applications of ureolytic biomineralization: a review. *Biofouling*, *29*(6), 715-733. https://doi.org/10.1080/08927014.2013.796550

Quan, Z.-X., Jin, Y.-S., Yin, C.-R., Lee, J. J., & Lee, S.-T. (2005). Hydrolyzed molasses as an external carbon source in biological nitrogen removal. *Bioresource Technology*, *96*(15), 1690-1695. https://doi.org/https://doi.org/10.1016/j.biortech.2004.12.033

Ramirez, J. E., Rangel-Mendez, J. R., Lopes, C. L., Gomes, S. D., Buitron, G., & Cervantes, F. J. (2018). Denitrification of metallurgic wastewater: mechanisms of inhibition by Fe, Cr and Ni. *Journal of Chemical Technology and Biotechnology*, *93*(2), 440-449. https://doi.org/10.1002/jctb.5374

Rasouli, R., Hayashi, K., & Zen, K. (2016). Controlled Permeation Grouting Method for Mitigation of Liquefaction. *Journal of Geotechnical and Geoenvironmental Engineering*, *142*(11), 04016052. https://doi.org/10.1061/(ASCE)GT.1943-5606.0001532

Rebata-Landa, V., & Santamarina, J. C. (2012). Mechanical Effects of Biogenic Nitrogen Gas Bubbles in Soils. *Journal of Geotechnical and Geoenvironmental Engineering*, *138*(2), 128-137. https://doi.org/10.1061/(asce)gt.1943-5606.0000571

Rittmann, B., & McCarty, P. (2020). *Environmental Biotechnology: Principles and Applications*. McGraw-Hill Companies, Incorporated.

Rittmann, B., McCarty, P., McCarty, P. L., & Bruce, R. (2001). *Environmental Biotechnology: Principles and Applications*. McGraw-Hill Companies,Incorporated.

Rittmann, B. E., Banaszak, J. E., Cooke, A., & Rowe, R. K. (2003). Biogeochemical Evaluation of Mechanisms Controlling CaCO3(s) Precipitation in Landfill Leachate-Collection Systems. *Journal of Environmental Engineering*, *129*(8), 723-730. https://doi.org/10.1061/(ASCE)0733-9372(2003)129:8(723)

Rittmann, B. E., Banaszak, J. E., VanBriesen, J. M., & Reed, D. T. (2002). Mathematical modeling of precipitationand dissolution reactions in microbiological systems. *Biodegradation*, *13*(4), 239-250. https://doi.org/10.1023/A:1021225321263

S., C., G.L., M.-L., & JP., P. (2000). Bacterial Roles in the Precipitation of Carbonate Minerals. In A. S. M. Riding R.E. (Ed.), *Microbial Sediments*. Springer.

Salek, S. S., van Turnhout, A. G., Kleerebezem, R., & van Loosdrecht, M. C. M. (2015). pH control in biological systems using calcium carbonate [https://doi.org/10.1002/bit.25506]. *Biotechnology and Bioengineering*, *112*(5), 905-913. https://doi.org/https://doi.org/10.1002/bit.25506

Scholten, J. C. M., van Bodegom, P. M., Vogelaar, J., van Ittersum, A., Hordijk, K., Roelofsen, W., & Stams, A. J. M. (2002). Effect of sulfate and nitrate on acetate conversion by anaerobic microorganisms in a freshwater sediment. *Fems Microbiology Ecology*, *42*(3), 375-385, Article Pii s0168-6496(02)00359-8. https://doi.org/10.1016/s0168-6496(02)00359-8

Senga, Y., Mochida, K., Fukumori, R., Okamoto, N., & Seike, Y. (2006). N2O accumulation in estuarine and coastal sediments: The influence of H2S on dissimilatory nitrate reduction. *Estuarine, Coastal and Shelf Science*, *67*(1), 231-238. https://doi.org/https://doi.org/10.1016/j.ecss.2005.11.021

Shi, C., Huang, Z., Zhou, Y., He, J., Yang, F., & Hang, L. (2019). Soil Desaturation Methods for the Improvement of Liquefiable Ground. *IOP Conference Series: Materials Science and Engineering*, *562*, 012015. https://doi.org/10.1088/1757-899x/562/1/012015

Silva, V., Amo-Oduro, D., Calderon, A., Dabbeek, J., Despotaki, V., Martins, L., Rao, A., Simionato, M., Vigano, D., Yepes, C., Acevedo, A., Crowley, H., Horspool, N., Jaiswal, K., Journeay, M., & Pittore, M. (2018). *Global Earthquake Model (GEM) Risk Map* [Report]. F. Global Earthquake Model. http://pubs.er.usgs.gov/publication/70201394

Singurindy, O., Berkowitz, B., & Lowell, R. P. (2004). Carbonate dissolution and precipitation in coastal environments: Laboratory analysis and theoretical consideration. *Water Resources Research*, *40*(4), Article W04401. https://doi.org/10.1029/2003wr002651

Sirivedhin, T., & Gray, K. A. (2006). Factors affecting denitrification rates in experimental wetlands: Field and laboratory studies. *Ecological Engineering*, *26*(2), 167-181. https://doi.org/10.1016/j.ecoleng.2005.09.001

Soto, O., Aspé, E., & Roeckel, M. (2007). Kinetics of cross-inhibited denitrification of a high load wastewater. *Enzyme and Microbial Technology*, *40*(6), 1627-1634. https://doi.org/https://doi.org/10.1016/j.enzmictec.2006.11.014

Spanos, N., & Koutsoukos, P. G. (1998). Kinetics of Precipitation of Calcium Carbonate in Alkaline pH at Constant Supersaturation. Spontaneous and Seeded Growth. *The Journal of Physical Chemistry B*, *102*(34), 6679-6684. https://doi.org/10.1021/jp981171h

Tugtas, A. E., & Pavlostathis, S. G. (2007). Effect of sulfide on nitrate reduction in mixed methanogenic cultures [https://doi.org/10.1002/bit.21338]. *Biotechnology and Bioengineering*, *97*(6), 1448-1459. https://doi.org/https://doi.org/10.1002/bit.21338

Umar, M., Kassim, K. A., & Chiet, K. T. P. (2016). Biological process of soil improvement in civil engineering: A review. *Journal of Rock Mechanics and Geotechnical Engineering*, *8*(5), 767-774. https://doi.org/10.1016/j.jrmge.2016.02.004

Vaid, Y. P., & Sivathayalan, S. (2000). Fundamental factors affecting liquefaction susceptibility of sands. *Canadian Geotechnical Journal*, *37*(3), 592-606. https://doi.org/10.1139/cgj-37-3-592

van den Berg, E. M., Rombouts, J. L., Kuenen, J. G., Kleerebezem, R., & van Loosdrecht, M. C. M. (2017). Role of nitrite in the competition between denitrification and DNRA in a chemostat enrichment culture. *AMB Express*, *7*(1), 91. https://doi.org/10.1186/s13568-017-0398-x

van der Star, W., van Wijngaarden-van Rossum, W. K., van Paassen, L., van Baalen, L. R., & van Zwiete, G. (2011). *Stabilization of gr avel deposits using microorganisms* 15th European Conference on So i l Mechan i cs and Geotechn i cal Eng i neer i ng, Amsterdam, Netherlands.

van Paassen, L. A., Daza, C. M., Staal, M., Sorokin, D. Y., van der Zon, W., & van Loosdrecht, M. C. M. (2010). Potential soil reinforcement by biological denitrification. *Ecological Engineering*, *36*(2), 168-175. https://doi.org/10.1016/j.ecoleng.2009.03.026

van Paassen, L. A., Ghose, R., van der Linden, T. J. M., van der Star, W. R. L., & van Loosdrecht, M. C. M. (2010). Quantifying Biomediated Ground Improvement by Ureolysis: Large-Scale Biogrout Experiment. *Journal of Geotechnical and Geoenvironmental Engineering*, *136*(12), 1721-1728. https://doi.org/10.1061/(asce)gt.1943-5606.0000382

van Paassen, L. A., Pham, V., Mahabadi, N., Hall, C. A., Stallings, E., & Kavazanjian, E. (2017). Desaturation via Biogenic Gas Formation as a Ground Improvement Technique. *PanAm Unsaturated Soils 2017*, 244-256. https://doi.org/doi:10.1061/9780784481677.013

van Turnhout, A. G., Kleerebezem, R., & Heimovaara, T. J. (2016). A toolbox to find the best mechanistic model to predict the behavior of environmental systems. *Environmental Modelling & Software*, *83*, 344-355. https://doi.org/10.1016/j.envsoft.2016.05.002

Vavilin, V. A., & Rytov, S. V. (2015). Nitrate denitrification with nitrite or nitrous oxide as intermediate products: Stoichiometry, kinetics and dynamics of stable isotope signatures. *Chemosphere*, *134*, 417-426. https://doi.org/10.1016/j.chemosphere.2015.04.091

Veshareh, M. J., Kjeldsen, K. U., Findlay, A. J., Nick, H. M., Røy, H., & Marietou, A. (2021). Nitrite is a more efficient inhibitor of microbial sulfate reduction in oil

reservoirs compared to nitrate and perchlorate: A laboratory and field-scale simulation study. *International Biodeterioration & Biodegradation*, *157*, 105154. https://doi.org/https://doi.org/10.1016/j.ibiod.2020.105154

Vink, J. P. M., & Meeussen, J. C. L. (2007). BIOCHEM-ORCHESTRA: A tool for evaluating chemical speciation and ecotoxicological impacts of heavy metals on river flood plain systems. *Environmental Pollution*, *148*(3), 833-841. https://doi.org/10.1016/j.envpol.2007.01.041

Wang, L., van Paassen, L., Gao, Y., He, J., Gao, Y., & Kim, D. (2020). Laboratory Tests on Mitigation of Soil Liquefaction Using Microbial Induced Desaturation and Precipitation. *Geotechnical Testing Journal*, *44*(2), 520-534. https://doi.org/10.1520/GTJ20190432

Weston, N. B., Vile, M. A., Neubauer, S. C., & Velinsky, D. J. (2011). Accelerated microbial organic matter mineralization following salt-water intrusion into tidal freshwater marsh soils. *Biogeochemistry*, *102*(1-3), 135-151. https://doi.org/10.1007/s10533-010-9427-4

Whiffin, V. S., van Paassen, L. A., & Harkes, M. P. (2007). Microbial carbonate precipitation as a soil improvement technique. *Geomicrobiology Journal*, *24*(5), 417-423. https://doi.org/10.1080/01490450701436505

Wilderer, P. A., Jones, W. L., & Dau, U. (1987). COMPETITION IN DENITRIFICATION SYSTEMS AFFECTING REDUCTION RATE AND ACCUMULATION OF NITRITE. *Water Research*, *21*(2), 239-245. https://doi.org/10.1016/0043-1354(87)90056-x

Yamamoto-Ikemoto, R., Matsui, S., Komori, T., & BosqueHamilton, E. J. (1996). Symbiosis and competition among sulfate reduction, filamentous sulfur, denitrification, and poly-P accumulation bacteria in the anaerobic-oxic activated sludge of a municipal plant. *Water Science and Technology*, *34*(5-6), 119-128. https://doi.org/10.1016/0273-1223(96)00637-3

Yegian, M. K., Eseller-Bayat, E., Alshawabkeh, A., & Ali, S. (2007). Induced-partial saturation for liquefaction mitigation: Experimental investigation. *Journal of Geotechnical and Geoenvironmental Engineering*, *133*(4), 372-380. https://doi.org/10.1061/(asce)1090-0241(2007)133:4(372)

Yeomans, J. C., Bremner, J. M., & McCarty, G. W. (1992). DENITRIFICATION CAPACITY AND DENITRIFICATION POTENTIAL OF SUBSURFACE SOILS. *Communications in Soil Science and Plant Analysis*, *23*(9-10), 919-927. https://doi.org/10.1080/00103629209368639

Yongsiri, C., Vollertsen, J., Rasmussen, M., & Hvitved–Jacobsen, T. (2004). Air–Water Transfer of Hydrogen Sulfide: An Approach for Application in Sewer Networks

[https://doi.org/10.2175/106143004X141618]. *Water Environment Research*, *76*(1), 81-88. https://doi.org/https://doi.org/10.2175/106143004X141618

Zarga, Y., Ben Boubaker, H., Ghaffour, N., & Elfil, H. (2013). Study of calcium carbonate and sulfate co-precipitation. *Chemical Engineering Science*, *96*, 33-41. https://doi.org/10.1016/j.ces.2013.03.028

Zhu, I., & Liu, J. R. (2017). Introductory Chapter: Effects of Salinity on Biological Nitrate Removal from Industrial Wastewater. https://doi.org/10.5772/intechopen.69438

Zhu, I., X. and Liu, Jian R. (2017). Introductory Chapter: Effects of Salinity on Biological Nitrate Removal from Industrial Wastewater. https://doi.org/10.5772/intechopen.69438

Zumft, W. G. (1997). Cell biology and molecular basis of denitrification. *Microbiology and Molecular Biology Reviews*, *61*(4), 533-+. https://doi.org/10.1128/.61.4.533-616.1997

Šimek, M., & Cooper, J. E. (2002). The influence of soil pH on denitrification: progress towards the understanding of this interaction over the last 50 years [https://doi.org/10.1046/j.1365-2389.2002.00461.x]. *European Journal of Soil Science*, *53*(3), 345-354. https://doi.org/https://doi.org/10.1046/j.1365-2389.2002.00461.x

APPENDIX A

CONSTANTS USED IN BIOGEOCHEMICAL MODEL

Below are the constants used during modeling. These do not include constants found within the ORCHESTRA database for acid-base speciation (Meeussen, 2003), nor those dependent on electron donor and acceptor (e.g., K_a and K_d) that can be found within Chapter 5, Chapter 6, and Chapter 7.

Parameter	Value	Reference
$\Delta G_c^{0'}$ (kJ e$^-$ eq^{-1}): free energy of the carbon source	Acetate: 27.4 Glucose: 41.0 Molasses: 41.0	(Rittmann & McCarty, 2020)
ΔG_{pc} (kJ e$^-$ eq^{-1}): free energy to convert pyruvate carbon to cellular carbon, depending on the nitrogen source	Nitrate: 14.1 Ammonium: 19.5	(Rittmann & McCarty, 2020)
$\Delta G_a^{0'}$ (kJ e$^-$ eq^{-1}): free energy required to reduce an electron acceptor	Nitrate: -41.65 Nitrite: -92.56 Sulfate: 20.85 Oxygen: -78.72	(Rittmann & McCarty, 2020)
$\Delta G_d^{0'}$ (kJ e$^-$ eq^{-1}): free energy released to oxidize an electron donor	Acetate: 27.4 Glucose: 41.0 Molasses: 41.0	(Rittmann & McCarty, 2020)
$\hat{q}_e$: maximum flow of electrons (e-equivalent g^{-1} biomass d^{-1})	1.0	(Rittmann & McCarty, 2020)
RM_A: (g Chemical Oxygen Demand (donor e$^-$ equivalent)$^{-1}$)	8	(Rittmann & McCarty, 2020)
RM_B: (mol donor g^{-1} Chemical Oxygen Demand)	Acetate: 84 Glucose: 192 Molasses: 192	Calculated from half reactions (Rittmann & McCarty, 2020)
e^-_d (mol electron donor (donor e$^-$ equivalent)$^{-1}$) is the amount of donor per electron equivalent	Acetate: 0.13 Glucose: 0.04 Molasses 0.04	Calculated from RM_A, RM_B, and $\hat{q}_e$
ε: energy transfer efficiency term	0.6	(Rittmann & McCarty, 2020)
n: considers energy efficiency due to thermodynamics, depending on electron donor	Acetate: 1 Glucose: 1 Molasses: 1	(Rittmann & McCarty, 2020)
X_a (mmol biomass L^{-1}): Active biomass concentration	Denitrifiers: 0.5 Sulfate Reducers: 0.25	
k_La (d^{-1}): gas mass transfer constant	0.5	(Yongsiri et al., 2004)

$K_{sp(CaCO_3)}$: speciation constant for calcium carbonate	$10^{-8.3}$	
R (L atm K^{-1} mol^{-1}): universal gas constant	0.082057	
T (K): temperature	298	
K_H (L$_{aq}$ atm mol^{-1}): Henry's Law coefficients	N_2: 1600 CO_2: 29 H_2S: 10	
e (L$_{pore}$ L$_{soil}^{-1}$): void ratio	0.64	Within a value of acceptable ranges (Christopher et al., 2006)
ka (L d^{-1}): combined coefficient considering a constant mass transfer and the average crystal surface area	100	Within a value of acceptable ranges (Rittmann et al., 2003)
ρ_{soil} (g soil L$_{soil}^{-1}$): soil density	1950	Within a value of acceptable ranges (Christopher et al., 2006)